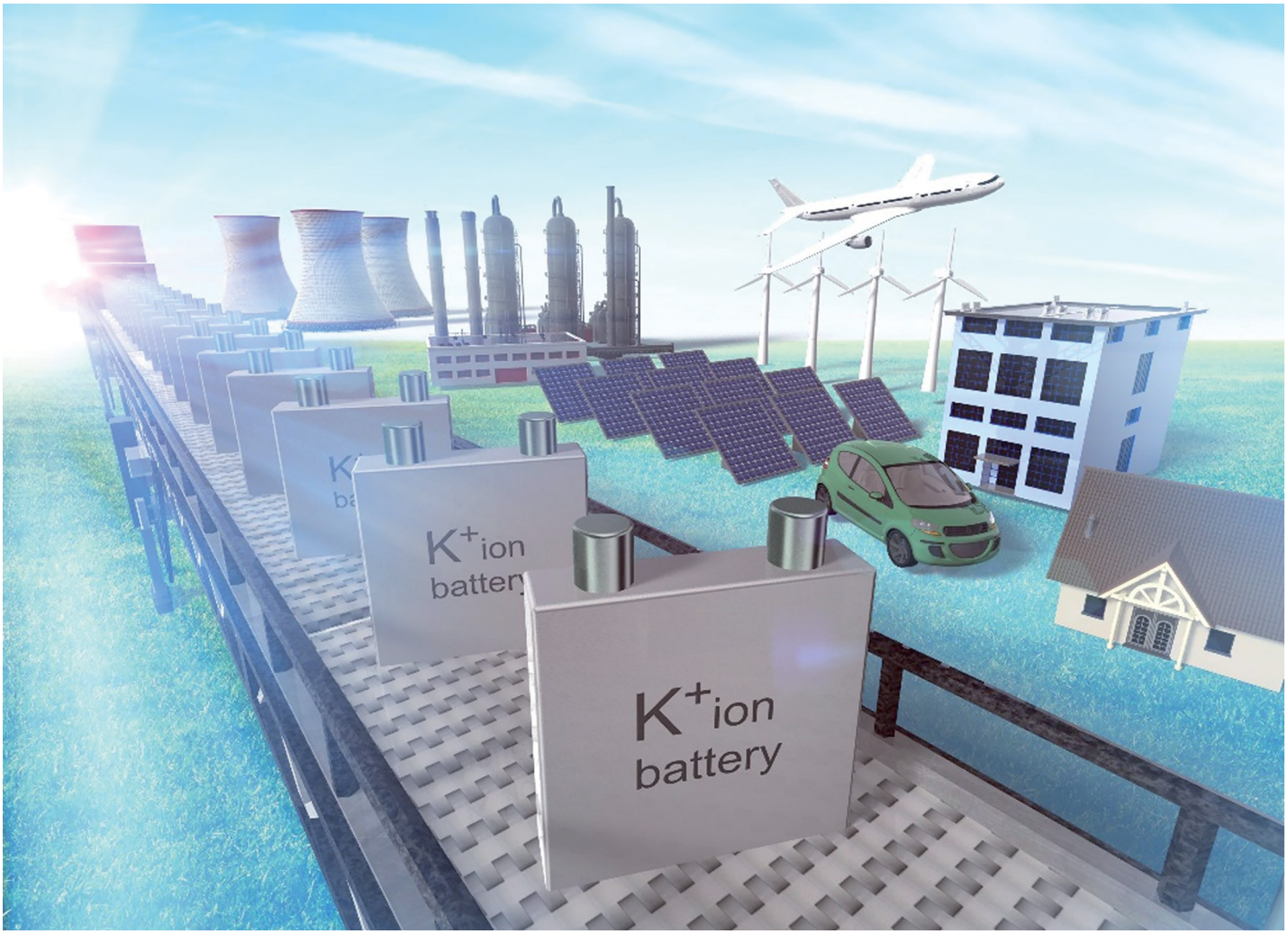

Showcasing research from Dr Titus Masese and Dr Godwill Mbiti Kanyolo's research group, National Institute of Advanced Science and Technology (AIST), Osaka, Japan.

Advancements in cathode materials for potassium-ion batteries: current landscape, obstacles, and prospects

This perspective highlights advancements in the development of positive electrode materials for potassium-ion batteries.

As featured in:

See Titus Masese and Godwill Mbiti Kanyolo, *Energy Adv.*, 2024, **3**, 60.

ROYAL SOCIETY OF CHEMISTRY

rsc.li/energy-advances

Registered charity number: 207890

Energy Advances

ROYAL SOCIETY OF CHEMISTRY

PERSPECTIVE

View Article Online
View Journal | View Issue

Check for updates

Cite this: *Energy Adv.*, 2024, 3, 60

Advancements in cathode materials for potassium-ion batteries: current landscape, obstacles, and prospects

Titus Masese *[ac] and Godwill Mbiti Kanyolo *[ab]

The development of advanced energy storage technologies has assumed paramount significance in addressing the escalating demands for sustainable and eco-friendly power sources. Amongst these innovative technologies, potassium-ion batteries (KIBs) have risen to the fore as viable contenders, chiefly owing to their cost-effectiveness and the abundant availability of potassium resources. Nevertheless, the realisation of efficient and high-performance KIBs hinges significantly upon the adept design and appropriate utilisation of cathode materials. Thus, this *Perspective* provides a comprehensive analysis of the present status, associated challenges, and prospective avenues concerning cathode materials for KIBs. We commence by discussing the significance of KIBs in the context of the global energy landscape and highlight their potential to revolutionise energy storage systems. Subsequently, we delve into cathode materials for KIBs, emphasising their pivotal role in determining the overall performance of these batteries. A systematic survey of the various cathode materials explored to date is presented, primarily encompassing layered oxides, polyanion-based compounds, Prussian analogues and organic moieties. The discussion focuses on the advantages, limitations, and performance metrics of each material class, unveiling the critical insights gained from experimental studies and theoretical investigations. Furthermore, this *Perspective* sheds light on the prominent challenges and obstacles hindering the widespread adoption of KIBs. These challenges include issues related to limited specific capacities, sluggish kinetics, and performance attenuation during cycling, as well as the scarcity of suitable electrolytes. We offer an authoritative evaluation of the efforts undertaken to address these obstacles, including novel material design strategies, advanced characterisation techniques, and the integration of nanotechnology. Finally, we conclude with a forward-looking perspective, outlining the future directions and potential breakthroughs in electrode materials for KIBs. We emphasise the importance of interdisciplinary collaborations, advancements in computational methods, and fundamental research to foster the development of high-performance and environmentally sustainable KIBs. In conclusion, this *Perspective* consolidates the current state of electrode materials for KIBs whilst elucidating the challenges that need to be overcome to unlock their full potential. By synthesising the collective knowledge from the latest research endeavours, this *Perspective* aims to inspire future research and innovation in the pursuit of efficient and scalable KIB technologies.

Received 20th August 2023,
Accepted 27th November 2023

DOI: 10.1039/d3ya00406f

rsc.li/energy-advances

Open Access Article. Published on 04 dicembre 2023. Downloaded on 11/06/2026 17:40:22.
This article is licensed under a Creative Commons Attribution-NonCommercial 3.0 Unported Licence.

1 Introduction

Meeting the immense energy demands of our society in a sustainable and environmentally responsible manner has become an urgent global imperative. Over the years, lithium-ion (Li-ion) battery (LIB) technology has reigned as the dominant energy storage system, finding widespread usage in portable electronics and scaling up to large-scale energy storage systems like the electric grid, facilitating the integration of intermittent renewable energy sources such as wind, tidal and solar power.[1] Fig. 1 shows the anticipated proliferation number of energy devices, encompassing portable electronics to large-scale energy storage systems intended for utilisation in electric vehicles. In this context, the applicability of rechargeable batteries, exemplified by the present-day LIB, is projected to be all-encompassing. However, the projected paucity and uneven global distribution of lithium resources,[2] along with the exponential growth of electric vehicles and our growing dependency on renewable energy, have catalysed the pursuit of

[a] *Research Institute of Electrochemical Energy, National Institute of Advanced Industrial Science and Technology (AIST), 1-8-31 Midorigaoka, Ikeda, Osaka 563-8577, Japan. E-mail: titus.masese@aist.go.jp, gm.kanyolo@aist.go.jp*
[b] *Department of Engineering Science, The University of Electro-Communications, 1-5-1 Chofugaoka, Chofu, Tokyo 182-8585, Japan. E-mail: gmkanyolo@mail.uec.jp*
[c] *AIST-Kyoto University Chemical Energy Materials Open Innovation Laboratory (ChEM-OIL), Sakyo-ku, Kyoto 606-8501, Japan*

© 2024 The Author(s). Published by the Royal Society of Chemistry

Open Access Article. Published on 04 dicembre 2023. Downloaded on 11/06/2026 17:40:22.
This article is licensed under a Creative Commons Attribution-NonCommercial 3.0 Unported Licence.

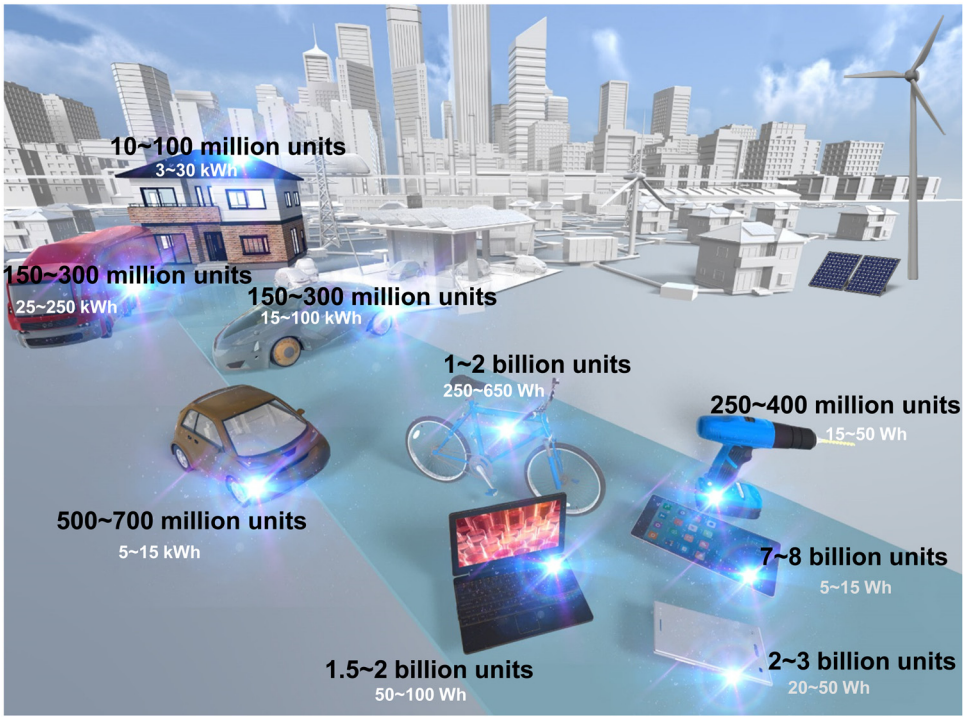

Fig. 1 Projected number of energy devices and battery size,[3] including those for portable electronics and large-scale energy storage in electric vehicles. Rechargeable batteries, like the current LIB, are expected to be extensively utilised.

alternative battery systems to replace or complement commercial Li-ion batteries (LIBs).

1.1 Overall significance of potassium-ion batteries

As a promising contender, potassium-ion (K-ion) batteries (hereafter referred to as KIBs) have emerged as a viable alternative for energy storage,[4] offering a range of compelling advantages delved into below:

1. The remarkable abundance of potassium resources in the earth's crust (at approximately 17 000 parts per million (ppm)) compared to lithium (at around 20 ppm) has ignited extensive research focus on potassium-based chemistries as a promising avenue for cost-effective grid-scale energy storage solutions. In

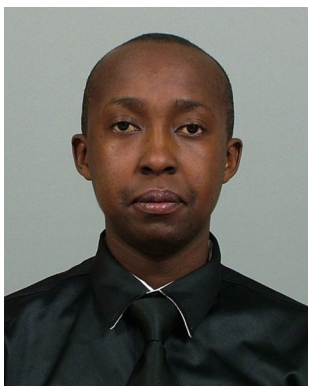

Titus Masese

Titus Nyamwaro Masese is a materials scientist specialising in the development of functional materials for a wide range of rechargeable batteries, including potassium-ion, silver, magnesium, and calcium battery systems. His research encompasses a multidisciplinary approach, where he leverages principles from electrochemistry, solid-state chemistry, solid-state physics, and mathematics. Currently, his primary focus revolves around the in-depth exploration of emerging phenomena and theory inherent in honeycomb layered oxide frameworks, a class of materials that holds significant promise not only in the advancement of energy storage technologies, but also opening up new frontiers in fundamental science and engineering.

Godwill Mbiti Kanyolo

Godwill Mbiti Kanyolo is a mathematical physicist studying quantum materials and their applications as functional materials and analogue systems for quantum gravity. He is currently fascinated with geometry and topological treatments of the condensed matter physics and chemistry inherent in optimised lattices of cations within honeycomb layered frameworks. His research includes the characterisation of peculiar electronic properties of valence electrons and their host ions on the honeycomb lattice, such as anomalous subvalent states and metallophilicity. He has also leveraged his broad expertise on honeycomb layered oxides to discovering novel high-performance materials for renewable energy storage applications such as potassium-ion batteries.

Open Access Article. Published on 04 dicembre 2023. Downloaded on 11/06/2026 17:40:22.
This article is licensed under a Creative Commons Attribution-NonCommercial 3.0 Unported Licence.

reality, the Clarke's number, a significant parameter denoting the relative crustal abundance of elements, exemplifies the remarkable disparity between potassium (2.3 wt%) and lithium (0.006 wt%).[6] The prevalence of potassium vastly surpasses that of lithium, emphasising the pronounced variation in their respective occurrences within the Earth's crust (Fig. 2a). Potassium-based salts are thus widely available in substantial quantities worldwide, offering a cost advantage.[7] For instance, raw materials such as K_2CO_3, employed as precursors for the design of electrode materials, are not only abundant but also more economically accessible than Li_2CO_3. Additionally, potassium resources are more evenly distributed across the globe, eliminating concerns about geopolitical constraints that can impede the supply of lithium. Thus, the sustainable nature of potassium-based alternatives becomes evident, providing a compelling rationale for their exploration in energy storage applications;

2. Potassium possesses electrochemical properties that are notably similar to lithium:[8]

(a) In fact, a potassium-ion battery operates on a mechanism that closely resembles that of a lithium-ion battery (Fig. 2b), wherein potassium ions shuttle between the electrodes through the electrolyte during the charging and discharging processes, in what was initially referred to as a 'shuttle' or 'rocking-chair' battery technology.

Like other rechargeable batteries, the potassium-ion battery (KIB) comprises an ionically conductive electrolyte containing a potassium-based salt, two current collectors (one negative and one positive), a separator and two electrodes with distinctive chemical potentials. The positive electrode can be constructed using diverse materials, such as layered oxides (*e.g.*, K_xCoO_2, $KCrO_2$, *etc.*),[9–11] polyanion compounds (*e.g.*, $KVPO_4F$, $KFeSO_4F$),[12–19] organic compounds (*e.g.*, poly(anthraquinonyl sulphide (abbreviated as PAQS)),[20,21] polyaniline (PANI),[22] 3,4,9,10-perylene-tetracarboxylic acid-dianhydride (commonly referred to as Pigment Red 224 ($C_{24}H_8O_6$) and abbreviated as PTCDA),[23] *etc.*), as well as Prussian analogues (*e.g.*, $K_2MnFe(CN)_6$, $K_2FeFe(CN)_6$, $K_2NiFe(CN)_6$, *etc.*).[24–34] Conversely, the negative electrode can be constituted of carbonaceous materials such as graphite, which stands as a prevalent choice due to its proficient facilitation of reversible extraction/insertion of K-ions. As for the electrolyte, customary formulations comprise mixtures of organic carbonate solvents, such as diethyl carbonate or ethyl carbonate, in conjunction with non-coordinating anion salts, prominently exemplified by potassium hexafluorophosphate (KPF_6), potassium bis(fluorosulphonyl)imide ($KN(SO_2F)_2$ (typically abbreviated as KFSI or KFSA)), potassium trifluoromethanesulphonate (KCF_3SO_3 (KOTf)), potassium (3-methoxypropyl)((trifluoromethyl)-sulphonyl)-imide (abbreviated as KMPSA) and potassium bis(trifluoromethanesulphonyl)imide ($KN(CF_3SO_2)_2$ (KTFSI or KTFSA)). A slender separator film, designed from insulation material, serves to efficaciously segregate the two electrodes, thereby preventing the occurrence of an internal short circuit.

During the charging phase, a cathodic oxidation half-reaction occurs at the positive electrode (cathode), where a positively charged external power source facilitates the extraction of

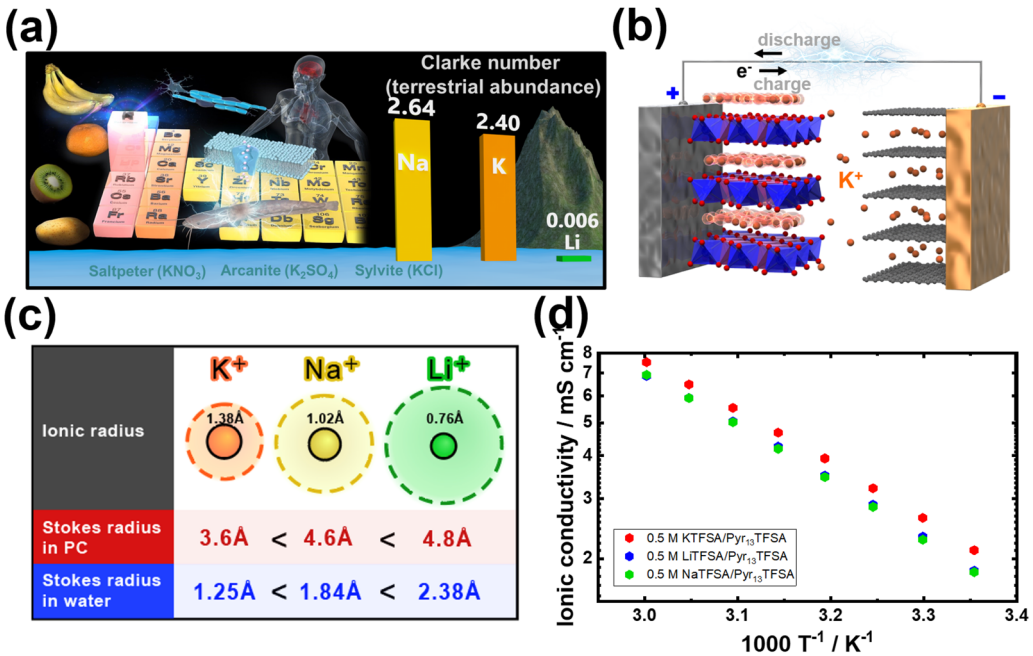

Fig. 2 (a) Abundance of potassium resources. (b) Schematic representation of the operation mechanism of potassium-ion battery (KIB), wherein the positive electrode consists of, for instance, layered oxide, and the negative electrode comprises graphite. Analogous to other secondary battery systems (rechargeable batteries), such as those involving lithium ions, the potassium ions efficiently traverse between the electrodes *via* the electrolyte. (c) Stokes radii of solvated states of alkali metal cations. (d) Arrhenius plots showing the ionic conductivity of pyrrolidinium-based ionic liquid electrolytes based on 1-methyl-1-propylpyrrolidinium bis(trifluoromethanesulphonyl)amide (abbreviated as $Pyr_{13}TFSA$ or $Pyr_{13}TFSI$) ionic liquids dissolved in KTFSA (KTFSI), NaTFSA and LiTFSA alkali metal salts.[5] Figure (d) reproduced from ref. 5 with permission. Copyright 2019 Wiley-VCH.

© 2024 The Author(s). Published by the Royal Society of Chemistry

Open Access Article. Published on 04 dicembre 2023. Downloaded on 11/06/2026 17:40:22.
This article is licensed under a Creative Commons Attribution-NonCommercial 3.0 Unported Licence.

electrons from the potassium atoms within the cathode material (*e.g.*, $KCrO_2$). Subsequently, these extracted electrons direct potassium ions (K^+) through an external circuit to the negative electrode (anode) (*e.g.*, graphite). This process engenders an electrical disequilibrium within the cell, prompting the migration of potassium ions through the electrolyte towards the negatively charged anode. The layered structure of loosely bonded graphene sheets in graphite facilitates a reduction half-reaction, enabling the intercalation of potassium ions into its layers and leading to the formation of potassiated graphite (KC_8) in a phenomenon known as potassiation or potassium intercalation/insertion. This potassiation process continues until the graphite achieves full potassiation, resulting in the maximal electrical potential difference between the two electrodes, commonly referred to as the fully charged state. In the discharge process, a converse sequence occurs. Electrons liberated from the graphite anode travel back to the cathodic side, compelling the departure of K^+ from the potassiated graphite in a process referred to as depotassiation or potassium de-intercalation/extraction. Concurrently, potassium ions traverse the electrolyte and recombine with the cathode material. This discharge process persists until the graphite is entirely depotassiated, leading to the diminishing of the potential difference between the two electrodes to the minimum voltage level.

(b) Potassium-ion batteries can benefit from the utilisation of electrolyte formulations similar to those used in lithium-ion batteries. For instance, electrolytes such as potassium hexafluorophosphates (KPF_6), where potassium replaces lithium in conventional $LiPF_6$-containing electrolytes, can be effectively employed. This compatibility extends to other battery components as well, allowing for the use of graphite and similar materials utilised in the production line of commercial lithium-ion batteries. As a result, the adoption of potassium-ion batteries not only benefits from existing manufacturing infrastructure but also offers potential cost reductions, making potassium-ion technology a promising 'drop-in' post-lithium-ion technology.

3. In its solvated state, potassium-ion exhibits a smaller Stokes radius compared to solvated lithium (Fig. 2c). This is primarily due to the larger ionic radius of K^+ ions compared to Li^+ and Na^+ ions.[37] As a result, K^+ ions experience reduced solvation compared to Na^+ and Li^+ ions, resulting in a smaller radius for solvated K^+ ions. This characteristic leads to weaker Lewis acidity for potassium and facilitates the faster movement of solvated K-ions in electrolytes containing potassium salts (Fig. 2d). The comparatively larger ionic radius of K^+ (*e.g.*, 1.38 Å when coordinated octahedrally with ligands) compared to Li^+ (0.76 Å) results in a smaller Stokes radius for K^+ when solvated in propylene carbonate,[38] as illustrated in Fig. 2c. Consequently, K^+ exhibits low desolvation energies and enhanced ionic mobility in electrolytes (Fig. 3).[39] Indeed, a comparative analysis of the ionic conductivity in K-based electrolytes as opposed to Na- and Li-based counterparts (*e.g.*, APF_6 in propylene carbonate, APF_6 in ethylene carbonate: dimethyl carbonate, and AFSI in propylene carbonate, where A = K, Na, Li) demonstrates that K-based electrolytes exhibit the highest ionic conductivity, primarily attributed to the weak Lewis acidity of the K^+ ions.[40–42] Furthermore, the similarities in chemistries between K^+ and Li^+ ions enable the utilisation of well-established Li-based electrolyte compositions as analogues, which have been instrumental in the exploration of high-performance K-based electrolytes.

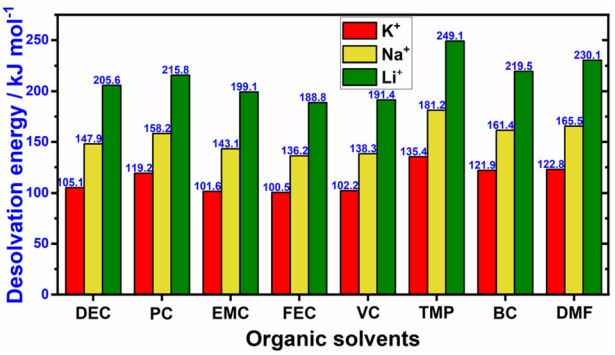

Fig. 3 Desolvation energy values of K^+, Na^+, and Li^+ in typical organic solvents. Abbreviations: dimethyl formamide (DMF), butylene carbonate (BC), trimethyl phosphate (TMP), vinylene carbonate (VC), fluoroethylene carbonate (FEC), ethyl methyl carbonate (EMC), propylene carbonate (PC), diethyl carbonate (DEC). The data was derived from ref. 35 and 36.

4. Potassium demonstrates a similar or even lower standard redox potential than lithium in non-aqueous electrolytes commonly used in conventional batteries,[44] paving the way for potentially high-voltage battery systems. Notably, nature itself has chosen potassium ions as charge carriers for transmitting synaptic impulses, whilst electric eels employ a combination of potassium and sodium ions in 'potassium pumps' to generate remarkably high voltages. From a technical perspective, the electrode potential of K/K^+ relative to the standard hydrogen electrode (SHE) (at −2.93 V *vs.* SHE for K/K^+) is comparable to that of Li^+/Li (at −3.04 V *vs.* SHE for Li/Li^+) in aqueous solvents. Furthermore, in certain non-aqueous solvents, K^+/K exhibits slightly more negative redox potentials than Li^+/Li (Fig. 4), resulting in higher voltage outputs and contributing to enhanced energy density in potassium-ion batteries.

5. Graphite, a commonly used anode material in commercial LIBs, can also serve as a direct anode material in KIBs (Fig. 5a). Remarkably, potassium ions can be reversibly inserted and extracted from graphite due to the inherent stability of the potassium-graphite compound (KC_8).[44–46] This unique characteristic enables the seamless utilisation of the well-established battery processing systems originally designed for LIBs in the context of KIBs. As a result, the transition and utilisation of graphite-based anodes become significantly easier and more efficient for KIBs compared to other rechargeable battery systems. Graphite anode demonstrates a reversible capacity, amounting to approximately 372 mA h g^{-1} in a Li cell, attributed to the formation of LiC_6 through a series of transitional stages: C ↔ LiC_{24} ↔ LiC_{18} ↔ LiC_{12} ↔ LiC_6. In contrast, whilst negligible capacity is observed in a Na cell, K^+ can be efficiently and reversibly inserted into graphite in a K cell (as illustrated in Fig. 5a and b). Reversible capacities commensurate

Open Access Article. Published on 04 dicembre 2023. Downloaded on 11/06/2026 17:40:22.
This article is licensed under a Creative Commons Attribution-NonCommercial 3.0 Unported Licence.

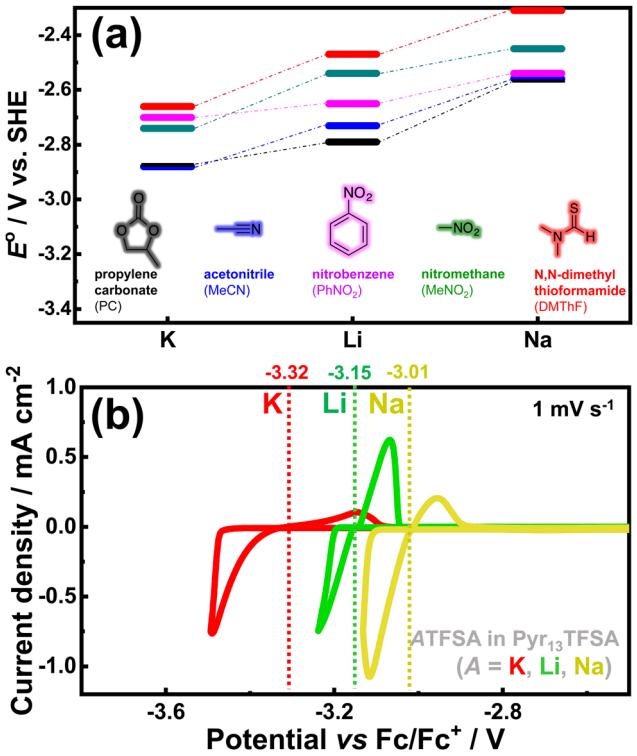

Fig. 4 (a) Alkali metal dissolution/deposition potential in organic solvents. Data plotted from ref. 43. (b) Alkali metal dissolution/deposition potential in pyrrolidinium-based ionic liquid electrolytes. Figure (b) reproduced and adapted from ref. 5 with permission. Copyright 2019 Wiley-VCH.

with the theoretical capacity of 279 mA h g^{-1} are commonly achieved in K cells (Fig. 5c), aligning closely with the reversible formation of stable KC_8 through a series of transitional stages that are yet polemical:[47] C ↔ KC_{36} ↔ KC_{24} ↔ KC_8[48] or C ↔ KC_{24} ↔ KC_{16} ↔ KC_8[49] or C ↔ KC_{60} ↔ KC_{48} ↔ KC_{36} ↔ KC_{24}/KC_{16} ↔ KC_8[50] or C ↔ KC_{48} ↔ KC_{36} ↔ KC_{24} ↔ KC_8[51] or C ↔ KC_{84} ↔ KC_{72} ↔ KC_{36} ↔ KC_{36}/KC_{24} ↔ KC_{24} ↔ KC_8.[52] It is indeed pertinent to note that these translational stages occur concurrently with graphite intercalation compounds manifesting electrochromism (Fig. 5d), thereby introducing novel applications of K^+ intercalation/de-intercalation electrochemistry within the realm of electrochromic device technologies. Moreover, potassium graphite intercalation compounds, namely KC_{12n} (where n = 2, 3, 4), KC_8, *etc.* can be synthesised through potassium-vapour-based methods, but an alternative approach involves a facile and scalable procedure achieved by combining graphite powder and potassium metal (with sodium as a catalyst) at room temperature (Fig. 5d). Hence, graphite, being an unquestionably inexpensive and extensively utilised anode material in commercial LIBs, can be readily adapted as an anode in KIBs. This noteworthy compatibility implies that the existing infrastructure and supply chain used for manufacturing graphite electrodes in LIBs can be smoothly transitioned to KIBs, thereby facilitating the commercial deployment of KIBs. Graphite can be envisaged as a widely employed anode material in KIBs, owing to its advantageous attributes, including low operation potential, high electronic conductivity, and significant volumetric and gravimetric capacities. The relatively low operation potential of graphite in KIBs (approximately 0.3 V *versus* (*vs.*) K/K^+, slightly higher than that in Li-cell as shown in Fig. 5a and c) enables the utilisation of the full cell voltage when combined with suitable high-voltage cathode materials. Additionally, this characteristic may mitigate the formation of dendritic potassium metal, a phenomenon typically observed at lower potentials (near 0 V *vs.* K/K^+). Furthermore, K/graphite cells have demonstrated superior rate capabilities compared to Li/graphite cells. Consequently, it becomes feasible to design a KIB system with essentially the same material configuration as current LIBs but with a higher power density.

6. Aluminium exhibits electrochemical alloying with lithium, forming β-LiAl, when employed as a current collector for the anode in lithium-ion batteries. However, when utilised as a current collector on the anode side of potassium-ion batteries, aluminium does not undergo the same electrochemical alloying reaction.[44] As a result, aluminium foil can be utilised as the current collector for the anode in potassium-ion batteries, eliminating the need for expensive copper foils used in the anode side of lithium-ion batteries. This utilisation of low-cost aluminium solely as the current collector in the anode side of potassium-ion batteries not only reduces costs but also decreases the weight of large battery packs. Notably, aluminium boasts a significantly lower density (2.7 g cm^{-3}) in comparison to copper (8.96 g cm^{-3}).

7. In contrast to lithium atoms, potassium atoms exhibit a broader range of coordination geometries with elements like oxygen. This characteristic gives rise to a greater diversity of potassium-based compounds, particularly inorganic compounds, offering a wider array of functionalities compared to lithium-based compounds. Furthermore, potassium-based layered oxides can accommodate potassium-deficient or non-stoichiometric compositions whilst maintaining stability,[54–103] which is not commonly observed in lithium-based layered oxides. For instance, the commercially utilised $LiCoO_2$ layered oxide cathode material cannot exist in a stable lithium-deficient form, such as $Li_{0.5}CoO_2$. However, related potassium-deficient layered oxides, such as $K_{0.3}CoO_2$, $K_{0.5}CoO_2$, $K_{0.67}CoO_2$, and so on, can be formed as stable materials. This implies that potassium-based compounds offer a vast landscape of battery materials with diverse electrochemistries.

1.2 Objective and scope of the perspective

Due to the aforementioned advantages, research on potassium-ion batteries (KIBs) has gained significant traction in recent years. Given the larger size of K^+ ions in comparison to both Na^+ and Li^+, considerable research efforts have been dedicated to designing electrode materials that can efficiently accommodate the reversible extraction/insertion of these larger K^+ ions. This *Perspective* presents a comprehensive overview of the progress in non-aqueous KIBs, with a primary focus on high-voltage cathode materials, whilst addressing the challenges that necessitate resolution. Perspectives and directions for the development of high-performance cathode materials in KIBs are also provided, drawing insights from relevant literature and our collective expertise. Additionally, we summarise effective

© 2024 The Author(s). Published by the Royal Society of Chemistry

Open Access Article. Published on 04 dicembre 2023. Downloaded on 11/06/2026 17:40:22.
This article is licensed under a Creative Commons Attribution-NonCommercial 3.0 Unported Licence.

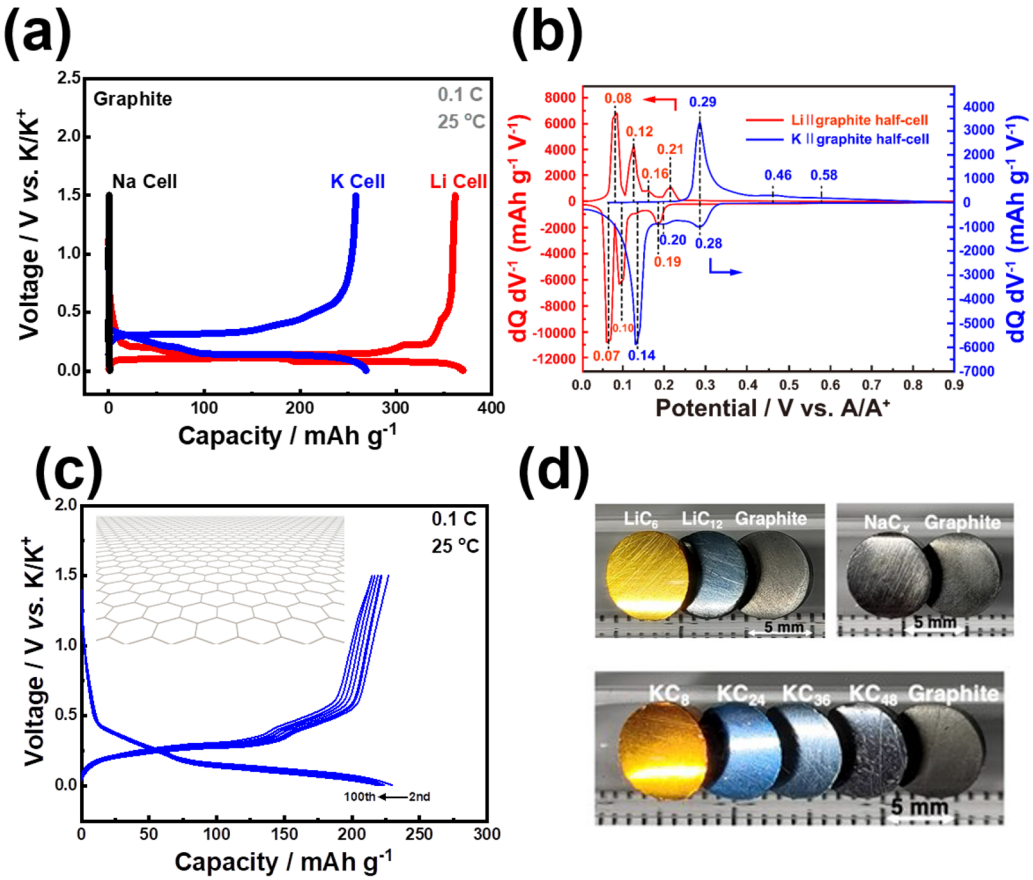

Fig. 5 Electrochemical Na^+, K^+ and Li^+ insertion/extraction behaviour in graphite. (a) Voltage–(dis)charge curves of graphite in an electrochemical Li, Na, K half-cell setups. (b) Differential capacity-potential plots of graphite in a Li half-cell and K half-cell showing peaks that correspond to the staging processes. (c) Voltage–(dis)charge profiles of graphite in a K half-cell (1C = 279 mA g^{-1}). (d) Photographs of LiC_{12}, LiC_6, KC_{12n} (n = 2, 3, 4), KC_8, and graphite pellets. Potassium graphite intercalation compounds display distinct colour with varying potassium content, suggesting that the electrochemical potassiation/depotassiation of graphite could have implications in electrochromic applications. Figure (b) reproduced from ref. 42 with permission. Copyright 2020 American Chemical Society. Figure (d) reproduced and adapted from ref. 53 with permission. Copyright 2023 Wiley-VCH.

strategies to enhance the electrochemical performance of both electrodes and electrolytes. Ultimately, we deliberate on the prospects for achieving high-performance non-aqueous KIBs. The *Perspective* aims to offer a holistic view and valuable guidance for researchers engaged in the pursuit of materials for high-voltage (and consequently, high energy density) non-aqueous KIBs. It is worth noting that, as of the present, there exists no universally standardised abbreviation for "potassium-ion battery" in the literature. Various publications have employed either "PIB" or "KIB" as the abbreviated form for "potassium-ion battery". Given the substantial volume of research papers adopting the abbreviation "KIB" across numerous scientific databases, in this *Perspective*, we shall abbreviate "potassium-ion battery" as "KIB".

2 High performance cathode materials

Cathode materials for KIBs can be classified broadly into four main groups: (i) Prussian analogues,[24–29] (ii) organic compounds, (iii) polyanion-based compounds, and (iv) layered oxides and chalcogenides.[104–109] In addition, perovskite compounds (such as $K(Mn_{0.95}Ni_{0.05})F_3$), conversion compounds (such as $CuSO_4$) and tunnel-structured compounds (such as cryptomelane-type KMn_8O_{16}) have emerged,[110–113] *albeit* less explored. Fig. 6 illustrates the average voltages attained by various cathode materials, along with their theoretical specific capacities. Hereafter, we will provide a concise summary of the advancements made in the development of high-voltage cathode materials for KIBs, with a particular emphasis on the strengths and weaknesses observed within each category of developed cathode materials.

2.1 Prussian analogues

Potassium-based Prussian analogues are hexacyanometallate compounds,[24–34] comprising cyanide-bridged coordination polymers formed by reacting transition metal cyanometallates with potassium ions. These compounds possess open three-dimensional (3D) crystalline frameworks and can be represented by the chemical composition $K_aL[L'(CN)_6]_{1-b}\cdot cH_2O$ ($0 \leq a \leq 2$, $0 \leq b < 1$, $c \geq 0$), where L and L' represent various transition metals like Zn, Cu, Ni, Co, Fe, Cr, and Ti, or alkaline-earth metals such as Mg, coordinated to cyano groups.

Open Access Article. Published on 04 dicembre 2023. Downloaded on 11/06/2026 17:40:22.
This article is licensed under a Creative Commons Attribution-NonCommercial 3.0 Unported Licence.

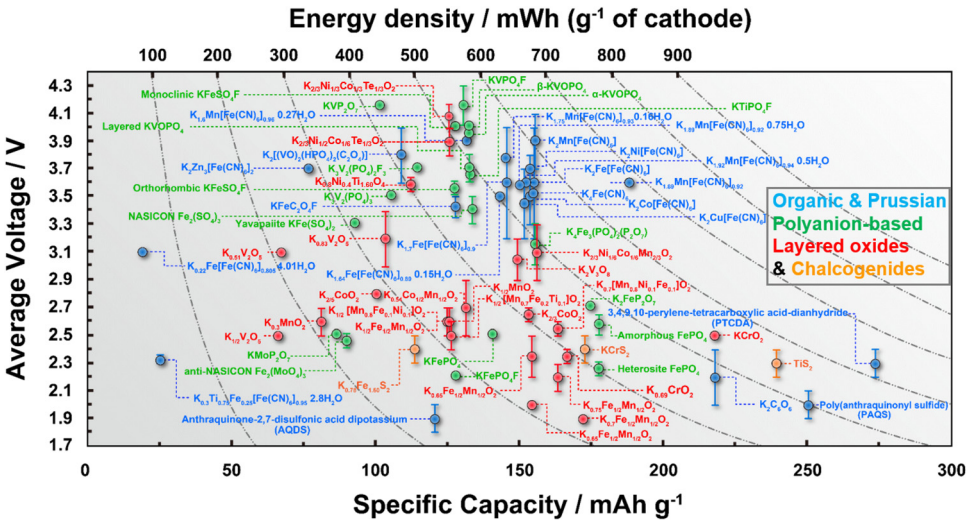

Fig. 6 Ragone plots of representative cathode materials for potassium ion batteries. Figure adapted from ref. 114 with permission.

Both L and L' are typically redox-active, and the fraction of $[L'(CN)_6]$ vacancies is denoted as b. By selecting different combinations of L and L', along with the concentration of interstitial potassium ions, the electrochemistry of Prussian analogues can be tailored for various performance metrics. The structure of a representative hexacyanoferrate, such as $K_2MnFe(CN)_6$, is shown in Fig. 7a, demonstrating an open channel structural framework where Fe and Mn are coordinated with C and N, respectively. The open 3D framework structure of Prussian analogues facilitates the easy diffusion of large K-ions, resulting in fast rate capabilities. These compounds have drawn attention owing to their scalable synthesis, high redox potential, and high theoretical capacity. For instance, $K_2FeFe(CN)_6$ exhibits a theoretical capacity of 155 mA h g^{-1}, based on the following two-electron reactions:

$$K_2Fe^{2+}[Fe^{2+}(CN)_6] \leftrightarrow KFe^{3+}[Fe^{2+}(CN)_6] + K^+ + e^-, \quad (1a)$$

$$KFe^{3+}[Fe^{2+}(CN)_6] \leftrightarrow Fe^{3+}[Fe^{3+}(CN)_6] + K^+ + e^-. \quad (1b)$$

A significant majority of Prussian analogues, such as $K_2MnFe(CN)_6$,[115] $K_2FeFe(CN)_6$,[24,26,115–118] $K_2CoFe(CN)_6$,[24] $K_2NiFe(CN)_6$,[24,119] $K_4Fe(CN)_6$,[120] and others, demonstrate notably high voltages, reaching up to 4 V. These voltages surpass those achieved by their lithium- and sodium-containing counterparts, such as $Li_2MnFe(CN)_6$, $Na_2MnFe(CN)_6$, $Li_2FeFe(CN)_6$ and $Na_2FeFe(CN)_6$ (Fig. 7b).[121–125] Additionally, Prussian blue analogues exhibit theoretically high gravimetric capacities, as depicted in Fig. 6, which have been experimentally realised. Consequently, Prussian analogues hold immense promise as cathode materials, particularly for high-energy-density KIBs. $K_2Mn[Fe(CN)_6]$ and $K_2Fe[Fe(CN)_6]$ demonstrate remarkable electrochemical performance within the Prussian analogues (as shown in Fig. 7c–f). This is attributed to the elevated Mn^{3+}/Mn^{2+} redox potential, which contributes to the superior characteristics of $K_2Mn[Fe(CN)_6]$ and its related derivatives. These materials showcase impressive capacities, exceeding 130 mA h g^{-1}, and maintain high average discharge voltages in the range of 3.8–3.9 V *versus* K/K^+. Consequently, they exhibit a relatively high energy density comparable to conventional cathode materials for lithium-ion batteries, such as $LiCoO_2$. However, it should be noted that the presence of high-spin Mn^{3+} (which is Jahn–Teller active) in $K_2Mn[Fe(CN)_6]$ introduces structural distortions during successive K^+ extraction/insertion cycles. This phenomenon results in $K_2Mn[Fe(CN)_6]$ experiencing multiple phase transitions, as evidenced by the following transformations: $K_2Mn^{2+}[Fe^{2+}(CN)_6]$ (monoclinic phase) ↔ $KMn^{2+}[Fe^{3+}(CN)_6]$ (cubic phase) ↔ $Mn^{3+}[Fe^{3+}(CN)_6]$ (tetragonal phase).[42] These structural changes compromise the cyclability of the material. In contrast, $K_2Fe[Fe(CN)_6]$ and its related derivatives, characterised by high-spin Fe^{2+} and low-spin Fe^{3+}, exhibit minimal Jahn–Teller distortion. As a consequence, they display robust cycling stability, which is highly desirable for practical applications.

Further advantages of Prussian blue analogues include facile synthesis, non-toxicity, and rapid rate capability.[42] Moreover, stable electrochemical performance in non-aqueous electrolytes can be achieved with Prussian analogues, provided that their water content, defects, and particle morphologies are carefully controlled.

However, similar to organic compounds (discussed subsequently), Prussian analogues also exhibit low material densities, typically below 2 g cm^{-3}, which significantly limits their achievable volumetric capacity. Whilst improving their volumetric capacities presents challenges, Prussian analogues, along with organic compounds, may find valuable applications in energy storage where volumetric energy density is of lesser importance. Furthermore, a significant scholarly effort is currently dedicated to addressing a dual set of concerns: water and $[Fe(CN)_6]^{4-}$ vacancies. Whilst the intricate role of water in the electrochemical performance of Prussian analogues is well acknowledged, $[Fe(CN)_6]^{4-}$ vacancies are believed to exert a deleterious impact on their maximal capacity and structural integrity. This is attributed to their reduction of potassium

© 2024 The Author(s). Published by the Royal Society of Chemistry

Open Access Article. Published on 04 dicembre 2023. Downloaded on 11/06/2026 17:40:22.
This article is licensed under a Creative Commons Attribution-NonCommercial 3.0 Unported Licence.

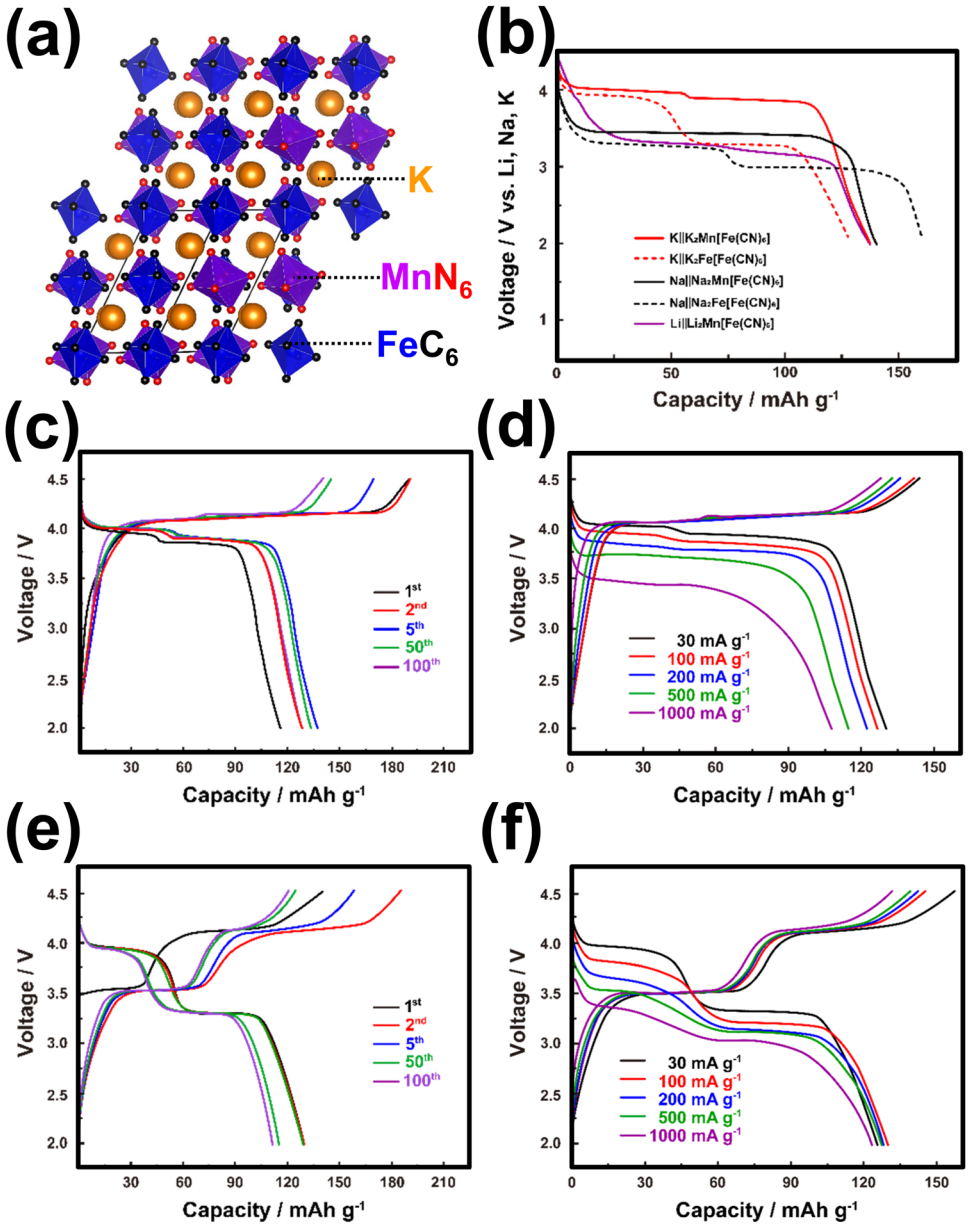

Fig. 7 (a) Crystal structural framework of $K_2MnFe(CN)_6$. (b) Voltage comparison of Prussian analogues when cycled in K, Na and Li half-cells. (c) Voltage-capacity profiles of $K_2MnFe(CN)_6$ and (d) corresponding rate performance. (e) Voltage-capacity profiles of $K_2FeFe(CN)_6$ and (f) corresponding rate performance. Figure (b) reproduced with permission from ref. 42. Copyright 2020 American Chemical Society. Figures (c)–(f) reproduced with permission from ref. 115. Copyright 2017 Royal Society of Chemistry.

occlusion capacity and the availability of redox-active Fe^{2+}. To date, the most outstanding performers amongst Prussian blue cathode analogues are those characterised by particles on the nanometric scale (nanoparticles), coupled with minimised $[Fe(CN)_6]^{4-}$ vacancies.[126]

On a different note, the safety considerations, encompassing aspects such as toxicity and thermal stability, remain inadequately understood. It can be contended that significant thermal runaways and the liberation of O_2 gas are unlikely to occur in the utilisation of Prussian blue analogues (such as $K_2MnFe(CN)_6$) within large-scale battery configurations, given their sole incorporation of cyanide ligands. Nonetheless, the decomposition of Prussian blue analogues does lead to the formation of cyanogen and hydrogen cyanide as byproducts.[126] Therefore, a more comprehensive inquiry into their safety and thermal stability becomes imperative.

2.2 Organic compounds

Organic-based cathode materials have attracted substantial interest due to their cost-effectiveness and environmentally friendly nature.[42,138–140] These materials consist of Earth-abundant elements, such as hydrogen, carbon, oxygen, and sulphur, which have a minimal environmental impact.[139] Moreover, the relatively low atomic weight of the constituent

Open Access Article. Published on 04 dicembre 2023. Downloaded on 11/06/2026 17:40:22.
This article is licensed under a Creative Commons Attribution-NonCommercial 3.0 Unported Licence.

elements bestows organic moieties with theoretically high gravimetric capacities. Additionally, organic compounds possess flexible molecular structures, enabling them to easily accommodate the facile and reversible insertion/extraction of large potassium-ions, thus facilitating fast potassium-ion kinetics.[141] Furthermore, the tunability of organic molecules allows for easy functionalisation to adjust their redox electrochemistry, making them versatile for various battery applications. Furthermore, the capability of reversibly inserting/extracting not only cations but also anions in organic molecules extends their potential applications to other high-voltage energy storage systems, such as potassium dual-ion batteries.[134]

A diverse array of organic compounds has been systematically designed and effectively demonstrated to enable the reversible insertion/extraction of K-ions, showcasing considerably higher capacities when compared to cathode materials like layered sulphides, layered oxides, polyanion-based compounds, and Prussian analogues. Organic compounds, including poly(anthraquinonyl sulphide),[21] perylene-3,4,9,10-tetracarboxylic dianhydride, poly(pentacenetetrone sulphide),[127] *etc.*,[141,142] have been extensively investigated as high-capacity cathode materials, showing promise as contenders for flexible KIBs with stable cycle performance. However, most reported organic materials have low average voltages, typically below 3 V, leading to reduced specific energy densities. Imides, anhydrides, quinones, and pyrazinyl compounds are pursued for enabling K^+ insertion/extraction through n-type reactions (Fig. 8). These materials accept electrons from electrolytes whilst facilitating K^+ cation insertion. However, their n-type redox reactions usually occur at voltages below 3 V, compromising the energy densities of KIBs. To enhance electrochemical performance, molecular fine-tuning is considered to elevate the voltages of organic moieties that undergo n-type redox reactions. It is worth noting that not all organic electrode materials solely undergo K^+ insertion/extraction through n-type redox reactions.

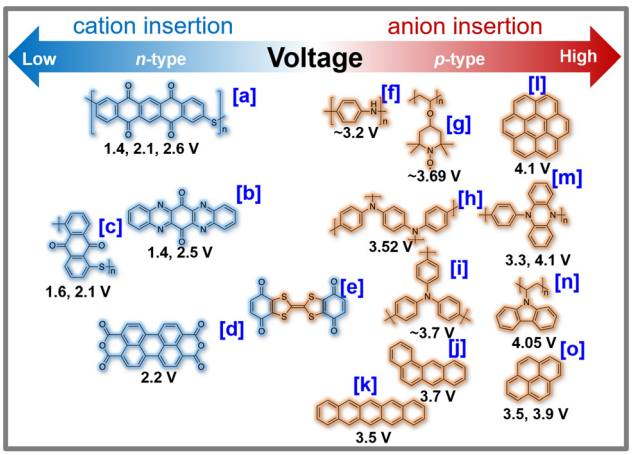

Fig. 8 Voltage attained from representative organic cathode materials for potassium-ion batteries. For the sake of clarity, we hereby present the chemical names of each organic moiety as follows. [a] PPTS (poly(pentacenetetrone sulphide)),[127] [b] TAPQ (5,7,12,14-tetraaza-6,13-pentacenequinone),[128] [c] PAQS (poly(anthraquinonyl sulphide)),[21] [d] PTCDA (3,4,9,10-perylene-tetracarboxylic acid dianhydride),[23] [e] QTTFQ ((2,3)-(6,7)-bis(1,4-dioxo-1,4-dihydrobenzo)tetrathiafulvalene),[129] [f] PANI (polyaniline),[130] [g] PTMA (poly(2,2,6,6-tetramethylpiperidinyloxy methacrylate)),[131,132] [h] PDPPD (poly(*N*,*N*′-diphenyl-*p*-phenylenediamine)),[133] [i] PTPAn (polytriphenylamine),[134] [j] *p*-DPPZ (poly(*N*-phenyl-5,10-dihydrophenazine)),[135] and [k] PVK (poly(*N*-vinylcarbazole)).[136] Figures reproduced with permission from ref. 137. Copyright 2021 Royal Society of Chemistry.

Other organic materials can exhibit high voltages through p-type reactions, losing electrons alongside anion insertion/extraction during battery operations. For example, conductive polymers[147,148] like polyaniline and polypyrrole undergo p-type reactions, leading to higher voltages compared to organic materials that undergo n-type redox reactions. Amine-derived polymers (such as poly(*N*,*N*′-diphenyl-*p*-phenylenediamine) (PDPPD), polytriphenylamine (PTPA), poly(*N*-phenyl-5,10-dihydrophenazine) (*p*-DPPZ), *etc.*) exhibit significant potential as viable organic cathode materials, owing to their inherent capacity to potentially yield high specific capacities, coupled with favourable discharge potentials approximating ~4 V, high (dis)charging rates, and good cyclability. Fig. 9 illustrates the electrochemical performance of polyarylamine poly(*N*-phenyl-5,10-dihydrophenazine) utilising a meticulously tailored electrolyte composition, resulting in the attainment of exemplary performance parameters.[135] Notably, polyarylamine poly(*N*-phenyl-5,10-dihydrophenazine) exhibits high power and energy density concomitant with good cyclability, thereby establishing crucial foundational criteria warranting contemplation for its prospective practical applications. Polycyclic aromatic hydrocarbons (Fig. 10) have also been extensively investigated for their p-type reactions and show promise as high-voltage organic cathode materials for potassium dual-ion batteries. In fact, organic compounds such as coronene (Fig. 11a), polyaniline, *etc.*, which function *via* the insertion of anions (*e.g.*, ClO_4^-, PF_6^-, FSI^-, $TFSI^-$, *etc.*), demonstrate voltages reaching 4 V, positioning them as high-voltage cathode candidates for potassium dual-ion batteries. Furthermore, the abundance of polycyclic aromatic hydrocarbons, exemplified by compounds like coronene,[137] and their utilisation in the scalable synthesis of carbonaceous anode materials, such as graphite, amplify the feasibility of high-voltage dual-ion batteries incorporating polycyclic aromatic hydrocarbons as cathodes coupled with graphite anodes. This innovative approach presents a promising avenue for the development of sustainable energy storage systems exclusively based on hydrocarbons, ushering in a greener and more environmentally conscious energy landscape.

A significant drawback associated with the utilisation of a majority of organic compounds is their tendency to undergo dissolution into the electrolyte, necessitating the careful selection of compatible electrolytes (such as highly concentrated electrolytes or ionic liquids) and the adoption of special synthetic routes (*e.g.*, oligomerisation or polymerisation).[139] Furthermore, a majority of organic compounds tend to exhibit low electronic conductivity. To address this issue, nanosizing of organic compounds and the use of special synthetic routes

© 2024 The Author(s). Published by the Royal Society of Chemistry

Open Access Article. Published on 04 dicembre 2023. Downloaded on 11/06/2026 17:40:22.
This article is licensed under a Creative Commons Attribution-NonCommercial 3.0 Unported Licence.

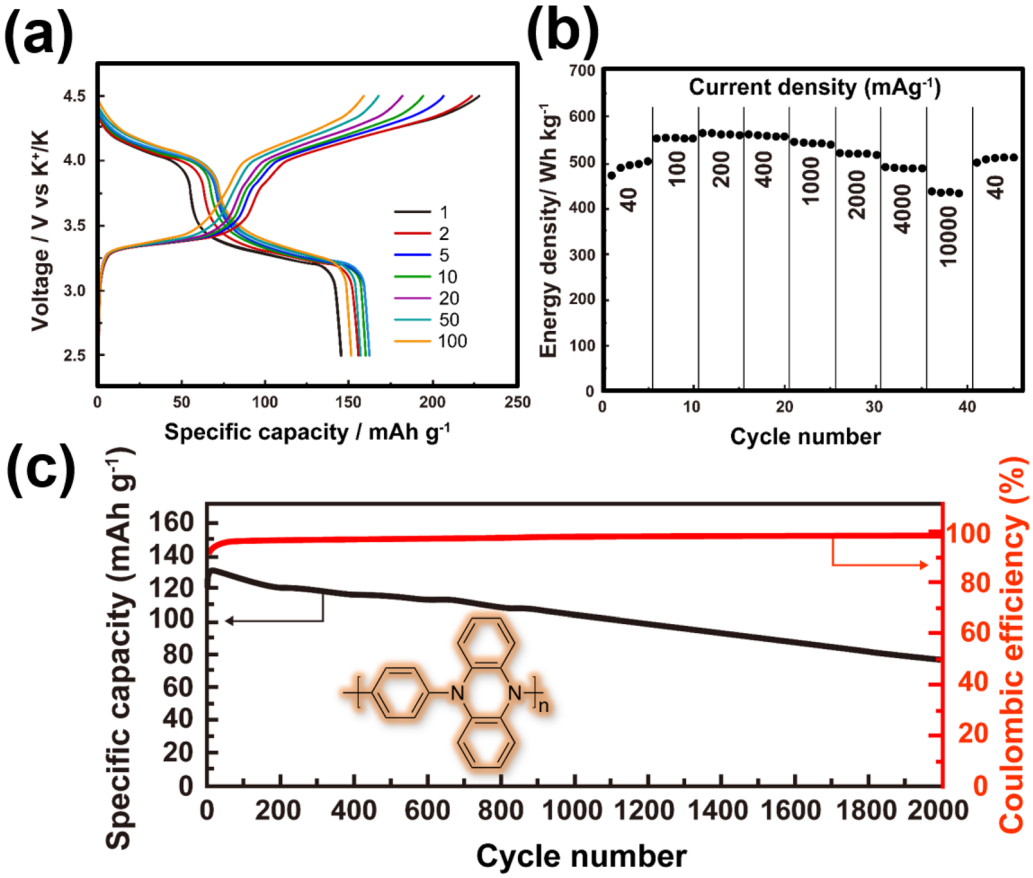

Fig. 9 Electrochemical performance of poly(*N*-phenyl-5,10-dihydrophenazine) as a high-voltage and high-capacity cathode material for KIBs. (a) Voltage-capacity profiles at a current density of 200 mA g^{-1}. The theoretical capacity for poly(*N*-phenyl-5,10-dihydrophenazine) is approximately 209 mA h g^{-1}. (b) Energy density at various current densities. (c) Cycle performance at a current density of 2 A g^{-1}. A highly concentrated electrolyte entailing 2.2 M KPF_6 in diglyme solvent was used in a potassium half-cell setup. Figures reproduced and adapted with permission from ref. 135. Copyright 2019 American Chemical Society.

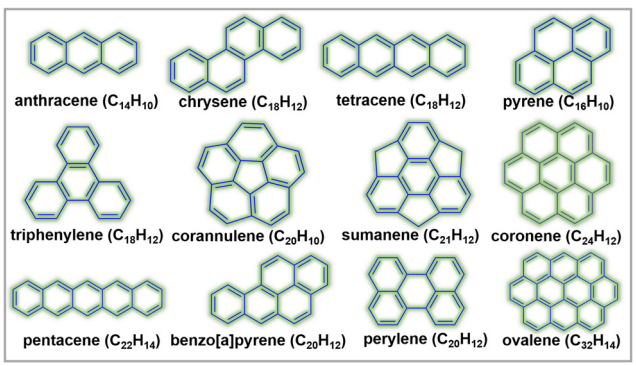

Fig. 10 Representative polycyclic aromatic hydrocarbons (including supertriphenylene,[143] superphenalene[143,144] and circumcoronene[145,146]), which can operate at high voltages *via* the insertion/extraction of anions such as PF_6^-, BF_4^-, FSI^-, $TFSI^-$, *etc.*

(*e.g.*, *in situ* polymerisation) can be envisaged to enhance their electronic conductivity.[139] Additionally, hybrid materials based on the fusion of inorganic and organic components, such as $K_2[(VO)_2(HPO_4)_2(C_2O_4)]$[149] and $K_2[(VOHPO_4)_2(C_2O_4)]$[150] metal–organic phosphates, have demonstrated not only high voltages (reaching up to 4 V) but also fast rate capabilities. Despite the fact that the theoretical capacities of these hybrid materials may be lower than those of pure organic compounds, their exceptional fast rate capabilities and high voltage render them as ideal cathode candidates for the development of high-performance 4 V-class KIBs. However, it is important to note that, similar to Prussian analogues, organic compounds also share the intrinsic drawback of having low tap density (material density), significantly impacting their volumetric energy densities.

Nonetheless, opportunities for improvement persist, particularly in the pursuit of organic molecules with precisely tailored structures that can be engineered into high-capacity cathode materials. An example of such promise (*albeit* necessitating caution in handling) appears to lie in trinitroaromatic salts, such as $C_6H_2(NO_2)_3OK$ which present as nitro-rich organic cathode materials with elevated discharge capacity and voltage due to the strong delocalisation effect between aromatic rings and $-NO_2$.[151] Theoretical calculations predict that $C_6H_2(NO_2)_3OK$ (potassium picrate) undergoes a 6-electron charge-transfer process, resulting in a high discharge capacity of 606 mA h g^{-1}.[151] Octahydroxytetraazopentacene, with a

Open Access Article. Published on 04 dicembre 2023. Downloaded on 11/06/2026 17:40:22.
This article is licensed under a Creative Commons Attribution-NonCommercial 3.0 Unported Licence.

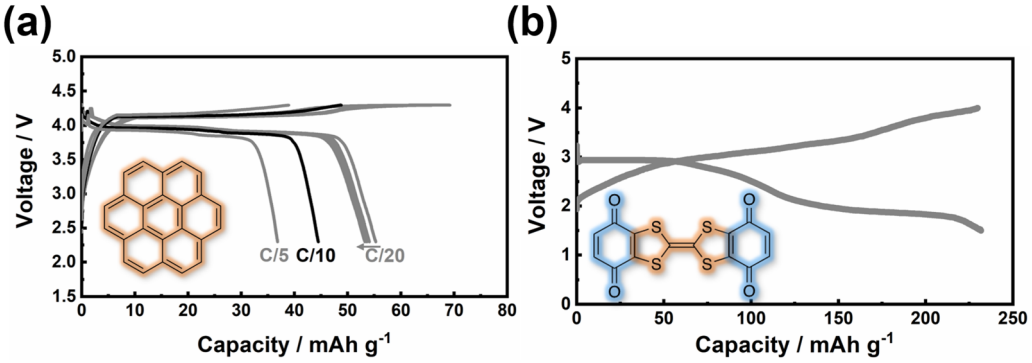

Fig. 11 Electrochemical performance of (a) p-type coronene ($C_{24}H_{12}$) and (b) bipolar (2,3)-(6,7)-bis(1,4-dioxo-1,4-dihydrobenzo)tetrathiafulvalene (QTTFQ) as cathode materials for potassium-ion batteries. The theoretical capacity for $C_{24}H_{12}$ and QTTFQ is, respectively, 88 mA h g^{-1} and 441 mA h g^{-1}. A current density of 40 mA g^{-1} was used in (b). Figures reproduced and adapted from ref. 129 and 137 with permission. Copyright 2019 and 2021 Royal Society of Chemistry.

theoretical capacity of close to 520 mA h g^{-1}, has been experimentally reported as a high-capacity organic material.[152] Additionally, bipolar organic molecules like tetrathiafulvalene, which enable reversible insertion/extraction of both anions and K^+ (*e.g.*, $TFSI^-$, FSI^-, PF_6^-, *etc.*), can be further explored as high-capacity materials. Fig. 11b shows the electrochemical performance of (2,3)-(6,7)-bis(1,4-dioxo-1,4-dihydrobenzo)tetrathiafulvalene (QTTFQ) which operates *via* both the p-type and n-type reactions to attain high capacity.[129] Moreover, a wide range of organic materials, including N-containing heteroatomic compounds, organosulphur compounds, quinone/phenoxide derivatives, carbonyl compounds, polymeric arylamines, and conductive polymers, hold potential for investigation to design cathode materials with both high capacity and high voltage.[139,153–157] Furthermore, the pursuit of organic molecules with high rate capability and electronic conductivity can be anticipated, for instance, through the use of (i) conjugated polymer poly(quinones) with electron-withdrawing groups and (ii) π-conjugated aromatic compounds comprising heteroatoms (such as S, N, and O) with lone electron pairs.

2.3 Polyanion-based compounds

Polyanion-based materials share a similar open three-dimensional (3D) framework with Prussian analogues, characterised by metalloid or non-metal atoms coordinated with oxygen atoms to form polyhedral units.[158] The polyhedral units embody a composition of $(AO_4)^{n-}$, with *A* representing elements such as Si, S, P, Ge, As, B, Mo, W, *etc.*, and *n* varying from 2 to higher values. These $(AO_4)^{n-}$ polyhedra intricately interlink with polyhedral units of transition metal atoms $(LO_a)^{n-}$, where '*a*' represents an integer such as 4, 5, 6, and so forth, and '*L*' denotes a transition metal like Ni, Co, Mn, Fe, *etc.* This arrangement generates voids within the structure, which serve as sites for accommodating or facilitating the movement of potassium ions. The 3D arrangement of K-ions with polyanion units reduces the effective K^+–K^+ repulsion strength, leading to an elevated working voltage.[159] Polyanion-based compounds have undergone extensive investigation in both sodium and lithium-ion batteries, and their material compositions have served as a basis for designing polyanion cathode materials for KIBs. Fig. 12 shows crystal structures of representative polyanion cathode materials for potassium-ion batteries. The inherent open structure of polyanion-based compounds facilitates rapid diffusion of K^+ ions and effectively accommodates the significant volume changes that occur during the insertion and extraction of large K-ions. Moreover, polyanion-based materials showcase remarkable thermal stability, making them exceptionally suitable as cathode materials for a wide range of battery applications, spanning from intermediate to high-temperature operations. Notably, they demonstrate theoretically high voltages, with some exceeding 4 V, along with high gravimetric capacities. The high voltage is attributed to a reduction in the covalency of the *A*–O bonds, a consequence of the pronounced covalent nature of the *L*–O bonds. This phenomenon (or what is referred to as 'inductive effect')[160] is contingent upon the electronegativity of the transition metal '*L*', leading to an augmentation in the redox voltage of the transition metal *L* ions. Additionally, their material density is relatively higher, generally surpassing 2.5 g cm^{-3} compared to organic compounds and Prussian analogues.

Polyanion-based frameworks, exemplified by $KFeSO_4F$,[12–17] $KCuSO_4F$, $KVPO_4F$,[18,19] $KVOPO_4$,[18] amongst others, boast higher material densities, typically ranging from 2.5 to 3.5 g cm^{-3} and exhibit high voltages, reaching up to 4 V and even surpassing 4 V in KIBs. Fig. 12 shows crystal structures of representative polyanion cathode materials for KIBs. Their synthesis protocols involve the use of cost-effective salt precursors and appear to be relatively straightforward. For instance, $KFeSO_4F$ and related compositions can be synthesised *via* a solid-state reaction at intermediate temperatures (300–400 °C), yielding various polymorphs: KF + $FeSO_4F$ → $KFeSO_4F$.[17] $KVPO_4F$ can be synthesised at slightly higher temperatures through the following reaction: KF + VPO_4 → $KVPO_4F$.[159]

$KVPO_4F$, characterised by its specific crystal structure with an open framework of $KTiOPO_4$-type (Fig. 12), allowing for rapid diffusion of K^+ ions, has emerged as a widely investigated polyanion-based cathode material. It exhibits the ability to reversibly release nearly one K^+ per formula unit, equating to

© 2024 The Author(s). Published by the Royal Society of Chemistry

Open Access Article. Published on 04 dicembre 2023. Downloaded on 11/06/2026 17:40:22.
This article is licensed under a Creative Commons Attribution-NonCommercial 3.0 Unported Licence.

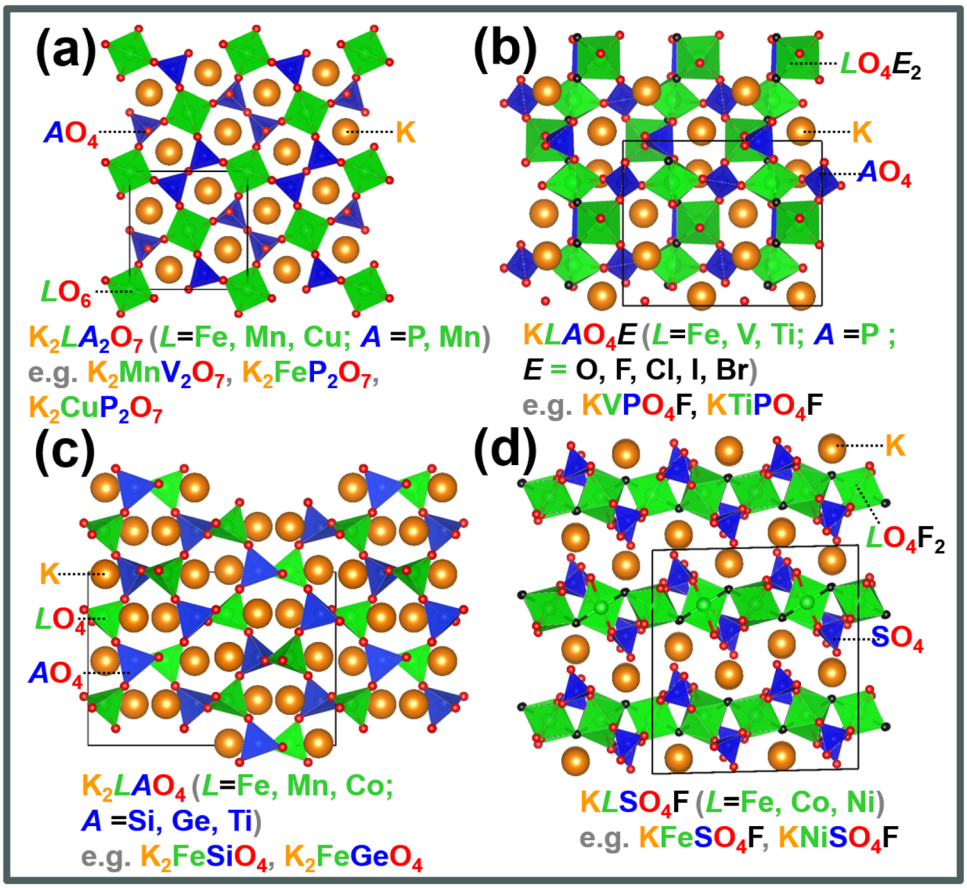

Fig. 12 Selected crystal structural frameworks of polyanion-based compounds. (a) Pyrophosphates and pyrovanadates, (b) $KTiOPO_4$ and derivative compounds, (c) cristoballite-type orthosilicates, orthogermanates and orthotitanates, and (d) fluorosulphates. Unit cells are highlighted in black boxes.

approximately 131 mA h g^{-1}, at an average potential of 4.02–4.3 V.[18,159] Consequently, $KVPO_4F$ offers a material-level specific energy density of 527–563 W h kg^{-1}, comparable to that of $LiFePO_4$, a widely used polyanion-based cathode material for LIBs, which presents an energy density of approximately ~580 W h kg^{-1}. Related $KVPO_4F$ compositions such as ($KVPO_4O$ ($KVOPO_4$), $KVPO_4Cl$, *etc.*) display high redox voltages (Fig. 13). Fig. 14a and b show the voltage-capacity profiles of $KVOPO_4$ and $KVPO_4F$, respectively. The average voltages for $KVPO_4F$ and $KVOPO_4$ are reported to be 3.95 V and 4.02 V respectively, ascribed to the V^{4+}/V^{5+} and V^{3+}/V^{4+} redox.[18] An appreciable irreversible capacity is observed during the initial charging process of $KVPO_4F$ and $KVOPO_4$ (Fig. 14a and b), which has been attributed to the substantial decomposition of the electrolyte solution.[18]

Researchers have been striving to narrow the energy density gap between $KVPO_4F$ and $LiFePO_4$ by exploring compounds such as $K_3V_2(PO_4)_2F_3$,[161] $K_3V_2(PO_4)_3$,[162] $K_3V_2O_2(PO_4)_2F$,[163] *etc.*,[164–166] which exhibit more than one K^+ per formula unit as high-capacity polyanion-based materials. Notably, the feasibility of extracting more than two K^+ per formula unit in $K_3V_2(PO_4)_2F_3$ has been demonstrated by harnessing the electrochemical activity of the third potassium in $K_3V_2(PO_4)_2F_3$, leading to the formation of $K_xV_2(PO_4)_2F_3$.[161] Vanadium-based polyanion compounds are poised to attract significant interest in the forthcoming years due to vanadium's capability to adopt various oxidation states, with oxidation states of 3+, 4+, and 5+ (V^{3+}, V^{4+} and V^{5+}) being particularly common in battery materials. This unique property enables vanadium to engage in multi-redox reactions, facilitating the reversible extraction/insertion of more than one K^+ ion, as demonstrated in compositions like $K_6V_2(PO_4)_4$.[167] The Ragone plot in Fig. 6 showcases the average voltages achieved by various polyanion-based cathode compounds reported thus far for KIBs. Vanadium-based orthophosphates (*e.g.*, $K_3V_3(PO_4)_4$,[168] $K_3V_3(PO_4)_4H_2O$,[169] $K_3V_2(PO_4)_3$[162,170]), fluorophosphates ($KV_{0.5}Ti_{0.5}PO_4F$,[171] $KVPO_4F$,[18,159] $K_{1.5}VOPO_4F_{0.5}$,[172] $K_3V_2O_2(PO_4)_2F$,[163] $KVPO_4F_{0.5}O_{0.5}$[173]), $K_3(VO)(HV_2O_3)(PO_4)_2(HPO_4)$,[174] oxyphosphates ($KVOPO_4$),[18,175] and pyrophosphates (KVP_2O_7)[176,177] exhibit high voltages, reaching 4 V and even beyond, whilst maintaining fast rate capabilities and good cyclability. Mixed polyanion compounds, such as $K_6(VO)_2(V_2O_3)_2(PO_4)_4(P_2O_7)$,[178,179] also exhibit high voltages surpassing 4 V.

Titanium-based fluorophosphates like $KTiPO_4F$ exhibit voltages of 3.6–3.7 V (Fig. 14c), which is remarkably high for titanium redox transitions (Ti^{3+}/Ti^{4+}), attributed to the $KTiOPO_4$-type framework it adopts.[180] It should be noted here that sustaining the Ti^{3+} oxidation state necessitates the

Open Access Article. Published on 04 dicembre 2023. Downloaded on 11/06/2026 17:40:22.
This article is licensed under a Creative Commons Attribution-NonCommercial 3.0 Unported Licence.

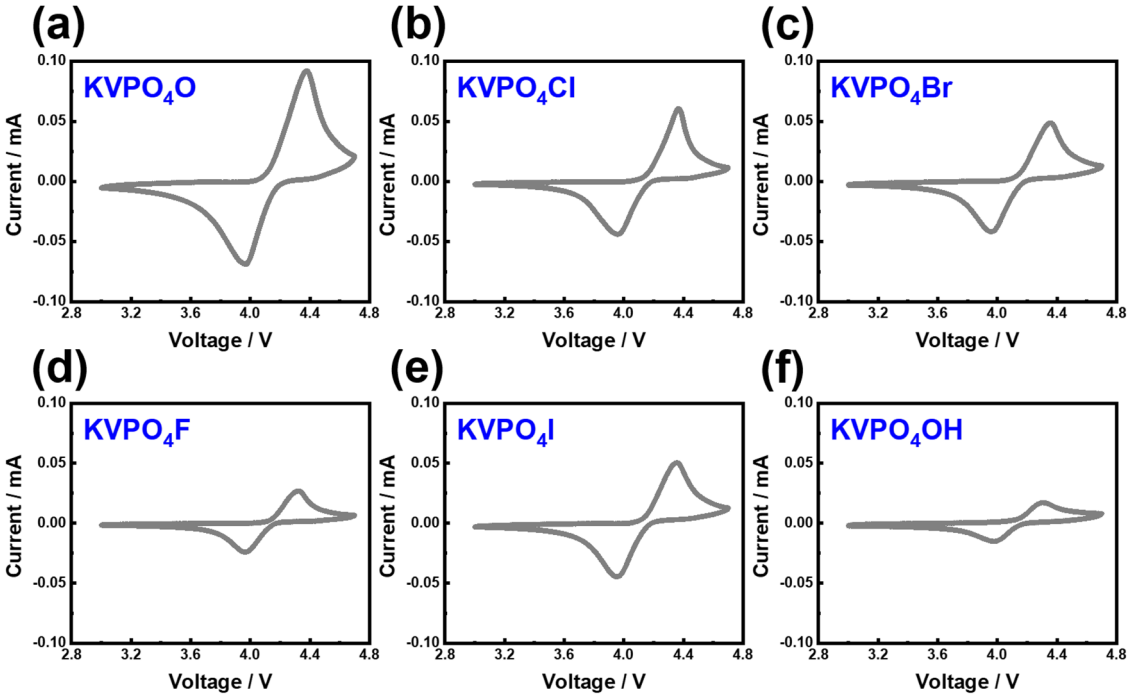

Fig. 13 Electrochemical performance of representative potassium-based vanadium phosphates showing high redox voltages. Cyclic voltammograms of (a) $KVPO_4$, (b) $KVPO_4Cl$, (c) $KVPO_4Br$, (d) $KVPO_4F$, (e) $KVPO_4I$ and (f) $KVPO_4OH$. The measurements were taken at a scanning speed of 0.1 mV s^{-1} at a cut-off voltage of 3.0–4.6 V. Potassium half-cells were used with 0.5 M KTFSI in $Pyr_{13}TFSI$ ionic liquid as the electrolyte. Figures reproduced and adapted from ref. 114 with permission.

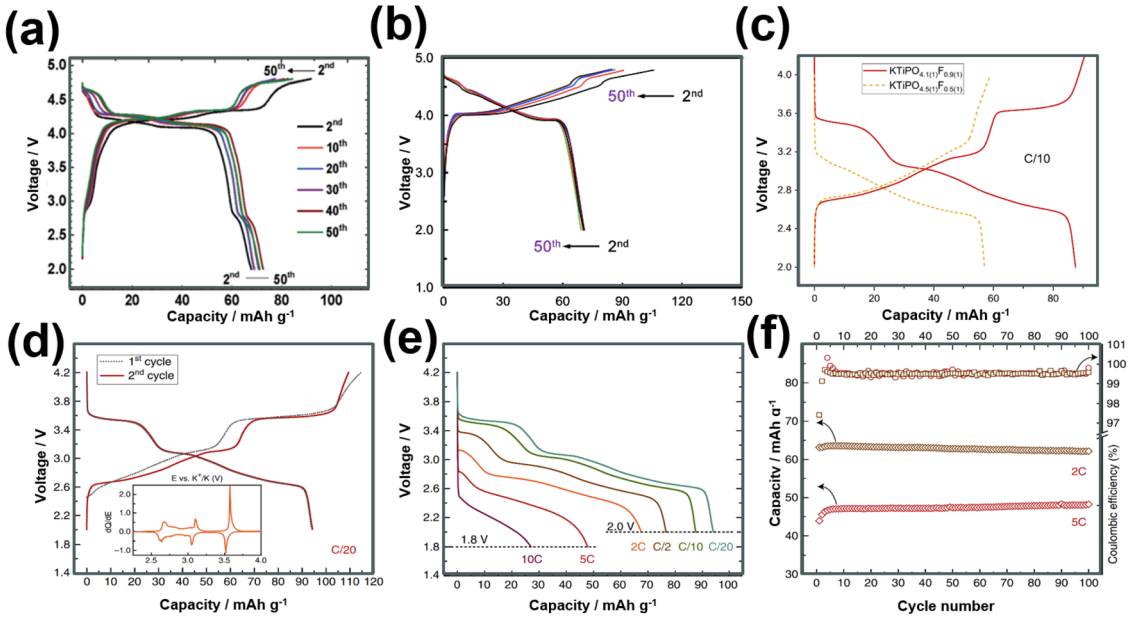

Fig. 14 Voltage-capacity profiles of (a) $KVPO_4$ (α-polymorph) and (b) $KVPO_4F$. The theoretical capacity of $KVPO_4$ and $KVPO_4F$ is 133.3 mA h g^{-1} and 131.4 mA h g^{-1}, respectively. (c) Voltage profile comparisons of $KTiPO_4F$ and $KTiPO_{4.5}F_{0.5}$. (d) Voltage profiles of $KTiPO_4F$ at C/20 rate, (e) corresponding rate performance and (f) cycle performance at various current densities. The theoretical capacity of $KTiPO_4F$ and $KTiPO_{4.5}F_{0.5}$ is 133.4 mA h g^{-1} and 134.4 mA h g^{-1}, respectively. Figures (a) and (b) reproduced from ref. 18 with permission. Copyright 2017 Royal Society of Chemistry. Figures (c), (d)–(f) reproduced with permission from ref. 180. Copyright 2020 Springer Nature.

maintenance of inert or reducing conditions at every stage encompassing synthesis and electrode material preparation of $KTiPO_4F$. Nonetheless, $KTiPO_4F$ demonstrates intricate voltage-capacity profiles, characterised by three distinct reversible

© 2024 The Author(s). Published by the Royal Society of Chemistry

Open Access Article. Published on 04 dicembre 2023. Downloaded on 11/06/2026 17:40:22.
This article is licensed under a Creative Commons Attribution-NonCommercial 3.0 Unported Licence.

processes at 3.6, 3.1, and 2.7 V (Fig. 14d), with all three processes exhibiting flat voltage profiles that indicate a biphasic transition. The utilisation of carbon-coated $KTiPO_4F$ has been experimentally validated to deliver a noteworthy capacity of 94 mA h g^{-1} (equivalent to the extraction of 0.8 K^+) whilst maintaining high cycle stability at a rate of C/20 along with good rate performance (Fig. 14e and f). This exceptional performance is attributed to the remarkably elevated potential for the Ti^{4+}/Ti^{3+} redox activity, which has been hypothesised to originate from a synergistic interplay between the material's structural attributes (*e.g.*, electrostatic interactions, vacancy/charge ordering) and chemical properties (*e.g.*, inductive effect) specific to the $KTiOPO_4$-type $KTiPO_4F$.[181,182] Such distinctive features position $KTiPO_4F$ as a promising high-energy-density cathode material candidate. Whilst the related Mn- and Fe-based compositions of the phosphates may show inferior voltages, with some (*e.g.*, $K_2FeP_2O_7$, $K_2MnP_2O_7$, *etc.*)[165] being deemed electrochemically inactive, their sulphate counterparts, such as $KFeSO_4F$, demonstrate high voltages (>3.5 V) with both good rate capabilities and cycle stability (Fig. 15), positioning them not only as cost-effective but also as high-voltage cathode candidates for sustainable and high-energy-density KIBs.

A significant challenge faced with polyanion-based compounds lies in their intrinsically low electronic conductivities. Addressing this limitation requires the incorporation of significant quantities of conductive materials, such as carbon, to fully harness and optimise their electrochemical performance. However, this practice can lead to reduced volumetric energy densities. Many polyanion-based cathode materials investigated by us and other research groups, such as langbeinite-type $K_2M_2(SO_4)_3$ (M = Cu, Co, Ni, Mn, Fe), $KM(PO_3)_3$, $K_2MV_2O_7$ (M = Mn, Co), $K_2MP_2O_7$,[165] KMP_2O_7 (M = Fe, Mn, Ti, Cr, V), $K_2VOP_2O_7$,[183] $KMPO_4$, $KMnVO_4$, fedotovite-type $K_2Cu_3O(SO_4)_3$,[184] $KFePO_4F$, $K_3Fe_2(PO_4)_3$, buetschliite-type $K_2Mn(SeO_3)_2$, yavapaiite-type $KFe(SO_4)_2$, $KFeGeO_4$, $KFeSiO_4$, amongst others, require both nanosizing and carbon nanocoating to fully exploit their electrochemical behaviour; otherwise, many of them may appear essentially 'electrochemically inactive' or behave as insulators. Nanosizing, carbon-coating, and doping have also been utilised to enhance the electronic conductivity of polyanion-based compounds such as $KFePO_4$,[185] $K_3V(PO_4)_2$,[186] $K_3V_2(PO_4)_3$,[162,187] $KFe_{0.95}Mg_{0.05}SO_4F$,[16] $K_{3-x}Rb_xV_2(PO_4)_3$ (x = 0.03, 0.05 and 0.07),[188] *etc.* As illustrated in Fig. 6, polyanionic compounds typically exhibit lower theoretical gravimetric capacities than Prussian

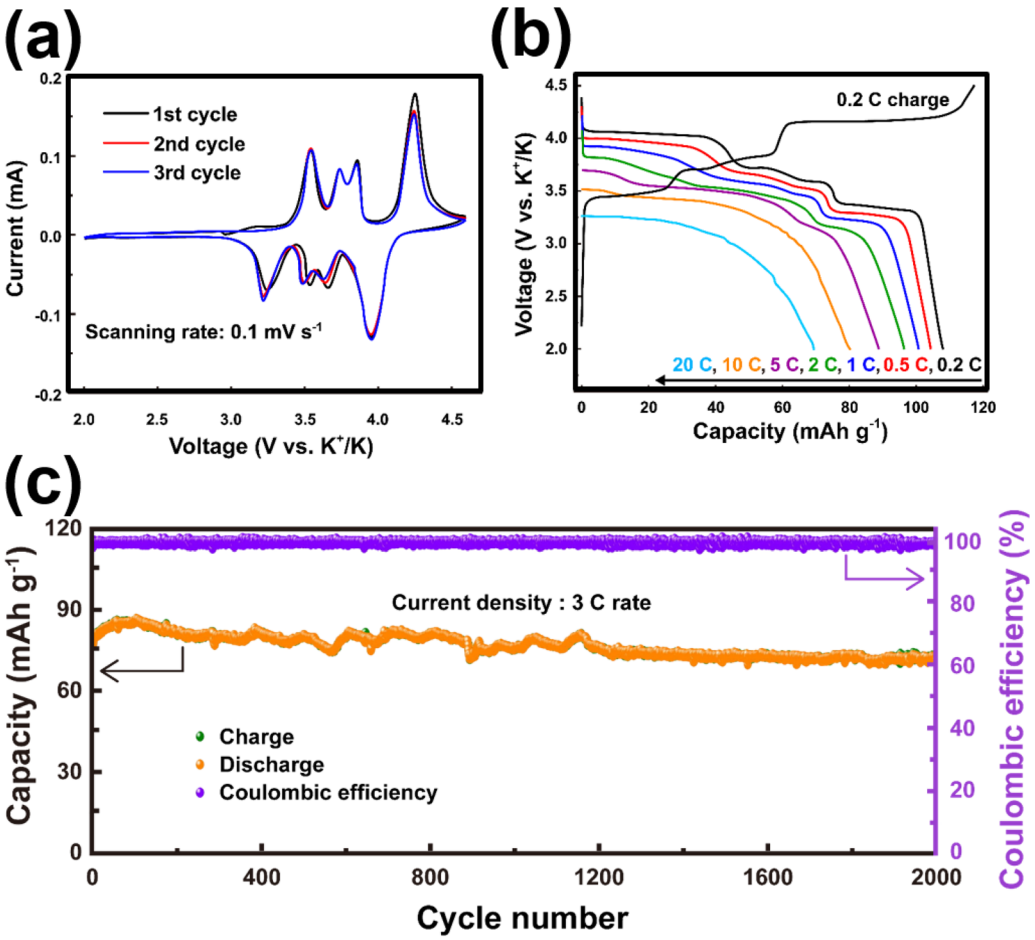

Fig. 15 Electrochemical performance of $KFeSO_4F$. (a) Cyclic voltammogram of $KFeSO_4F$ taken at a scanning rate of 0.1 mV s^{-1}. (b) Rate performance of $KFeSO_4F$ and (c) cycle performance at a current density commensurate to 3C. The theoretical capacity for $KFeSO_4F$ is 127.6 mA h g^{-1} (1C = 127.6 mA g^{-1}). Figures reproduced from ref. 14 with permission. Copyright 2022 Elsevier.

Open Access Article. Published on 04 dicembre 2023. Downloaded on 11/06/2026 17:40:22.
This article is licensed under a Creative Commons Attribution-NonCommercial 3.0 Unported Licence.

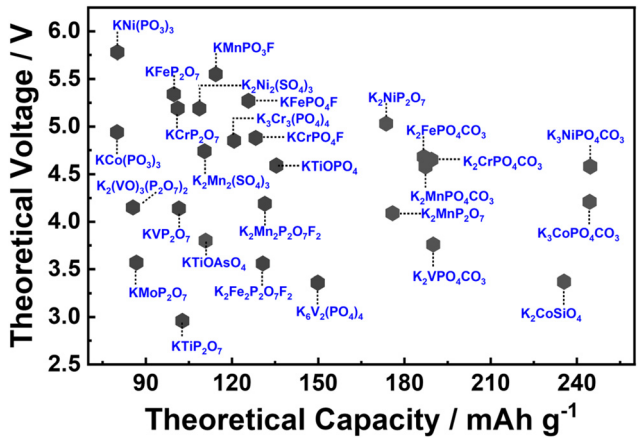

Fig. 16 Theoretical voltages calculated for polyanion compounds for potassium-ion batteries. Graph plotted based on the data derived from ref. 167, 176 and 189–192.

analogues, which may compromise their energy density. However, the high voltages demonstrated by polyanion-based compounds can potentially counterbalance their intrinsic low electronic conductivities. As a result, a careful material screening process becomes essential, with a focus on identifying polyanion-based compounds that exhibit not only high voltages (>4.5 V) but also high gravimetric capacities (>130 mA h g^{-1}). Fig. 16 showcases the projected voltages in polyanion cathode materials, underpinned by computational screening, alongside their corresponding theoretical capacities. The realm of theoretical computations unveils a plethora of polyanion compounds that manifest both high voltages and high theoretical capacities.[167,176,189–192] Additionally, electrochemical ion-exchange utilising sodium- or rubidium-based polyanion compounds can serve as another strategy for obtaining new potassium-based polyanion compounds with favourable electrochemical properties, as demonstrated in the design of $K_3V_2(PO_4)_2F_3$.[161]

Moreover, most polyanionic compounds tend to exhibit lower theoretical capacities compared to both Prussian blue analogues and organic compounds, primarily due to their heavy polyanion formula weights. Nonetheless, ample opportunities remain to explore high-capacity polyanion-based materials, such as pyrophosphates (*e.g.*, $K_2MnP_2O_7$,[165] $K_2FeP_2O_7$,[165] $K_2NiP_2O_7$, $K_2CoP_2O_7$, $K_2MnP_2O_7F_2$,[167] *etc.*), orthophosphates (*e.g.*, $K_6V_2(PO_4)_4$[167]), silicates (including various emerging slow-release fertilisers,[193,194] *e.g.*, K_2FeSiO_4 (Fig. 17a), K_2MnSiO_4, *etc.*), vanadates (*e.g.*, $K_2MnV_2O_7$,[195] $K_2CoV_2O_7$[196]), borates (*e.g.*, $K_2Fe_2B_2O_7$ (isostructural with $K_2Al_2B_2O_7$),[197,198] $KFeBO_3$, $KMnBO_3$, *etc.*), and sulphates (*e.g.*, $K_2Fe(SO_4)_2$), most of which involve two K^+ ions per formula unit, resulting in a K-to-transition metal content ratio of ≥ 2.

Iron-based polyanion compounds, exemplified by K_2FeSiO_4, exhibit significant theoretical capacities (Fig. 17b) and thus hold promise for integration into the composition of iron-based materials tailored for utilisation as high-energy-density cathode material systems (Fig. 17c). Whilst we acknowledge the apparent impracticality of vanadium-based polyanionic compounds due to vanadium's toxicity, it is worth noting that delving into unconventional vanadium-based materials can furnish valuable insights into maximising the potential of cathode materials for KIBs. Our preliminary exploration of the K_2O–V_2O_5–V_2O_4–SO_3 phase system (depicted in Fig. 17d)[199,200] has brought to light a suite of novel vanadium-based polyanion cathode materials, exemplified by compounds like $K_2VO(SO_4)_2$,[201] $KV(SO_4)_2$[202] and $V_2O_3(SO_4)_2$.[203] These materials exhibit noteworthy attributes, including high voltages (up to 4 V) and high theoretical capacities, opening vistas for further investigation. The lability of the polyanion moiety also contributes to the polymorphism exhibited by polyanionic compounds such as $KFeSO_4F$[17] and $K_2CuP_2O_7$,[204,205] leading to a rich variety of crystal structures with distinct electrochemical performance. Notably, polyanionic compounds offer a diverse array of crystal structures compared to Prussian analogues, thereby providing tunable electrochemistry that can be exploited to optimise both their volumetric energy densities and rate capabilities. Furthermore, the electrochemistry of polyanion compounds, such as pyrophosphates,[176] has revealed captivating optical characteristics. For instance, the extraction of potassium from compounds like $KMoP_2O_7$, KVP_2O_7, and $KTiP_2O_7$ induces noticeable colour shifts,[176] suggesting potential applications in electrochromic devices.

The broad class of fluorosulphates and fluorophosphates holds significant potential for further exploration. Preliminary investigations have already demonstrated the feasibility of designing new fluorosulphates through solid-state reactions involving inexpensive potassium salts, such as KCl, KBr, KI, K_2SO_4, KOH, and others. For instance, derivative compositions of new fluorosulphates and fluorophosphates can be designed *via* the following reactions at intermediate temperatures: $KA + FeSO_4 \rightarrow KFeSO_4A$ (A = Cl, Br, I, OH); $KA + NiSO_4 \rightarrow KNiSO_4A$ (A = Cl, Br, I, OH); $KA + CoSO_4 \rightarrow KCoSO_4A$ (A = Cl, Br, I, OH); $KA + NiSO_4 \rightarrow KNiSO_4A$ (A = Cl, Br, I, OH); $KA + FePO_4 \rightarrow KFePO_4A$ (A = Cl, Br, I, OH); $KA + VPO_4 \rightarrow KVPO_4A$ (A = Cl, Br, I, OH); $KA + VOSO_4 \rightarrow KVOSO_4A$ (A = F, Cl, Br, I, OH); $K_2SO_4 + VOSO_4 \rightarrow K_2VO(SO_4)_2$; $KF + VOSO_4 \rightarrow KVO(SO_4)F$. Additionally, oxyphosphates, such as $KVOPO_4$, can be synthesised through carbothermal reduction processes at intermediate temperatures: $K_2CO_3 + V^{5+}OPO_4 + C \rightarrow KV^{4+}OPO_4$.

Furthermore, the exploration of mixed polyanion compounds, replicating chemical compositions like $KFePO_4NO_3$,[206] $K_4Fe_3(PO_4)_2(P_2O_7)$,[207] $K_4[Mn_2Fe](PO_4)_2(P_2O_7)$,[208] $K_2M_3(SO_4)_3(OH)_2(H_2O)_2$ (M = Co, Fe), $KFe_3(SO_4)_2(OH)_6$,[209] $(K(Mo_2PO_6))(P_2O_7)_2$,[210] $K_3(VO)(V_2O_3)(PO_4)_2(HPO_4)$,[211] $K_3(VO)(HV_2O_3)(PO_4)_2(HPO_4)$,[211] $K_2Mn_3(VO_4)_2(CO_3)$,[212] *etc.*, presents an opportunity to further enhance the electrochemical performance of polyanion-based materials. The broad class of mixed polyanion compounds encompasses polyoxyanion groups such as PO_4–CO_3, C_2O_4–SO_4, PO_4–NO_3, SO_4–OH, PO_4–SO_4, SO_4–S_2O_3, BO_3–B_2O_5, PO_4–P_2O_7, and others,[213] offering ample room for exploration and optimisation. In addition, the exploration of high- and medium-entropy polyanion compounds (*e.g.*, $K_3Mn_{2/3}V_{2/3}Ti_{2/3}(PO_4)_3$) can provide a pathway for designing new polyanion frameworks with enhanced rate capabilities, as demonstrated for their Na-based analogues.[214]

© 2024 The Author(s). Published by the Royal Society of Chemistry

Open Access Article. Published on 04 dicembre 2023. Downloaded on 11/06/2026 17:40:22.
This article is licensed under a Creative Commons Attribution-NonCommercial 3.0 Unported Licence.

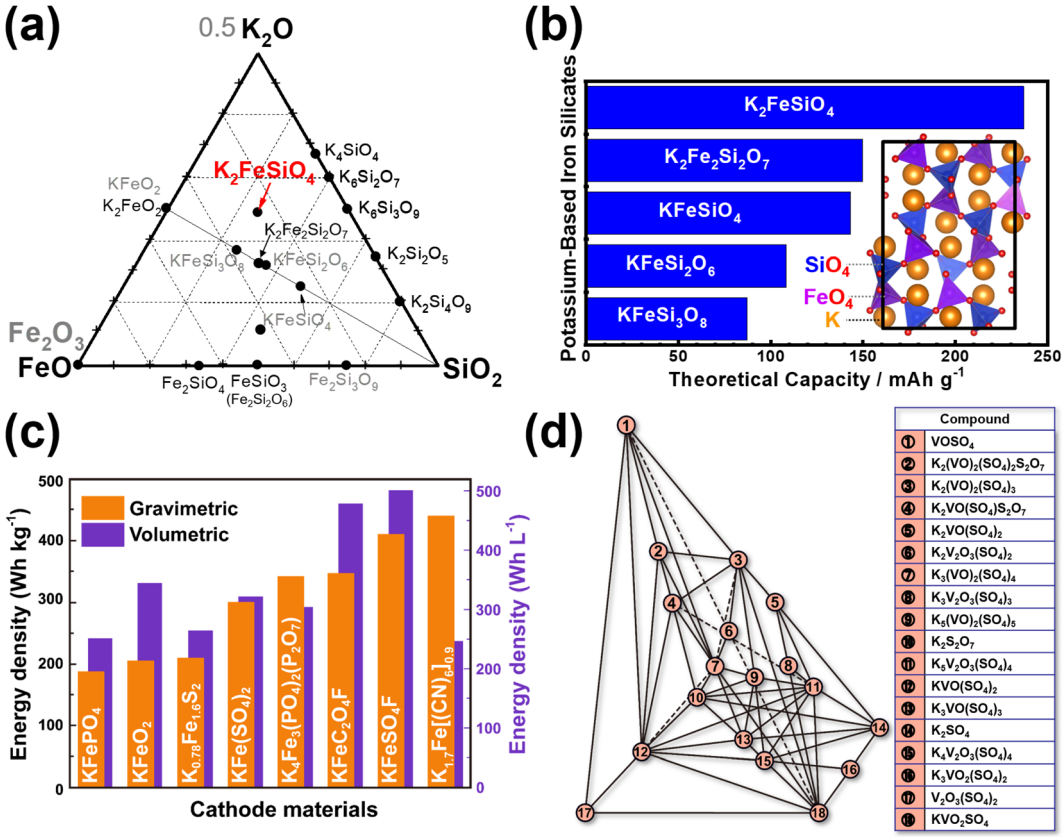

Fig. 17 Exploration of new polyanion-based cathode compound for potassium-ion batteries. (a) Ternary phase diagram of K_2O–FeO(Fe_2O_3)–SiO_2 showing new silicate-based polyanion compounds (such as K_2FeSiO_4). (b) Theoretical specific capacities of new iron-based silicates that can be explored as high-capacity cathode materials. Inset shows the crystal structure of cristobalite-type K_2FeSiO_4. (c) Plot showing gravimetric and volumetric energy densities attainable with iron-based cathode materials reported in literature. (d) K_2O–V_2O_5–V_2O_4–SO_3 ternary phase diagram unveiling new vanadium-based sulphates that can be assessed as high-voltage cathode materials. (c) Reproduced and adapted from ref. 14 with permission. Copyright 2022 Elsevier. (d) Adapted from ref. 199 and 200 with permission. Copyright 2007 Springer Nature.

2.4 Layered oxides and chalcogenides

Layered oxides, characterised by the composition A_xLO_2 (where A represents an alkali metal, L denotes primarily 3d transition metals, and $0 < x < 4/3$), have been subject to extensive investigation as potential cathode materials for both lithium-ion and sodium-ion batteries. This interest stems from the initial demonstration of electrochemical Li and Na extraction/insertion in the case of layered $LiCoO_2$ and $NaCoO_2$ back in 1980.[215,216] Notably, potassium-based layered oxides, such as K_xMO_2, were already a subject of exploration during the 1960s and 1970s.[217,218] Despite the discovery of these potassium-based layered oxides, it was not until 2016 that the electrochemical K-ion extraction/insertion in non-aqueous K cells was officially reported.[219]

Potassium-based layered oxide cathodes, emulating compositions found in sodium- and lithium-ion batteries, have been actively pursued as potential cathode materials for KIBs.[62,220–230] Typically, these layered oxides, adopting the general composition of A_xLO_2, consist of alkali metal atoms (A) arranged between transition metal oxide slab layers (LO_6 octahedra). As a result, various stacking sequences are observed (simply classifiable using the Hagenmuller–Delmas notation', or more elaborately using the face-centred cubic (FCC) notation), primarily influenced by (i) the type of alkali metal atom or transition metal present within the slab and (ii) the specific synthesis conditions. Due to the larger ionic radius of K^+ compared to the transition-metal ions in the slab, defects involving the mixing of transition-metal ions and K^+ are averted. This stands in stark contrast to Li-based layered oxides, where defects arise due to the similar ionic radius of Li^+ and transition metal ions, leading to their mixing. Moreover, the larger ionic radius of K^+ fosters weaker interlayer bonds, thereby facilitating facile 2D cationic diffusion during battery operation. This characteristic enables efficient movement of potassium ions within the layered framework.

Fig. 18a–c depict the crystal structures of archetypal layered frameworks (namely, $LiCoO_2$, $NaCoO_2$ and $K_{0.5}CoO_2$) which can be categorised within the Delmas notation as O3-, P3-, and P2-type, respectively. The numeric labels (1, 2, 3,...) correspond to the recurrent transition metal slabs that are oriented perpendicular to the layers of alkali metal within the unit cell. In contrast, the designations "P" or "O" are indicative of the alkali metal atoms' coordination with oxygen ligands, manifesting either as prismatic or octahedral arrangements. Table 1 shows representative layered cathode oxides classified in

Open Access Article. Published on 04 dicembre 2023. Downloaded on 11/06/2026 17:40:22.
This article is licensed under a Creative Commons Attribution-NonCommercial 3.0 Unported Licence.

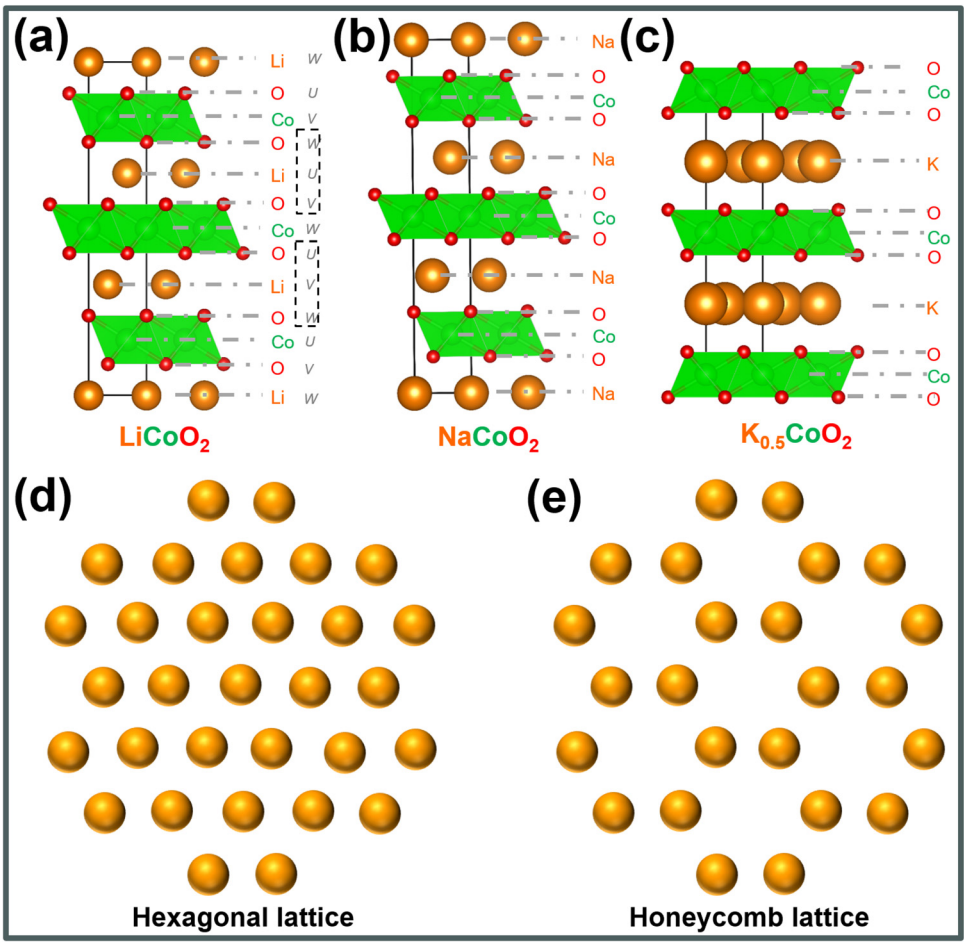

Fig. 18 Layered frameworks of (a) $LiCoO_2$, (b) $NaCoO_2$ and (c) $K_{0.5}CoO_2$. (d) Arrangement of mobile cations in a hexagonal lattice as exemplified in $LiCoO_2$ and $NaCoO_2$. (e) Arrangement of mobile cations in a honeycomb lattice as exemplified in potassium-deficient $K_{0.5}CoO_2$.

Delmas notation, for brevity. Within the framework of the FCC notation, the three-dimensional (3D) lattice configuration, exemplified for instance by $LiCoO_2$, manifests as an ordered $U_OV_{Co}W_OU_{Li}V_OW_{Co}U_OV_{Li}W_OU_{Co}V_OW_{Li}U_O$ sequence. This pattern iterates consistently to give rise to the layered structure of the material. The intrinsic value of adopting the FCC notation resides in its capacity to inherently encode the coordination phenomena between oxygen species and cationic entities. Concurrently, this notation provides an implicit exposition of information pertaining to the spatial arrangement of ions in the two-dimensional (2D) lattice layers.[235] Furthermore, the predominant occupation sites for alkali cations encompass either hexagonal lattices or honeycomb lattices, as schematically shown in Fig. 18d and e. The latter configuration is prominently observed within alkali-deficient or alkali-poor layered frameworks.

Layered transition metal oxides, such as K_xCrO_2 (x = 0.69, 0.8, and 1),[67,78,232] K_xMnO_2 (x = 0.3, 0.5 and 0.7),[85,236] K_xCoO_2 (x = 0.44 and 0.6),[65,66] $K_{0.48}Mn_{0.4}Co_{0.6}O_2$,[237] $K_xFe_{0.5}Mn_{0.5}O_2$ (x = 0.45, 0.65 and 0.7),[68,238] $K_{0.45}Mn_{0.5}Co_{0.5}O_2$,[60] $K_{0.5}Mn_{0.8}Co_{0.1}Ni_{0.1}O_2$,[55] $K_{0.67}Ni_{0.17}Co_{0.17}Mn_{0.66}O_2$,[239] $K_{1.39}Mn_3O_6$,[240] $K_xV_2O_5$,[68,241–246] $K_2V_3O_8$,[247] $K_{0.72}Li_{0.27}Ni_{0.6}Co_{0.2}Mn_{0.2}O_2$,[248] $K_{0.7}Fe_{0.05}Co_{0.1}Mn_{0.75}Ni_{0.05}V_{0.05}O_2$,[225] *etc.*, as well as layered chalcogenides (*e.g.*, $KCrS_2$,[231] $Cu_{0.11}TiSe_2$ superconductor[249] and $K_{0.78}Fe_{1.60}S_2$[250]), are considered promising cathode candidates owing to their theoretically high energy density and two-dimensional K^+ diffusion pathways. However, the large size of K^+ ions leads to increased K^+–K^+ electrostatic repulsion within the layered structure, resulting in multiple phase transitions and low operating voltages.[64] Fig. 19a shows the voltage profiles of $LiCoO_2$, $Na_{2/3}CoO_2$ and $K_{0.41}CoO_2$.[66] Layered oxides exhibit voltage profiles with a staircase-like pattern, the amplitude of which is contingent upon the separation distance between the layers. The interlayer spacing is subject to modulation by the size of the alkali atom intercalated within the slab. As illustrated in Fig. 19a, the inclusion of potassium atoms with substantial atomic radii within K_xCoO_2 results in increased interlayer distances, consequently impacting the ionicities of the transition metal constituents, thereby exerting a discernible influence upon the redox potentials. Moreover, vacancies are created or annihilated in the course of alkali ion intercalation or de-intercalation processes, thereby instigating a reconfiguration of alkali atom coordination within the layered framework. Illustrated in Fig. 19b are the distinct phases of transitions

© 2024 The Author(s). Published by the Royal Society of Chemistry

Open Access Article. Published on 04 dicembre 2023. Downloaded on 11/06/2026 17:40:22.
This article is licensed under a Creative Commons Attribution-NonCommercial 3.0 Unported Licence.

Table 1 Representative layered cathode oxides and sulphides for KIBs[54–103,231–234]

Delmas' notation	Layered compounds
O3-type	$KCrS_2$, $KCrO_2$
P2-type	$K_2Ni_2TeO_6$ ($K_{2/3}Ni_{2/3}Te_{1/3}O_2$), $K_{0.6}CoO_2$, $K_{0.5}Mn_{0.7}Fe_{0.2}Ti_{0.1}O_2$, $K_{0.6}Mn_{0.8}Ni_{0.1}Ti_{0.1}O_2$, $K_{2/3}Ni_{1/3}Co_{1/3}Te_{1/3}O_2$ ($K_2NiCoTeO_6$), $K_{0.75}[Ni_{1/3}Mn_{2/3}]O_2$, $K_{0.75}[Mn_{0.8}Ni_{0.1}Fe_{0.1}]O_2$, $K_{0.83}[Ni_{0.05}Mn_{0.95}]O_2$, $K_{0.21}MnO_2$, $K_{0.7}[Cr_{0.85}Sb_{0.15}]O_2$, $K_{0.76}Fe_{0.2}Mg_{0.1}Mn_{0.7}O_2$, $K_{5/9}Mn_{7/9}Ti_{2/9}O_2$, $K_{0.44}Ni_{0.22}Mn_{0.78}O_2$, $K_{0.75}[Ni_{1/3}Mn_{2/3}]O_2$, $K_{0.83}[Ni_{0.05}Mn_{0.95}]O_2$, $K_{0.6}Co_{0.67}Mn_{0.33}O_2$, $K_{0.6}Co_{0.66}Mn_{0.17}Ni_{0.17}O_2$, $K_{0.41}CoO_2$, $K_{0.65}Fe_{0.5}Mn_{0.5}O_2$, $K_{0.56}Ni_{0.52}Sb_{0.48}O_2$, $K_{0.86}Co_{0.62}Sb_{0.38}O_2$
P3-type	$K_2Ni_2TeO_6$, $K_{0.5}Mn_{0.8}Co_{0.1}Ni_{0.1}O_2$, $K_{0.5}Mn_{0.7}Ni_{0.3}O_2$, $K_{0.6}Cr_{0.6}Ti_{0.4}O_2$, $K_{0.45}Mn_{0.5}Co_{0.5}O_2$ $K_{0.70}[Cr_{0.86}Sb_{0.14}]O_2$, $K_{0.5}MnO_2$, $K_{0.69}CrO_2$, $K_{0.54}[Co_{0.5}Mn_{0.5}]O_2$, $K_{0.5}[Mn_{0.8}Fe_{0.1}Ni_{0.1}]O_2$, $K_{1/2}Mn_{5/6}Mg_{1/12}Ni_{1/12}O_2$, $K_{0.45}Mn_{1-x}Fe_xO_2$ (x = 0, 0.1, 0.2, 0.3, 0.4 and 0.5), $K_{0.8}CrO_2$, $K_{0.5}[Ni_{0.1}Mn_{0.9}]O_2$, $K_{0.5}[Mn_{0.85}Ni_{0.1}Co_{0.05}]O_2$, $K_{0.4}Fe_{0.1}Mn_{0.8}Ti_{0.1}O_2$, $K_{0.45}Co_{1/12}Mg_{1/12}Mn_{5/6}O_2$, $K_{0.45}Mn_{0.9}Mg_{0.1}O_2$, $K_{0.39}CrO_2$, $K_{0.23}MnO_2$, $K_{0.54}Mn_{0.78}Mg_{0.22}O_2$, $K_{0.45}Ni_{0.1}Fe_{0.1}Mn_{0.8}O_2$, $K_xMn_{0.7}Ni_{0.3}O_2$ (x = 0.4–0.7), $K_{0.4}Fe_{0.1}Mn_{0.8}Ti_{0.1}O_2$, $K_{0.5}Mn_{0.7}Co_{0.2}Fe_{0.1}O_2$, $K_{0.5}Mn_{0.72}Ni_{0.15}Co_{0.13}O_2$, $K_{0.45}Mn_{0.9}Al_{0.1}O_2$, $K_{0.67}Mn_{0.83}Ni_{0.17}O_2$, $K_{0.5}Mg_{0.15}[Mn_{0.8}Mg_{0.05}]O_2$, $K_{0.45}Ni_{0.1}Co_{0.1}Mg_{0.05}Mn_{0.75}O_2$, $K_{0.45}Ni_{0.1}Co_{0.1}Al_{0.05}Mn_{0.75}O_2$, $K_{0.48}Mn_{0.4}Co_{0.6}O_2$ $K_{0.45}Rb_{0.05}Mn_{0.85}Mg_{0.15}O_2$, $K_{0.35}Mn_{0.8}Fe_{0.1}Cu_{0.1}O_2$, $K_{0.5}Mn_{0.8}Fe_{0.2}O_2$, $K_{0.3}Mn_{0.95}Co_{0.05}O_2$ $K_{0.5}Ni_{0.5}Sb_{0.5}O_2$, $K_{0.5}Co_{0.5}Sb_{0.5}O_2$, $K_{0.5}Mn_{0.67}Fe_{0.33}O_{1.95}N_{0.05}$

(in Delmas' notation) in representative layered oxides that entail alterations in the manner by which alkali metal atoms are coordinated with the oxygen atoms belonging to the adjacent transition metal slabs. These multiple transitions transpire as a consequence of fluctuations in the alkali atom content. Fig. 19c delineates the voltage profiles exhibited by $K_{0.5}MnO_2$, illuminating the nature of phase transitions inherent in the course of K^+ intercalation and de-intercalation processes. The sequence of phase transformations during the K^+ de-intercalation or extraction process of $K_{0.5}MnO_2$ encompasses an initial P3 to O3 biphasic transition, subsequently progressing to another biphasic transition from O3 to a heretofore uncharacterised phase (designated as "X"). Computational results further predict the unidentified phase to assume an O1 configuration. X-ray diffraction investigations, as depicted in Fig. 19d, unveil the reversibility of the phase evolution during K^+ intercalation or insertion processes, signifying an absence of supplementary phase transitions. This observation implies a reversible intercalation and deintercalation process of potassium in $K_{0.5}MnO_2$.

Fig. 20a shows the voltage-capacity profiles of nanostructured $K_{0.5}MnO_2$ during successive cycles, along with electrochemical performance when subjected to various current densities (Fig. 20b).[75] The enhancement of electrochemical performance in layered oxides can be achieved through meticulous optimisation of particle morphology. Fig. 20c further showcases the voltage-capacity profiles of $K_{0.6}CoO_2$ microcubes, revealing their augmented electrochemical performance relative to both microspheres and microparticles (depicted in Fig. 20d).[56] The $K_{0.6}CoO_2$ microcubes demonstrate a substantial reversible capacity coupled with superior capabilities in terms of rate performance and long-term cycle stability (Fig. 20e). These improvements are attributed to the distinctive morphology inherent to the $K_{0.6}CoO_2$ microcubes.[56]

Whilst a vast majority of documented potassium-based layered oxides predominantly adopt the P2- and P3-type frameworks, which proffer notable advantages over O-type frameworks in relation to rate capabilities, they do, however, manifest diminished operational voltages (typically falling below 3 V). As previously alluded, the conspicuous Devil's staircase-like voltage profiles (akin to the Cantor–Vitali mathematical function[251–254]) are a consequence of the substantial size of the K^+ ion, which increases the electrostatic repulsion interactions between adjacent K^+ ions.[64] A strategic avenue for the amelioration of operational voltages within the domain of potassium-based layered oxides is to address this K^+–K^+ electrostatic repulsion phenomenon directly, accomplished through judicious structural design of the layered oxide framework. An illustrative exemplar involves the manipulation of K^+ ion concentrations, yielding a P3-type $K_{0.7}Mn_{0.7}Ni_{0.3}O_2$ variant characterised by a disordered vacancy/K^+ architecture, thereby evincing an elevated voltage plateau *vis-à-vis* its ordered $K_{0.4}Mn_{0.7}Ni_{0.3}O_2$ counterpart.[93] An alternative strategy encompasses the conception of a corrugated layered structure, whereby potassium atoms are sufficiently segregated so as to mitigate the repulsive K^+–K^+ interactions throughout successive K^+ intercalation and de-intercalation processes.

A series of corrugated layered titanates,[255] including $K_{0.8}M_{0.8}Ti_{1.2}O_4$ (M = V, Cr, Mn, Fe and Co), $K_{0.6}Cr_{0.6}Ti_{0.4}O_2$, *etc.*,[256] with longer K^+–K^+ distances (of ~3.9 Å) compared to conventional K_xMO_2 layered oxides' (typically ~3.0 Å),[232] have been found to effectively mitigate the K^+–K^+ electrostatic repulsion, resulting in high voltages with minimal phase transitions. For example, a representative layered titanate such as $K_{0.8}Ni_{0.4}Ti_{1.6}O_4$ (Fig. 21a) exhibits a high working voltage of 3.6 V.[256] Fig. 21b and c show the voltage-capacity profiles of $K_{0.8}Ni_{0.4}Ti_{1.6}O_4$ and $K_{0.8}Co_{0.8}Ti_{1.2}O_4$.[256] Although further material optimisation are required to enhance the capacity, these layered oxides display high voltages. Furthermore, our preliminary results indicate that layered stannates, like $K_xNi_{0.5}Sn_{0.5}O_2$ ($x < 1$), demonstrate high operating voltages of approximately 3.9 V, positioning related layered oxide compositions as promising high-voltage cathode materials that warrant further exploration.

Honeycomb layered oxides,[257] characterised by a honeycomb arrangement of mainly transition metal atoms in the

Open Access Article. Published on 04 dicembre 2023. Downloaded on 11/06/2026 17:40:22.
This article is licensed under a Creative Commons Attribution-NonCommercial 3.0 Unported Licence.

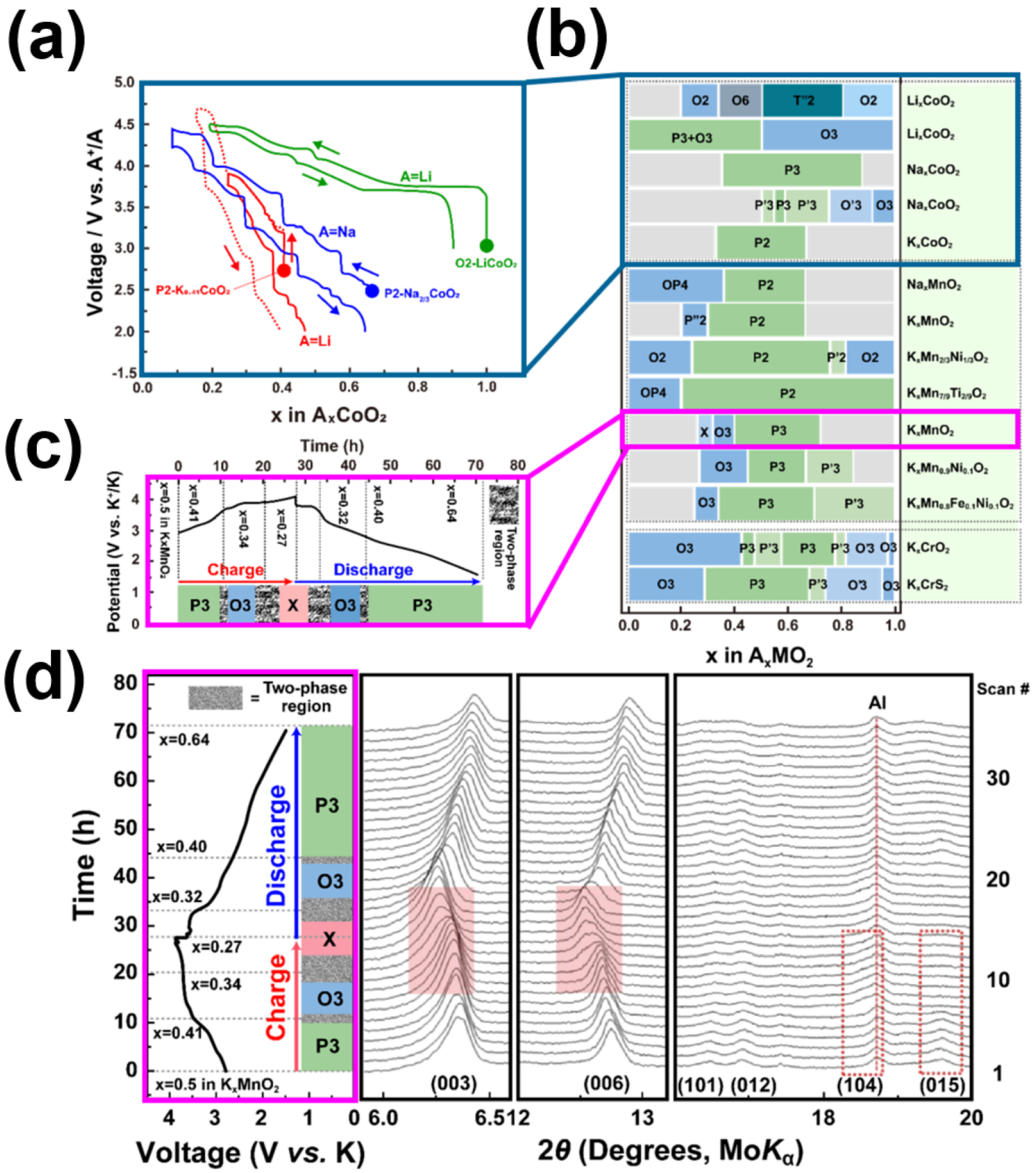

Fig. 19 (a) Voltage profiles comparison of $LiCoO_2$, $Na_{2/3}CoO_2$ and $K_{0.41}CoO_2$. (b) Phase transition in the stacking order of the slabs noted in layered oxides and sulphides during alkali-ion extraction. (c) Structural changes during K^+ extraction/insertion process of $K_{0.5}MnO_2$. (d) *In situ* X-ray diffraction data of $K_{0.5}MnO_2$ during initial charging and discharging processes. Figure (a) reproduced with permission from ref. 66. Copyright 2017 Royal Society of Chemistry. Figure (b) reproduced and adapted from ref. 229 with permission. Copyright 2021 Elsevier. Figures (c) and (d) reproduced from ref. 64 with permission. Copyright 2017 Wiley-VCH.

slab, represent an underrated class of cathode materials with exceptional properties. These materials not only exhibit high material densities, high voltages, and fast ion kinetics but also demonstrate excellent thermal stability, a feature distinct from conventional layered oxides.[257] Notable potassium-based honeycomb layered oxides include $K_2Ni_2TeO_6$ (or equivalently as $K_{2/3}Ni_{2/3}Te_{1/3}O_2$),[72,258] $K_2Ni_{1.5}Co_{0.5}TeO_6$ ($K_{2/3}Ni_{1/2}Co_{1/6}Te_{1/3}O_2$),[5,72] K_4NiTeO_6 ($K_{4/3}Ni_{1/3}Te_{1/3}O_2$), $K_4Ni_{0.5}Co_{0.5}TeO_6$ ($K_{4/3}Ni_{1/6}Co_{1/6}Te_{1/3}O_2$), amongst others. Fig. 22 displays high-resolution transmission electron microscopy (TEM) images of honeycomb layered $K_2NiCoTeO_6$, acquired through distinct zone axes. Clearly discernible within these TEM micrographs is the honeycomb arrangement of Ni/Co around Te atoms within the transition metal slab, as evidenced by the recurring –Te–Ni/Co–Ni/Co–Te– sequences. This spatial configuration becomes particularly pronounced when examining the TEM images taken along the[100] zone axis (as illustrated in Fig. 22a and b). Notably, the K atoms incorporated within $K_2NiCoTeO_6$ exhibit a prismatic coordination with oxygen atoms, thereby unveiling a P2-type layered framework. This mode of coordination is unequivocally substantiated by the TEM depictions captured along the [1$\bar{1}$0] direction (as presented in Fig. 22c and d). Furthermore, the TEM images divulge that potassium atoms also adopt a honeycomb lattice, as depicted in Fig. 18e. Honeycomb layered tellurates exhibit K–K distances approximating 3.0 Å. Consequently, the expectation of elevated

© 2024 The Author(s). Published by the Royal Society of Chemistry

Open Access Article. Published on 04 dicembre 2023. Downloaded on 11/06/2026 17:40:22.
This article is licensed under a Creative Commons Attribution-NonCommercial 3.0 Unported Licence.

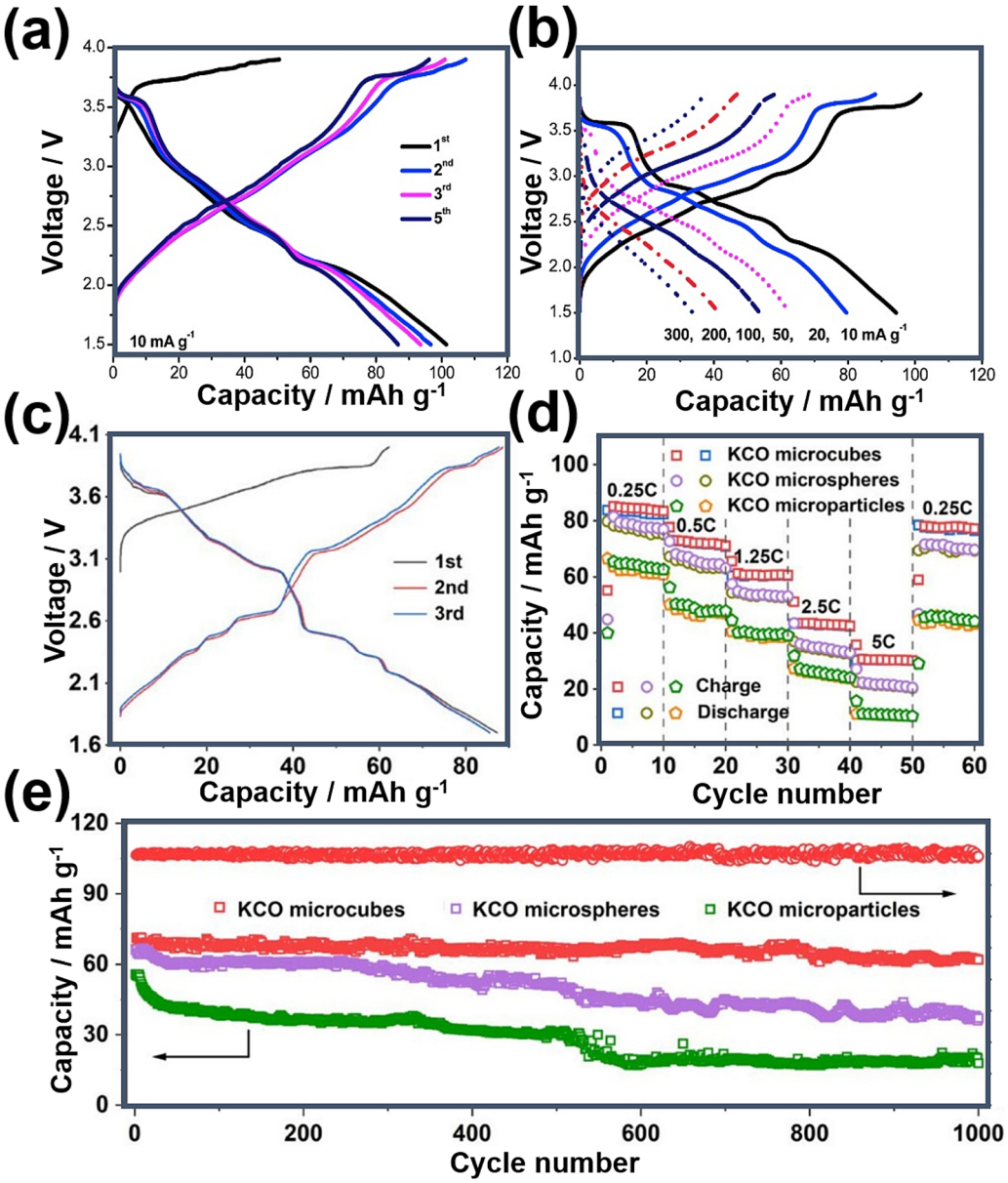

Fig. 20 (a) Voltage-capacity profiles of $K_{0.5}MnO_2$ and (b) corresponding rate performance. (c) Voltage-capacity profiles of $K_{0.6}CoO_2$ at a current density equivalent to C/4 (1C = 80 mA g^{-1}). (d) Rate performance of nanoarchitectured $K_{0.6}CoO_2$ (abbreviated as KCO) and (e) cycle performance at a current density commensurate to C/2. Figures (a) and (b) reproduced with permission from ref. 75. Copyright 2019 Elsevier. Figures (c), (d) and (e) reproduced with permission from ref. 56. Copyright 2023 American Chemical Society.

voltages similar to those observed in corrugated layered titanates such as $K_{0.8}Ni_{0.4}Ti_{1.6}O_4$ and $K_{0.8}Co_{0.8}Ti_{1.2}O_4$,[256] which possess significantly longer K^+–K^+ distances, should not be readily assumed. Cyclic voltammograms (Fig. 23a) of honeycomb layered tellurates with the composition of $K_2Ni_{2-x}Co_xTeO_6$ (x = 0, 0.25, 0.50 and 0.75) display redox voltages reaching 4 V, bringing to the fore honeycomb layered oxides as promising high-voltage cathode materials. Fig. 23b and c further show the voltage profiles of honeycomb layered $K_2NiCoTeO_6$ ($K_{2/3}Ni_{1/3}Co_{1/3}Te_{1/3}O_2$) and $K_2Ni_{1.5}Co_{0.5}TeO_6$ ($K_{2/3}Ni_{1/2}Co_{1/6}Te_{1/3}O_2$), demonstrating the honeycomb layered tellurates to exhibit high voltages reaching 4 V. The high voltage attained can be ascribed to the 'inductive effect'[160] imposed by the more electronegative $[TeO_6]^{6-}$ on the Ni/Co redox couple.

In addition to the achieved high voltages, honeycomb layered tellurates also manifest considerable material density (tap density). This notable characteristic bodes favourably for their prospective application as materials with high energy density, pending the complete optimisation of their capacity. However, the presence of chalcogens like tellurium in these honeycomb layered oxide compositions may hinder their practical realisation due to cost and scarcity concerns. Future research endeavours could be directed towards exploring tellurium-free honeycomb layered oxide compositions, such

Open Access Article. Published on 04 dicembre 2023. Downloaded on 11/06/2026 17:40:22.
This article is licensed under a Creative Commons Attribution-NonCommercial 3.0 Unported Licence.

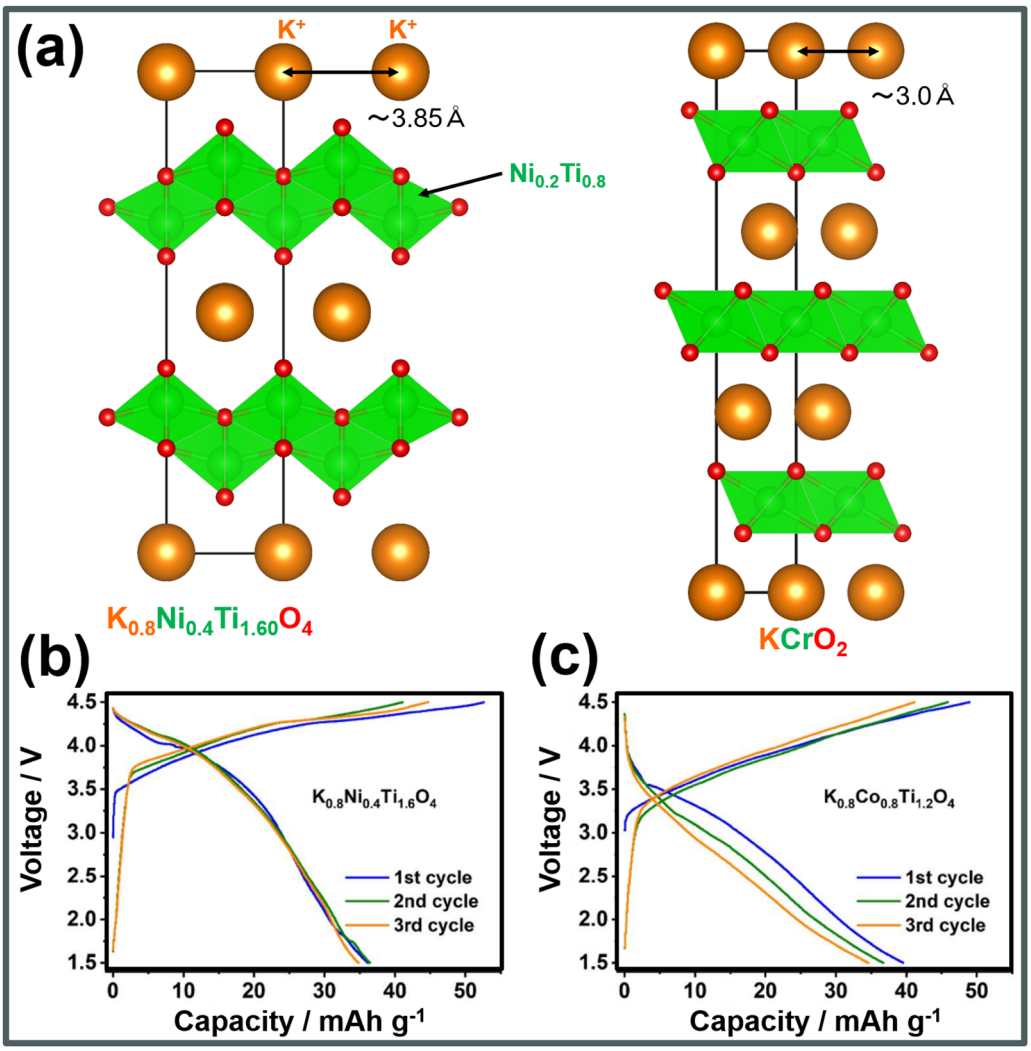

Fig. 21 Electrochemical performance of representative corrugated layered titanate cathode materials. (a) Comparison of the structural framework of corrugated layered titanates with that of conventional layered oxides, in terms of the K^+–K^+ distances. (b) Voltage-capacity profiles of $K_{0.8}Ni_{0.4}Ti_{1.6}O_4$ and (c) $K_{0.8}Co_{0.8}Ti_{1.2}O_4$. Figures (b) and (c) reproduced from ref. 256 with permission. Copyright 2022 American Chemical society.

as the bismuthates, antimonates, tungstenates, molybdenates, ruthenates, *etc.*, which offer the potential for both high voltages and high theoretical capacities.[257] Moreover, from a pedagogical perspective, the distinctive crystalline structure and inherent structural symmetries of these materials facilitate the prevalence of 2D atomistic interactions within their honeycomb layered heterostructures. This characteristic opens up opportunities for exploring unconventional magnetic phenomena, such as Heisenberg-Kitaev interactions, and investigating novel emergent properties, including quantum geometries and topologies.[257–266] The unique properties of these materials provide valuable insights into fundamental physics principles and can serve as excellent educational tools to foster a deeper understanding of advanced materials and their intriguing behaviours.

A significant challenge associated with many layered oxide materials is their delicate handling requirements, necessitating a controlled atmosphere, such as storage in argon-purged glove boxes or dry-rooms, due to their high sensitivity to air and moisture (hygroscopic nature). Nevertheless, their inherent instability can be effectively mitigated and controlled through meticulous tuning of their chemical composition. Partial substitution of constituent transition metal atoms has emerged as a promising and viable approach, as evident in Na-analogues like $NaNi_{2/3}Sb_{1/3}O_2$ ($Na_3Ni_2SbO_6$). In this case, even a minor amount of substitution with elements such as Mn, Mg, or Ru has been found to significantly improve the structural stability of the material.[267–269] A similar strategy can be adopted to improve the stability of hygroscopic potassium-based layered oxides. Additionally, the concept of utilising multiple transition metals in equivalent proportions, commonly referred to as 'high-entropy oxides',[270,271] has recently emerged as a novel approach for designing stable layered oxides with distinctive physicochemical properties. Whilst this concept presents exciting new possibilities for designing and implementing potassium-based layered oxides, it is still in its nascent stages

© 2024 The Author(s). Published by the Royal Society of Chemistry

Open Access Article. Published on 04 diciembre 2023. Downloaded on 11/06/2026 17:40:22.
This article is licensed under a Creative Commons Attribution-NonCommercial 3.0 Unported Licence.

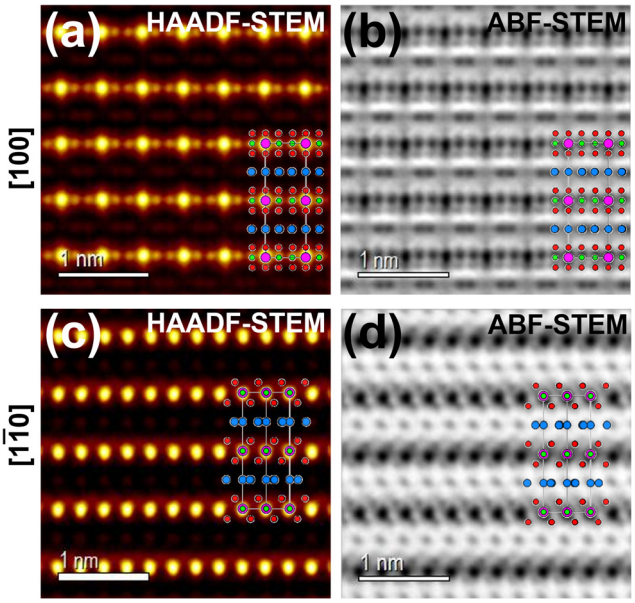

Fig. 22 High-resolution transmission electron microscopy images of honeycomb layered Rb(5%)-doped $K_2NiCoTeO_6$ ($K_{2/3}Ni_{1/3}Co_{1/3}Te_{1/3}O_2$) taken at various zone axes. (a) High-angle annular dark-field (HAADF) scanning transmission electron microscopy (STEM) image taken along[100] zone axis and (b) corresponding annular bright-field (ABF)–STEM image. (c) HAADF–STEM image taken along [1$\bar{1}$0] zone axis and (d) corresponding ABF–STEM image. K atoms are shown in blue, Ni/Co and Te atoms are shown in green and pink, respectively. Oxygen atoms are shown in red.

with substantial room for further exploration and development. Moreover, the application of plasma-enhanced sintering methodologies has demonstrated significant efficacy in augmenting the structural stability of layered oxides, exemplified by $K_{0.6}Ni_{0.2}Co_{0.3}Mn_{0.5}O_2$,[272] particularly when exposed to moisture.

A vast majority of potassium-based layered oxides and chalcogenides suffer from potassium deficiency, which limits their capacity to bring a sufficient amount of potassium into a potassium-ion battery (KIB). To overcome this limitation, one promising approach is the investigation of stoichiometric layered oxides (*e.g.*, $KCrO_2$[232] and $KCrS_2$[231]) or potassium-rich layered oxides, as found in, for instance, the aforementioned honeycomb layered oxide compositions or potassium hypomanganates such as K_3MnO_4.[273] Another strategy involves exploring materials that operate through the combined participation of both transition metal cation and oxygen/sulphide anion redox chemistry, enabling the full utilisation of the capacity in both potassium-rich and potassium-deficient layered oxide cathode materials. It is noteworthy that reversible anion-redox chemistry has been observed in certain layered oxide cathode materials, such as $K_{0.4}Fe_{0.5}Mn_{0.5}O_2$[238] and $K_{0.78}Fe_{1.60}S_2$.[250]

These approaches, including high-throughput materials screening,[274–276] hold promise in addressing the potassium deficiency challenge and unlocking the full potential of layered oxide cathode materials for high-performance KIBs. Further research in this direction is crucial for advancing the field of potassium-ion battery technology and enhancing its practical applications in energy storage.

2.5 Approaches to enhance material performance.

Fig. 24 below presents a summary of the distinct classes of cathode materials employed in rechargeable KIBs, along with the corresponding challenges to be addressed, and their respective solutions.

2.5.1 Organic materials. Organic materials have attracted tremendous attention due to their high capacity, flexibility, and cost-effectiveness.[42,138–141] Nevertheless, the significant majority of organic materials, particularly simple, low-molecular-weight quinones such as anthraquinone, naphthoquinone, and benzoquinone, tend to manifest poor cyclability (electrochemical reversibility), notwithstanding their high theoretical capacity. This phenomenon primarily stems from their propensity to dissolve into the electrolyte. Salinisation and polymerisation/oligomerisation have demonstrated effectiveness in alleviating the substantial dissolution of organic compounds into the electrolyte.[141] Polymers emerge as promising organic materials due to their restricted solubility in organic electrolytes, resulting in good cyclability. However, the polymerisation process inevitably introduces inert (inactive) components, consequently leading to a reduced reversible capacity compared to organic salts and small molecules. Therefore, the imperative lies in augmenting the proportion of active material components to enhance the energy density of polymers. Methods for optimising the electrolyte, including the incorporation of additives and the utilisation of highly-concentrated electrolytes, have been employed to improve the compatibility between the electrolyte and the electrode.[141] Furthermore, combining organic compounds with carbonaceous materials, such as carbon nanotubes and graphene, can increase electronic conductivity, thus enhancing their rate performance. Furthermore, the incorporation of molecular engineering strategies, including the extension of π-conjugated moieties (such as through π-d conjugate metal coordination design and π–π conjugate large plane molecular design),[277] can effectively facilitate electron delocalisation, thereby enabling facile intermolecular electron transport and consequently leading to the enhancement of rate capabilities. The redox potential of organic materials undergoing n-type reactions (electrophilic additions), such as organic carbonyl and imine compounds, is typically low (<3 V *versus* K/K^+). This low potential proves suboptimal for the enhancement of battery energy density. Conversely, anion insertion compounds that undergo p-type reactions (nucleophilic additions), exemplified by nitroxide free radicals, amino groups, and heteroatoms, generally exhibit potentials exceeding 3 V (*versus* K/K^+). Consequently, these materials can find utility as high-voltage organic cathode components ((Fig. 8–11a)). Bipolar organic materials, such as QTTFQ (Fig. 11b), which undergo both the n-type and p-type reactions, possess high theoretical capacity and wide voltage ranges, rendering them exceptionally appealing as high-energy-density cathode materials. Furthermore, increasing the number of carbonyls per molecular unit can aid in increasing the attainable capacity, as demonstrated

Open Access Article. Published on 04 dicembre 2023. Downloaded on 11/06/2026 17:40:22.
This article is licensed under a Creative Commons Attribution-NonCommercial 3.0 Unported Licence.

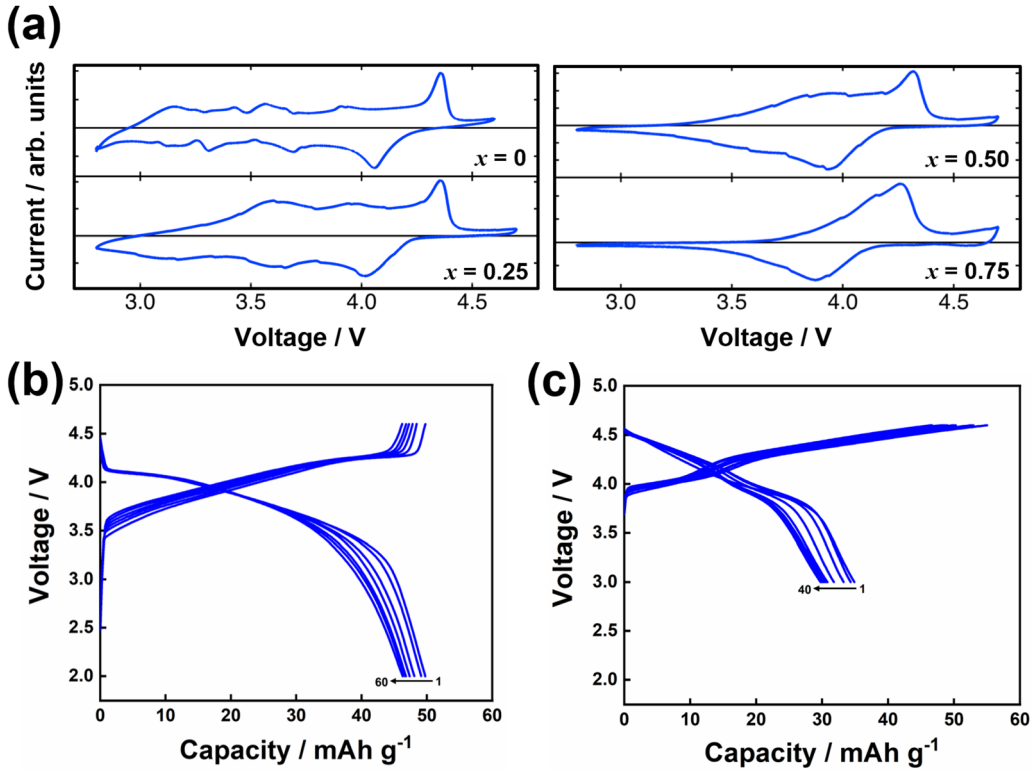

Fig. 23 (a) Cyclic voltammograms of $K_2Ni_{2-x}Co_xTeO_6$ ($K_{2/3}Ni_{(2-x)/3}Co_{x/3}Te_{1/3}O_2$) taken at a scanning speed of 0.1 mV s^{-1} and at a cut-off voltage of 2.8–4.7 V. 0.5 M KTFSI in Pyr_{13}TFSI ionic liquid was used as the electrolyte in potassium half-cells. (b) Voltage-capacity profiles of honeycomb layered $K_{2/3}Ni_{1/2}Co_{1/6}Te_{1/3}O_2$ using 0.5 M KTFSI in Pyr_{13}TFSI ionic liquid as the electrolyte in K half-cells. A current density commensurate to C/10 was applied (1C = 127.8 mA g^{-1}). (c) Voltage-capacity profiles of honeycomb layered $K_{2/3}Ni_{1/3}Co_{1/3}Te_{1/3}O_2$ (5% Rb-doped) using 1 M KFSI in Pyr_{13}FSI ionic liquid as the electrolyte in K half-cells. Tungsten foils were used as the current collector to avert corrosion from FSI^-. A current density commensurate to C/10 was applied (1C = 127.8 mA g^{-1}). Figure (a) reproduced and adapted with permission from ref. 5. Copyright 2019 Wiley-VCH.

in 5,7,12,14-pentacenetetrone (with a theoretical capacity of 317 mA h g^{-1}).[141] In this case, the addition of four carbonyl groups to anthraquinone (with a theoretical capacity of 257 mA h g^{-1}) results in a larger conjugated moiety with a higher theoretical capacity. Although quinone moieties generally exhibit low operating voltages, the incorporation of electron-withdrawing groups is a well-known strategy for increasing the voltage. Ultimately, employing computational predictions for the design of novel organic cathode moieties represents a formidable undertaking. Nevertheless, it is a viable pathway that can be leveraged for the *in silico* design of new high-energy-density organic cathode materials.

2.5.2 Prussian analogues. Prussian analogues have garnered substantial attention due to their high specific capacity and sustainability.[24–34] Prussian white ($K_2Fe[Fe(CN)_6]$) exhibits a greater potassium content than Prussian blue and Berlin green derivatives, resulting in a theoretical capacity twice that of Prussian blue. $K_2Fe[Fe(CN)_6]$ and $K_2Mn[Fe(CN)_6]$ consist of cost-effective elements and generally demonstrate high energy density (Fig. 6 and 7). Effective strategies,[28,278,279] such as nanocomposite design, potassium content regulation, elemental substitution, morphology control, and crystallinity tuning, can be implemented to address challenges associated with low electronic conductivity, intrinsic $[Fe(CN)_6]^{4-}$ vacancies, and crystal water content in Prussian blue analogues. In the present context, $K_2Mn[Fe(CN)_6]$ and related compositions, despite their low material density, present themselves as promising candidates for commercial applications due to their high operating voltage, superior energy density, excellent air stability, and cost-effective production processes. The most efficient method for synthesising Prussian blue analogues is the water co-precipitation approach,[28,278,279] which combines cost-effectiveness with the simplicity necessary for upscaling. However, this aqueous synthesis environment inadvertently introduces challenges such as crystal defects and water inclusion. These imperfections can compromise electrochemical performance and hinder thermal stability, although a comprehensive understanding of the precise impact of defects and water inclusion on electrochemical performance is yet to be achieved. Two potential strategies have emerged as leading approaches in the effort to mitigate these imperfections in Prussian analogues: (i) the utilisation of high-temperature drying and dehydration processes and (ii) the introduction of suitable chelating agents. Another challenge involves the quest for suitable electrolytes capable of withstanding high-voltage operation whilst ensuring safety. Prussian analogues, such as $K_2Mn[Fe(CN)_6]$ and their derivatives, exhibit voltage plateaus exceeding 4 V.[24–34] Unfortunately, conventional organic electrolytes falter

© 2024 The Author(s). Published by the Royal Society of Chemistry

Open Access Article. Published on 04 dicembre 2023. Downloaded on 11/06/2026 17:40:22.
This article is licensed under a Creative Commons Attribution-NonCommercial 3.0 Unported Licence.

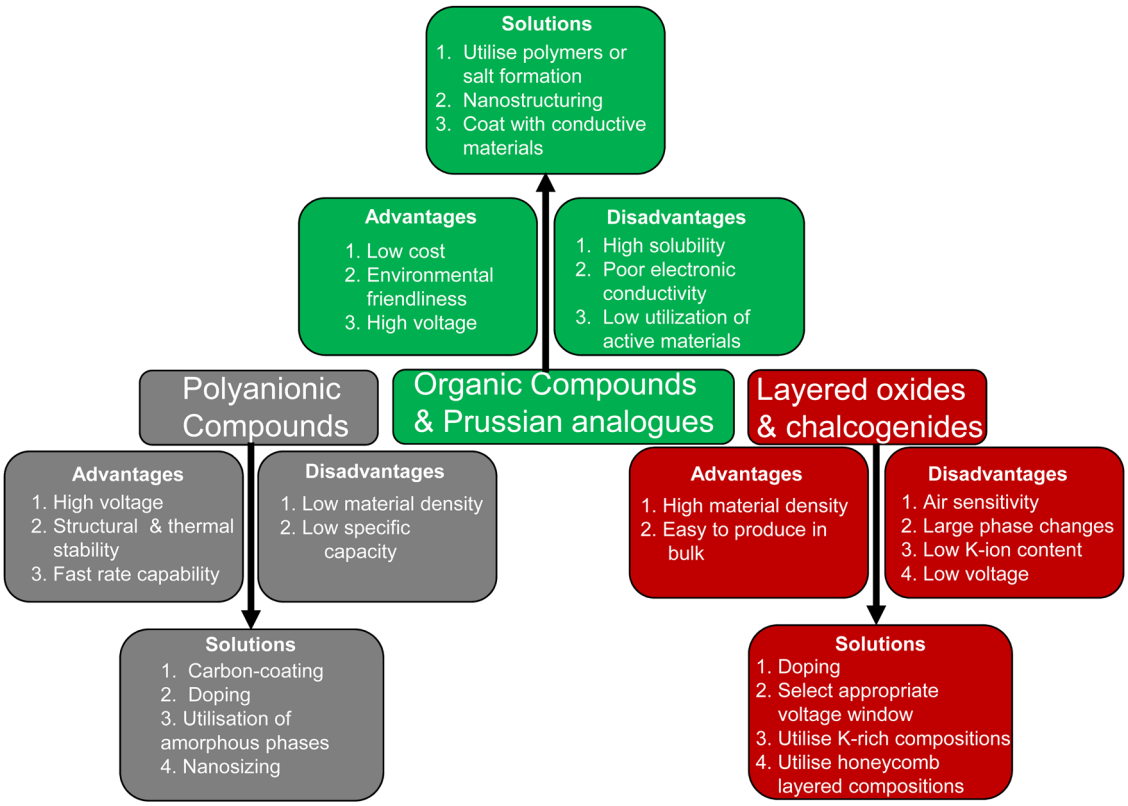

Fig. 24 Pros/cons of various positive electrode (cathode) materials for KIBs, along with their solutions. Figures adapted from ref. 4 with permission. Copyright 2020 Wiley-VCH.

when employed in high-voltage battery systems. The primary challenge lies in their propensity to undergo various side reactions when subjected to high voltages, resulting in capacity degradation. Additionally, safety concerns stemming from the flammable nature of many organic electrolytes cannot be disregarded. The use of highly concentrated electrolytes and ionic liquids has demonstrated favourable cycling performance for Prussian analogues.[280,281]

2.5.3 Polyanion-based compounds. Polyanionic frameworks present an open and robust structural lattice (Fig. 12), facilitating the swift diffusion of large potassium ions. Furthermore, polyanion-based compounds display exceptional thermal stability and typically manifest heightened voltages attributed to the inductive effect.[164,165] Polyanion-based compounds that adopt structural configurations akin to $KTiOPO_4$, such as $KFeSO_4F$,[12–17,282] $KTiPO_4F$,[180] $KVPO_4F$,[18,19] and $KVOPO_4$,[18] have undergone thorough examination due to their relatively elevated operational voltages and favourable rate capabilities. Nevertheless, these compounds confront inherent challenges stemming from limited electronic conductivity and diminished theoretical specific capacities, primarily arising from the substantial atomic mass of the polyanion constituents. Mitigating the constraints associated with low electronic conductivity necessitates the implementation of pivotal strategies, including elemental substitution, the incorporation of conductive materials (*e.g.*, carbon), morphological engineering (*e.g.*, nanosizing), and structural modifications.[164,165] Additionally, the investigation of lightweight polyanion units, such as borates (*e.g.*, $K_2Fe_2B_2O_7$, $KMnBO_3$, $KFeBO_3$ (isotypic with $KMgBO_3$[283,284])), silicates (cristobalite-type K_2FeSiO_4, K_2MnSiO_4, K_2FeTiO_4, K_2FeGeO_4 and sorosilicates ($K_2Fe_2Si_2O_7$ (isotypic with $K_2Ca_2Si_2O_7$[285–288]), $K_2Mn_2Si_2O_7$)), and pyrophosphates ($K_2MnP_2O_7$,[165] $K_2FeP_2O_7$,[165] $K_2NiP_2O_7$, $K_2CoP_2O_7$), showcasing multi-electron redox reactions of transition metals ($Fe^{2+/3+/4+}$, $Mn^{2+/3+/4+}$, $Ni^{2+/3+/4+}$, $Co^{2+/3+/4+}$), represents a promising avenue for harnessing high-capacity cathode materials (Fig. 16 and 17). Moreover, the exploration of novel polyanion frameworks enabling multi-electron redox reactions of vanadium ($V^{2+/3+/4+/5+}$) or chromium ($Cr^{2+/3+/4+}$) can be pursued through computational screening.

2.5.4 Layered oxides and chalcogenides. Layered oxides and sulphides have garnered significant attention owing to their high theoretical capacity and ease of synthesis.[62,220–230] However, they encounter challenges, including capacity degradation upon repeated cycling due to structural deterioration, susceptibility to moisture, and inherently low operational voltages. To address these issues, various effective strategies are employed,[62,220–230] such as particle coating with protective surface layers (*e.g.*, Al_2O_3), elemental substitution within the transition metal layers (*e.g.*, employing Ti, Mg, Al, *etc.*), morphological engineering (*e.g.*, nanosizing), and rational composition design. Potassium-based layered oxides and sulphides (Table 1) typically exhibit relatively low operational voltages, which can be improved through structural modifications. Examples include the incorporation of honeycomb layered

Open Access Article. Published on 04 dicembre 2023. Downloaded on 11/06/2026 17:40:22.
This article is licensed under a Creative Commons Attribution-NonCommercial 3.0 Unported Licence.

oxides containing highly electronegative elements like Te (*e.g.*, K_4NiTeO_6, $K_2Ni_2TeO_6$,[5,72,258] $K_3Ni_{1.5}TeO_6$), or the utilisation of corrugated layered frameworks (*e.g.*, $K_{0.8}Ni_{0.4}Ti_{1.6}O_4$[256] and $K_{0.8}Co_{0.8}Ti_{1.2}O_4$[256]) with expanded K^+–K^+ bond distances (Fig. 21 and 23). Furthermore, moisture sensitivity of layered oxides and chalcogenides can be alleviated by employing synthesis techniques such as plasma-enhanced sintering, as demonstrated in $K_{0.6}Ni_{0.2}Co_{0.3}Mn_{0.5}O_2$.[272] High-entropy layered oxides, such as $K_{0.6}Ni_{0.05}Fe_{0.05}Mg_{0.05}Ti_{0.05}Mn_{0.0725}O_2$,[289] have also exhibited stability against moisture, underscoring the 'high-entropy' approach as a viable technique for designing moisture-resistant layered oxides.

2.5.5 Cathode-electrolyte interphase. The cathode-electrolyte interphase (CEI) typically forms instantaneously through electrochemical and chemical reactions when the cathode (positive electrode) makes contact with the electrolyte. The CEI plays a critical role as the electrochemical interphase governing cathode stability, cycle life, and rate performance. Whilst research in the field of CEI is advancing rapidly, our understanding of the CEI in potassium-ion batteries (KIBs) significantly lags behind that of lithium-ion batteries or even sodium-ion batteries.[290–296] Consequently, comprehending and, ultimately, controlling the CEI remains the primary challenge in establishing stable electrochemical interphases for cathode materials in KIBs. In summary, more work and effort should be directed towards further elucidating the structure–property relationship of the CEI, exploring the chemical characteristics of the CEI, and developing advanced characterisations for establishing the CEI model, amongst other aspects. Moreover, the judicious integration of artificial intelligence and machine learning stands as an auspicious avenue through which to expedite research and development endeavours related to the CEI for KIBs.

3 High-energy-density potassium-ion battery full cell design

As the quest for alternative energy storage systems gains momentum, the exploration of potassium-ion batteries (KIBs) as potential replacements for lithium-ion batteries has witnessed a notable surge. This comprehensive *Perspective* serves to expound on the current state of research endeavours in the domain of KIBs, focusing specifically on the advancements and challenges pertaining to cathode materials. In tandem with the intensive recent research, KIBs have emerged as highly promising contenders for next-generation battery technology, boasting attributes such as high voltage, high power capabilities, and cost-effectiveness. Nevertheless, to enable their practical implementation, further enhancements in energy density, cyclability, high-power operation, and safety must be achieved.

Within the confines of this *Perspective*, we hereafter also envisage innovative design strategies for both anode materials and electrolyte formulations, which play a pivotal role in realising a feasible potassium-ion battery. Additionally, we impart valuable perspectives and directions for designing materials tailored to suit KIBs, derived from our own experience and insights garnered from pertinent literature. It is our aspiration that these perspectives will not only underscore the potential of KIBs as a competitive energy-storage technology but also illuminate the pathways leading to its actualisation. We endeavour to elucidate the accessibility of the knowledge and strategies indispensable for the development of this technology. Nevertheless, it is imperative to clarify that the perspectives delineated herein represent the viewpoints of the authors and should not be misconstrued as an exhaustive compendium of strategies pursuable in the pursuit of high-performance KIBs.

3.1 Suitable anode materials for high-voltage cathode materials

The exploration of various anode materials that can be readily coupled with high-voltage/high energy density cathode materials for KIBs has yielded significant advancements.[51,306–334] Fig. 25a shows exemplars of anode materials reported for KIBs. Ragone plots showing the average voltages attained by selected anode materials along with theoretical capacities are shown in Fig. 25b. Fig. 25c shows the theoretical gravimetric and volumetric capacities attainable with alloy-based anode materials compared to carbonaceous materials such as carbon. Carbonaceous materials, including graphite and its derivatives such as hard carbon (non-graphitisable carbon (Fig. 26a)) and soft carbon (graphitisable carbon), emerge as promising candidates for anode materials.[335–359] This is attributed to their relatively low cost, high surface area, and ease of surface modification. Notably, graphite stands out as a viable option for achieving high-voltage KIBs, as its potassiation/depotassiation voltage plateau lies above 0.1 V *versus* K/K^+ (Fig. 5). Additionally, the design of hierarchical porous 2D and 3D nanostructures from graphene/graphite is a straightforward process, and further appropriate structural modifications hold the potential to enhance its energy density. Nonetheless, practical application of graphite anodes demands further improvement in terms of reaction kinetics and managing volume expansion during potassiation. Addressing these challenges would be crucial to unlocking the full potential of graphite as an anode material in high-performance potassium-ion batteries.[360] As research continues, advancements in anode materials are essential for achieving significant progress in KIB technology and meeting the demands of next-generation energy storage applications.

Layered titanates, including $K_2Ti_2O_5$, $K_2Ti_3O_7$, $K_2Ti_4O_9$, $K_2Ti_6O_{13}$, $K_2Ti_8O_{17}$, *etc.*, operating through topotactic K^+ insertion/extraction mechanisms similar to graphite, hold significant promise as anode materials.[361,365–368] These materials offer high capacity attainable through Ti^{4+}/Ti^{3+} redox reactions, with low volume change and relatively high operation potentials at around 0.5 V. Fig. 26b and c show the voltage-capacity plots for $K_2Ti_8O_{17}$ and $K_2Ti_4O_9$. One notable advantage of layered titanates over graphite and other carbonaceous materials is their higher material densities (tap densities), which contributes to their potential for enhanced performance in terms of volumetric energy density. To fully exploit the electrochemical capabilities of layered titanates, thoughtful electrode

© 2024 The Author(s). Published by the Royal Society of Chemistry

Open Access Article. Published on 04 dicembre 2023. Downloaded on 11/06/2026 17:40:22.
This article is licensed under a Creative Commons Attribution-NonCommercial 3.0 Unported Licence.

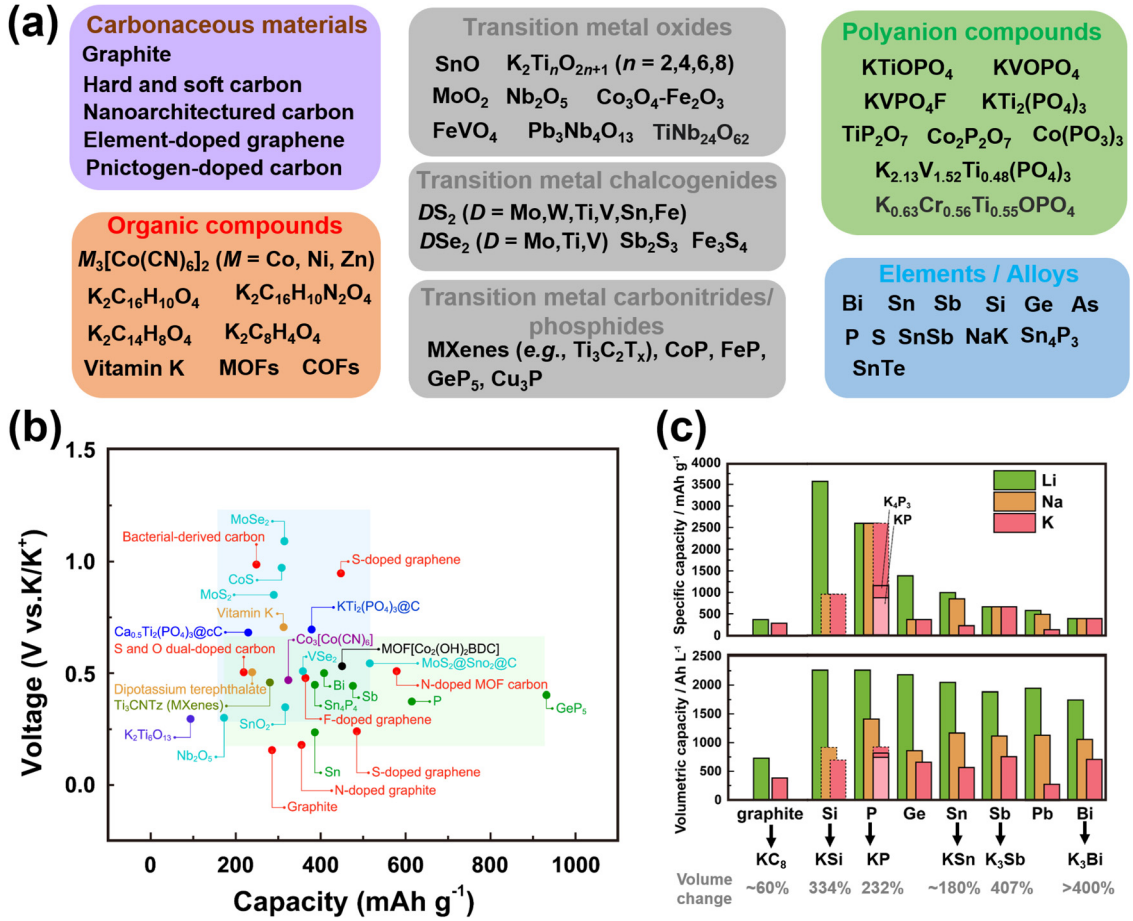

Fig. 25 (a) Exemplars of anode materials for potassium-ion batteries.[297–305] (b) Ragone plot showing the average voltages attained by selected anode materials along with their theoretical capacities. (c) Theoretical capacities of alloy-based anode materials compared to graphite in potassium-, sodium- and lithium-ion battery configurations, and (d) corresponding volumetric capacities. Figures adapted with permission.[42] Copyright 2020 American Chemical Society.

design strategies, such as nanostructuring, are imperative. These strategies can optimise the electrochemical performance of the materials, enabling them to achieve their full potential as anode materials for potassium-ion batteries. Additionally, titanium-based polyanion compounds like $KTiOPO_4$[369] and $KTi_2(PO_4)_3$,[370,371] whilst exhibiting theoretically low capacities, can play a pivotal role in ensuring the thermal stability of layered titanates during high-temperature operation. Moreover, the incorporation of polyanion-based compounds can further elevate the material densities and, consequently, improve the volumetric energy densities of layered titanates. For the successful development of polyanion-based anodes, it is essential to design materials with a reasonable operating potential and satisfactory capacity, striking a balance between these properties to ensure their effective utilisation in KIBs. Fig. 26d displays the voltage-capacity profiles of a representative polyanionic compound (i.e., $KVOPO_4$) evaluated also as an anode material for KIBs. Through systematic research and innovative design, layered titanates and polyanion-based compounds offer exciting prospects for advancing the performance of anode materials in KIBs.

Anodes operating *via* alloying reactions, such as those based on materials like Bi and Sn, show great promise as candidates for KIBs due to their high capacity.[373–375] Fig. 26e shows the voltage-capacity plots of Sb as an anode material for KIBs, operating *via* alloying reaction to form K_3Sb. However, certain challenges associated with these alloy anodes need to be addressed. These challenges include the low initial Coulombic efficiency, high operating potential, and significant volume expansion (see Fig. 25c) observed during the potassiation/depotassiation processes. Resolving these issues is crucial to fully harness the potential of alloy anodes and to enhance their performance in KIBs. Apart from alloying reactions, anodes operating *via* conversion reactions (such as SnO (shown in Fig. 26f)) offer alternative pathways for high-capacity anode materials in KIBs. Additionally, anode materials that undergo cumulative alloying and conversion reaction (such as Sb_2Se_3)[376] or cumulative (de)intercalation and conversion processes can be utilised to increase their energy density.[7]

Similarly, organic anodes (Fig. 27), including conjugate carboxylates and π-conjugated 2D and 3D covalent organic frameworks (COFs),[142,377–380] hold great potential for high-

Open Access Article. Published on 04 dicembre 2023. Downloaded on 11/06/2026 17:40:22.
This article is licensed under a Creative Commons Attribution-NonCommercial 3.0 Unported Licence.

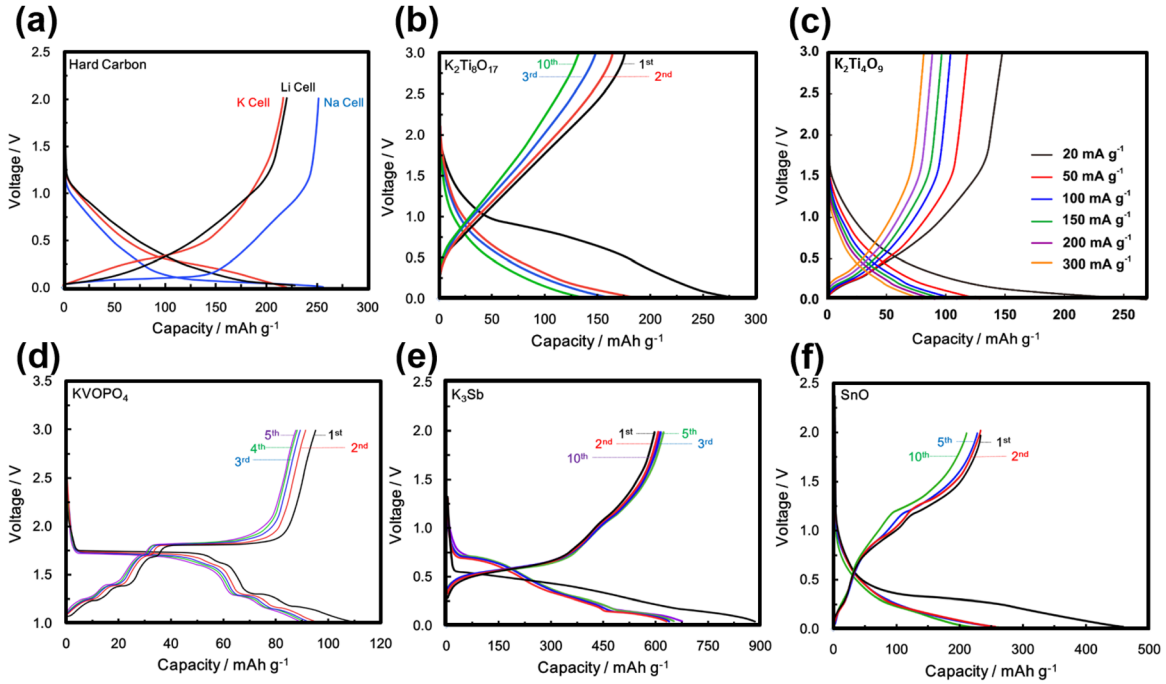

Fig. 26 Voltage-capacity profiles of (a) hard carbon (in potassium-ion, sodium-ion, and lithium-ion battery configurations),[42] (b) $K_2Ti_8O_{17}$,[361] (c) $K_2Ti_4O_9$ under various current densities,[362] (d) $KVOPO_4$,[42] (e) Sb[363] and (f) SnO.[364] Figures (a) and (d) reproduced from ref. 42 with permission. Copyright 2020 American Chemical Society. Figure (b) reproduced from ref. 361 with permission. Copyright 2016 Royal Society of Chemistry. Figure (c) reproduced from ref. 362 with permission. Copyright 2017 American Chemical Society. Figure (e) reproduced from ref. 363 with permission. Copyright 2015 American Chemical Society. Figure (f) reproduced from ref. 364 with permission. Copyright 2018 American Chemical Society.

capacity anode applications. The challenges that require addressing include the dissolution of active materials into the electrolyte and the inadequate electronic conductivity found in a majority of organic anodes. Organic anodes can be particularly well-suited for flexible organic KIBs, enabling innovative and versatile designs for next-generation energy storage devices. As research progresses, addressing the challenges faced by alloying anodes and exploring the potential of conversion-based and organic anodes will undoubtedly contribute to the development of high-performance KIBs and advance the field of energy storage technology.

In light of its scalability and suitability for commercialisable potassium-ion battery (KIB) anodes, graphite emerges as a promising candidate. The existing infrastructure established for manufacturing graphite electrodes in lithium-ion batteries (LIBs) can be leveraged and transitioned to accommodate KIBs, streamlining the commercialisation process for this novel battery system. Nevertheless, the key determinant lies in understanding and optimising the solid–electrolyte interphase layer and comprehending the K^+ extraction/insertion mechanism. Significant research efforts should be directed towards unraveling the intricacies of the solid–electrolyte interphase (SEI),[381–384] its interplay with the additives, electrolytes, and binders employed, as well as the mechanism of its growth and formation. The controlled, reliable, and safe growth of SEI on the graphite surface is pivotal to facilitating the adoption of graphite as an anode material for KIBs. Moreover, several theoretical models, such as the Daumas–Hérold model and Rüdorff–Hofmann model,[385–387] have been proposed to describe the intercalation process of alkali ions like K^+ into graphite (also referred to as the 'staging' process). However, these models still lack comprehensive understanding and need further exploration. Exploring the potential formation of ripplocations[388–392] during the process of potassium-ion intercalation and de-intercalation in graphite, through techniques such as transmission electron microscopy, can provide captivating insights. A holistic understanding of the mechanism governing electrochemical K^+ extraction/insertion mechanism of graphite is crucial,[393] including insights into the influence of current rate on the staging processes and the nature of phases present. Furthermore, addressing concerns related to high current-rate performance and safety of graphite in KIBs is of paramount importance. This is a major area of concern that persists in LIBs and requires careful examination and mitigation to ensure the successful and safe deployment of graphite in KIBs. In conclusion, whilst graphite shows promise as a viable anode material for KIBs, extensive research is imperative to elucidate and optimise the SEI formation,[394] K-ion insertion/extraction mechanisms, and ensure high current-rate performance and safety, thereby facilitating the successful integration of graphite in practical potassium-ion battery systems.[393]

3.2 Safe and compatible electrolytes for high-voltage cathode materials

Aside from electrodes, another pivotal aspect of battery technologies lies in the electrolyte, which profoundly governs their performance and lifespan. Ever since the discovery of reversible

© 2024 The Author(s). Published by the Royal Society of Chemistry

Open Access Article. Published on 04 dicembre 2023. Downloaded on 11/06/2026 17:40:22.
This article is licensed under a Creative Commons Attribution-NonCommercial 3.0 Unported Licence.

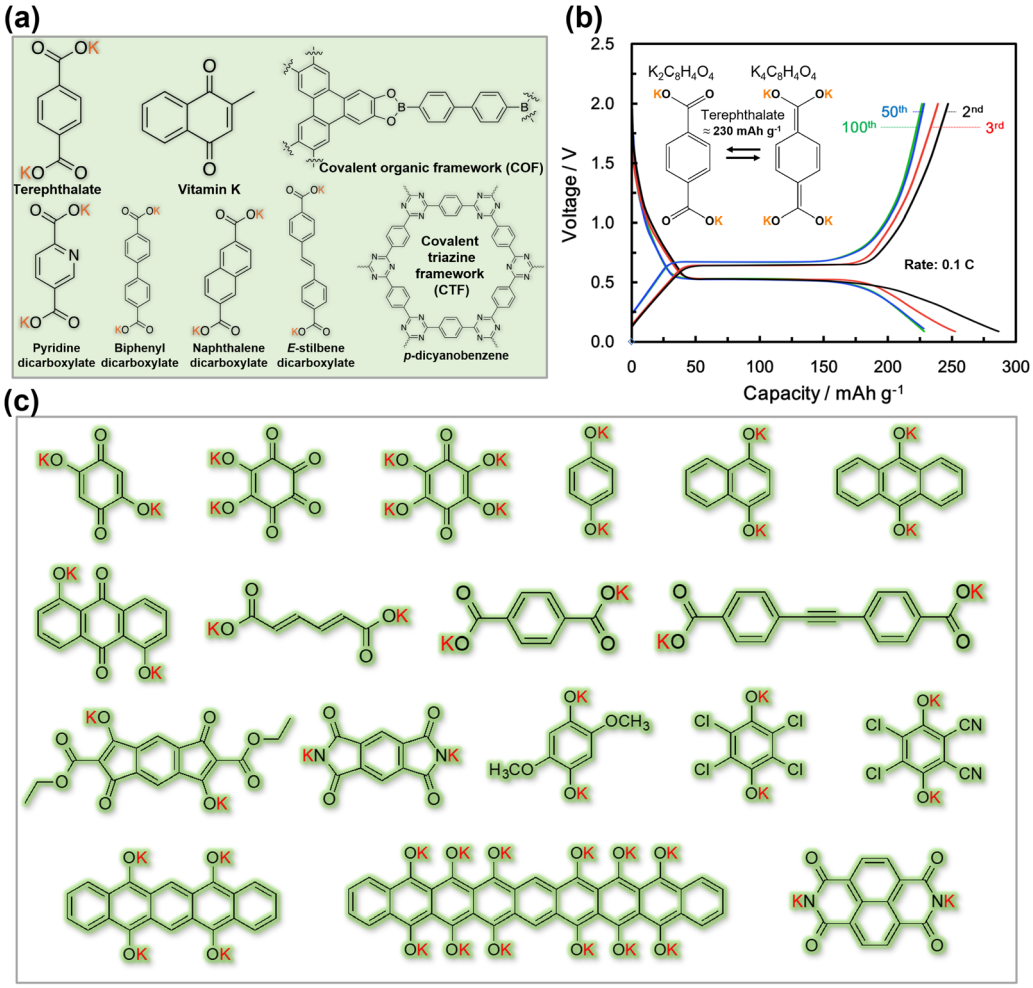

Fig. 27 (a) Representative organic moieties that have been explored as anode materials for potassium-ion batteries. (b) Voltage-capacity profiles of potassium terephthalate ($K_2C_8H_4O_4$) demonstrating good cyclability and rate performance. (c) Exemplars of new carboxylate organic compounds that can be explored as anode materials for potassium-ion batteries. Figure (b) reproduced from ref. 372 with permission. Copyright 2017 Royal Society of Chemistry.

electrochemical K^+ insertion/extraction in graphite, a plethora of electrolytes have been subjected to thorough investigation to unveil their physicochemical properties.[36,54,383,395–399] To date, an array of electrolyte systems has been extensively studied, encompassing organic-solvent-based electrolytes, ionic liquid electrolytes, aqueous electrolytes, and solid-state electrolytes. Notably, research endeavours have predominantly concentrated on organic liquid electrolytes.

Amongst the potassium salts employed in organic-solvent-based electrolytes, noteworthy candidates include potassium trifluoromethanesulphonate (KCF_3SO_3), potassium perchlorate ($KClO_4$), potassium tetrafluoroborate (KBF_4), potassium bis(trifluoromethylsulphonyl)imide (typically abbreviated as KTFSI, KTf_2N or KTFSA), potassium bis(fluorosulphonyl)imide (KFSI, Kf_2N or KFSA), potassium hexafluorophosphate (KPF_6), potassium (3-methoxypropyl)((trifluoromethyl)-sulphonyl)imide (abbreviated as KMPSA), potassium bis(2-(2-(2-methoxyethoxy)-ethoxy)ethyl) phosphate (KTEEP), potassium (bis(2-(2-ethoxy)-ethoxy)ethyl) phosphate (KDEEP), and more recently potassium hexafluoropropane-1,3-disulfonimide (KHFDF).[400] Notably, the molar solubility of KPF_6, KTFSI, and KFSI salts in organic solvents (Fig. 29a), suchlike propylene carbonate (PC), far exceeds that of $KClO_4$ and KBF_4, both of which at room temperature exhibit almost insolubility in PC solvent. Moreover, the pronounced interactions between BF_4^- and K^+ detrimentally impact the conductivity of KBF_4-based electrolytes, rendering them less suitable. Similarly, $KClO_4$ is sparingly used due to safety concerns pertaining to the reduction of ClO_4^- ions. Thus, it can be inferred that KBF_4 and $KClO_4$ are not ideal potassium salts for practical KIBs. It is pertinent to note that commonly utilised potassium salts typically entail fluorinated anions, as the electron-withdrawing attributes of fluorine atoms and the delocalised charge of the anions engender high solubility of these salts in organic non-aqueous (aprotic) solvents. Table 2 shows the physicochemical properties of representative potassium salts utilised in KIB electrolytes.[54,382]

Imides, such as KTFSI and KFSI, have garnered considerable traction owing to their exceptional solubility in both ether and

Open Access Article. Published on 04 dicembre 2023. Downloaded on 11/06/2026 17:40:22.
This article is licensed under a Creative Commons Attribution-NonCommercial 3.0 Unported Licence.

Table 2 Physicochemical properties of representative potassium salts for potassium-ion battery electrolytes[54,382]

Potassium salt	Decomposition temperature (°C)	Conductivity (mS cm^{-1}) (room temperature)	Solubility	Cost	Toxicity
$KClO_4$	610	1.1	Hardly dissolves in propylene carbonate	Low	High
KBF_4	530	0.2	Hardly dissolves in propylene carbonate	Low	High
KPF_6	575	5.75	0.9 mol kg^{-1} in propylene carbonate	Low	Low
KCF_3SO_3	238.5	—	22 mol L^{-1}	High	Slight
$KN(SO_2F)_2$ (KFSI)	102	7.2	7.5 mol kg^{-1} in dimethoxyethane	High	Slight
$KN(CF_3SO_2)_2$ (KTFSI)	198–203	6.1	6 mol kg^{-1} in dimethoxyethane	High	Slight

ester solvents. Electrolytes based on KFSI or KTFSI have exhibited superior ionic conductivity and enhanced electrochemical stability compared to KPF_6-based electrolytes, thus positioning them as prospective candidates amongst mainstream electrolytes for KIBs. However, it should be noted that typical KTFSI-based and KFSI-based electrolytes exhibit severe corrosion on the aluminium current collector at high voltages, particularly exceeding 4.0 V. Additionally, the use of ether solvents renders the electrolytes more susceptible to decomposition at relatively low voltages owing to the elevated highest occupied molecular orbital energy levels of ether molecules, impeding their application in high-voltage full-cell designs. Fortunately, both challenges can be circumvented through the adoption of highly concentrated electrolytes[280] or the implementation of current collectors based on tungsten or titanium nitride, albeit acknowledging the potential cost implications.

Despite their relatively high ionic conductivity, KPF_6 salts suffer from certain drawbacks, including susceptibility to hydrolysis and inadequate thermal stability. Thus, achieving a delicate balance amongst these properties becomes imperative. Electrolytes comprising binary salts, such as KFSI–KPF_6 in organic solvents like ethylene carbonate (EC) and diethylene carbonate (DEC), have demonstrated the ability to amalgamate the benefits of both KPF_6 and KFSI salts,[401] resulting in enhanced stability at high potentials and reduced viscosity. Furthermore, the solid electrolyte interphase (SEI) formed in KPF_6/KFSI electrolyte exhibits reduced thickness compared to that formed in KPF_6 single-salt electrolytes, thus ensuring favourable cyclability when employing binary-salt electrolytes.[396] Notably, research on binary-salt electrolytes for KIBs remains an unexplored territory, offering ample opportunities for further investigation and advancements.

Electrolyte optimisation strategies, such as the incorporation of additives like fluoroethylene carbonate (FEC), trimethylene sulphate,[402] ethylene sulphate, potassium difluorophosphate, vinylene carbonate, sulphate esters of 1,3,2-dioxathiolane 2,2-dioxide,[402,403] dimethylsulfamoyl fluoride,[404] 1,3-propane sultone,[403] butylene sulphite[403] amongst others, hold immense potential to enhance the electrochemical performance of potassium-ion battery (KIB) electrolytes. Despite their higher cost, FEC stands out as a dominant additive for high-voltage battery electrolytes, attributed to its robust oxidation resistance owing to the fluorine-containing structure. To fully exploit the potential benefits of various additives, particularly FEC, in the formation of SEI and the manipulation of K^+ solvation structures, further in-depth exploration is warranted. Numerous challenges persist in the quest to develop an ideal organic liquid electrolyte with exemplary reliability. Future research efforts can be directed towards controlling and mitigating side reactions between the electrolyte and potassium metal.[405] Additionally, the mechanism behind SEI layer formation and charge transfer kinetics in KIBs remains enigmatic, necessitating extensive investigations in the forthcoming studies. Given the high reactivity of potassium, the integration of advanced characterisation techniques, such as *in situ* transmission electron microscopy (TEM), cryo-electron microscopy, and *in situ* magnetometry,[406] in conjunction with computation, can offer valuable insights into the charge transfer kinetics, microstructures, and reaction mechanism of SEI.[407] Moreover, the advent of cutting-edge technologies like machine interaction, artificial intelligence, and big data analysis holds the potential to drive further advancements in electrolyte chemistry and the elucidation of SEI phenomena, as well as the development of compatible electrode materials for KIBs. By harnessing these multidisciplinary approaches, the path towards achieving highly efficient and reliable potassium-ion batteries can be substantially expedited.

A significant challenge faced by KIBs revolves around safety concerns, particularly in light of the negative publicity surrounding battery safety issues. However, the development of a reliable and safe KIB, even at a cost-to-performance ratio lower than LIBs, holds the potential to establish dominance in certain applications. One approach to ensure the safety and thermal stability of liquid aprotic electrolytes for KIBs involves the incorporation of functional additives such as flame retardants ((Fig. 29b)),[408–413] for example, triethylphosphate ($(C_2H_5)_3PO_4$), trimethylphosphate ($(CH_3)_3PO_4$), tributylphosphate ($(C_4H_9)_3PO_4$) and tris(2,2,2-trifluoroethyl) phosphate ($(C_6H_6)F_9PO_4$), into the organic solvents. This strategy helps to guarantee improved safety without compromising performance. Alternatively, ionic liquids present promising attributes in terms of better thermodynamic stability and wider electrochemical stability windows,[414] in comparison to both organic liquid and aqueous electrolytes. Furthermore, ionic liquids demonstrate exceptionally high solubilities with a diverse range of organic, inorganic, and polymer materials. This unique property enables the amalgamation of various cations and anions, thus bestowing unparalleled flexibility in the design of KIBs for a myriad of applications. However, the widespread adoption of ionic liquid-based electrolytes for KIBs has been hindered by their high cost. Despite this challenge, there have been some reports on the utilisation of KFSI- and KTFSI-based

© 2024 The Author(s). Published by the Royal Society of Chemistry

Open Access Article. Published on 04 dicembre 2023. Downloaded on 11/06/2026 17:40:22.
This article is licensed under a Creative Commons Attribution-NonCommercial 3.0 Unported Licence.

Table 3 Physicochemical properties of representative ionic liquid electrolytes for potassium-ion battery.[5,424] Electrochemical stability tests of representative ionic liquid (for instance, 0.5 M KTFSI in $Pyr_{13}TFSI$) are shown in Fig. 28

Concentration (M)	Potassium salt	Ionic liquid	Conductivity (room temperature) (mS cm^{-1})	Decomposition temperature (°C)	Electrochemical stability window (V)
0.5	KTFSI	$Pyr_{H4}TFSI$	1.49	300	4
1	KFSI	$Pyr_{13}FSI$	4.8	307	5.72
0.5	KTFSI	$Pyr_{14}TFSI$	7.96	350	6
0.5	KTFSI	$Pyr_{13}TFSI$	2.1	417	6.01

ionic liquid electrolytes, such as 1 M KFSI in $Pyr_{13}FSI$, 0.5 M KTFSI in $Pyr_{13}TFSI$, and 0.3 M KTFSI in $Pyr_{14}TFSI$, amongst others.[5,72,415–423] For brevity, 1-butyl-3-methylpyrrolidinium and 1-propyl-3-methylpyrrolidinium have been abbreviated as Pyr_{14} and Pyr_{13}, respectively. Table 3 shows the physicochemical properties of representative ionic liquid electrolytes for KIBs.[5,424] 0.5 M KTFSI in $Pyr_{13}TFSI$ ionic liquid demonstrates large electrochemical window, as shown in the cyclic and linear sweep voltammograms (Fig. 28a). Moreover, 0.5 M KTFSI in $Pyr_{13}TFSI$ ionic liquid shows stable deposition and dissolution of potassium with relatively low overvoltage (Fig. 28b).

Fig. 29c illustrates the configuration of typical ionic liquids, solvents, and salts integrated into the design of liquid-based electrolytes.[396,425] Ionic liquids investigated for use in KIBs predominantly employ pyrrolidinium cations, coupled with imide anions such as FSI^- and $TFSI^-$. The lowered melting point of these ionic liquids can be attributed to the asymmetry of their ions, which hinders the compact arrangement of the ions, thus imparting them with remarkable thermal stability. However, it is noteworthy that pyrrolidinium-based ionic liquids often exhibit high viscosity. In contrast, quaternary ammonium-based ionic liquids have displayed enhanced electrochemical stability when utilised in LIBs, yet their potential as electrolytes for KIBs remains largely unexplored.[426]

The drawbacks associated with ionic liquids can potentially be offset by the additional functional capabilities they offer when utilised in KIBs. These benefits include a wide applicable temperature range, high safety, and exceptional durability. One area of focus for future research is to address the cost issues related to ionic liquid electrolytes. An effective approach for cost reduction involves exploring more economical reaction pathways, exemplified by the implementation of ion exchange resins as an alternative to conventional batch metathesis reactions.[427] This methodological shift has demonstrated its efficacy in enhancing the cost-efficiency of deploying ionic liquids, particularly within sectors such as timber processing. A similar strategy can also be applied to the scalable design of ionic liquids for batteries. Another strategy to curtail the cost involves blending ionic liquids with organic solvents like propylene carbonate, which may meet the cost requirements whilst preserving the desirable properties of the ionic liquid electrolytes. Additionally, exploring the use of potassium single cation molten salts, which exclusively contain K^+ as the cationic species, presents another avenue to lower the cost of employing pyrrolidinium-based ionic liquids. However, it is essential to note that potassium single cation molten salts generally operate at elevated temperatures, necessitating further developments in room-temperature single cation molten salts. Recent advancements have shown that single cation molten salts composed of an almost equimolar mixture of potassium (fluorosulphonyl)(trifluoromethylsulphonyl)amide (KFTA) and potassium bis(fluorosulphonyl)amide (KFSA) exhibit low melting points of 67 °C.[428] This demonstrates the feasibility of preparing single cation molten salt electrolytes that can function at room temperature with potential adjustments to the potassium salt compositions (Fig. 30a). In fact, it has been

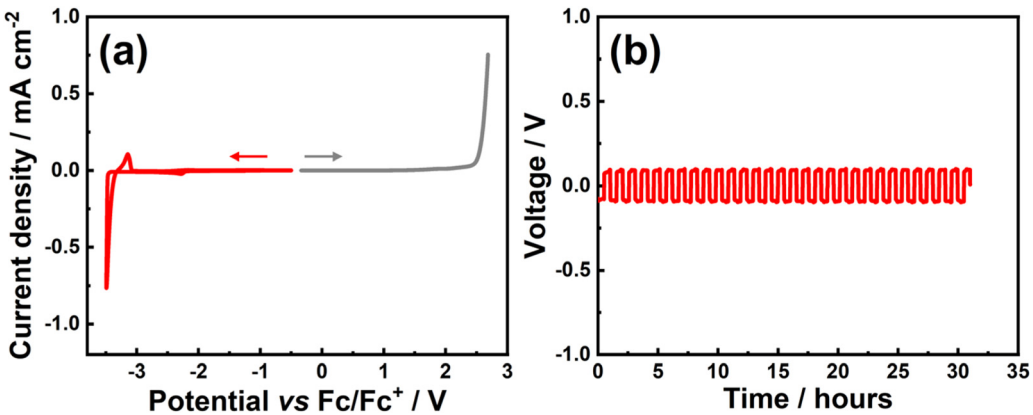

Fig. 28 Electrochemical stability of 0.5 M KTFSI in $Pyr_{13}TFSI$ ionic liquid at 298 K. (a) Cyclic and linear sweep voltammograms conducted at a scan rate of 1 mV s^{-1} to assess the cathodic (in red) and anodic (in grey) limit. (b) Voltage profiles during galvanostatic deposition and dissolution of potassium in potassium symmetric cells performed at a current density of 6.4 μA cm^{-2}. Figures adapted from ref. 5 with permission. Copyright 2019 Wiley-VCH.

Open Access Article. Published on 04 dicembre 2023. Downloaded on 11/06/2026 17:40:22.
This article is licensed under a Creative Commons Attribution-NonCommercial 3.0 Unported Licence.

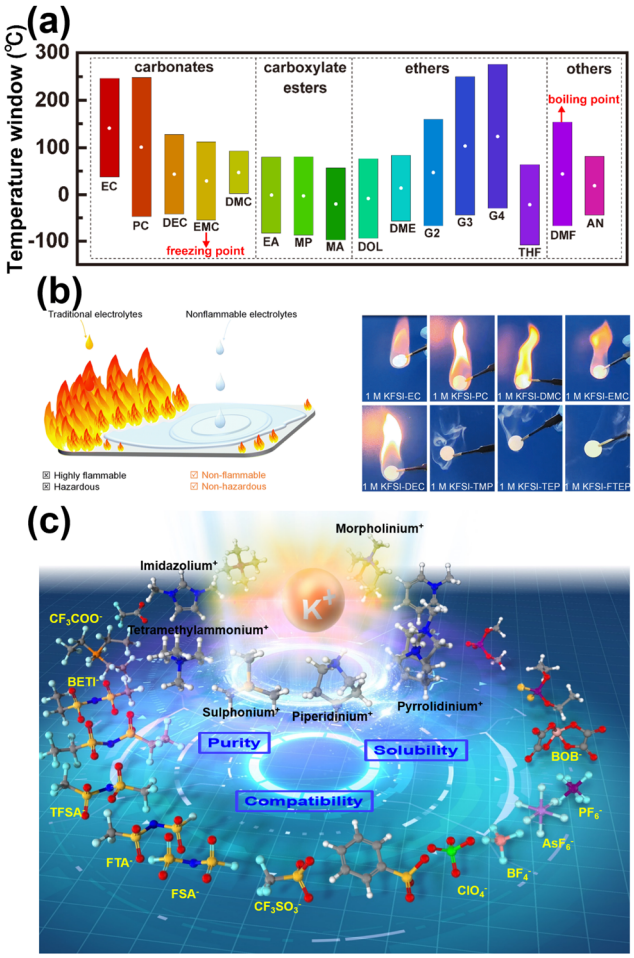

Fig. 29 (a) Representative organic solvents utilised in the formulation of liquid electrolytes for KIBs. (b) A visual representation depicting the contrasting hazardous attributes between non-flammable electrolytes based on phosphate esters and conventional/traditional electrolytes composed of ethers and carbonates. Experimental examination involving flame tests conducted on diverse electrolytes is also shown. (c) Selection of organic and inorganic salts for the purpose of formulating ionic liquids for KIBs. Ionic liquids, comprising of organic cations like piperidinium, imidazolium, pyrrolidinium, amongst others, are conjoined with either organic or inorganic anions such as ClO_4^-, PF_6^-, and BF_4^-. Notably, organic or inorganic anions are represented in yellow, whilst organic cations are denoted in black. During the formulation of appropriate ionic liquids for high-voltage operation, considerations encompassing factors like salt purity, solubility, and compatibility with the electrode materials are imperative. Abbreviations: ethylene carbonate (EC), propylene carbonate (PC), diethyl carbonate (DEC), ethyl methyl carbonate (EMC), dimethyl carbonate (DMC), ethyl acetate (EA), methyl propionate (MP), methyl acetate (MA), 1,3-dioxolane (DOL), 1,2-dimethoxyethane (DME), diglyme (G2), triglyme (G3), tetraglyme (G4), tetrahydrofuran (THF), *N*,*N*-dimethylformamide (DMF), acetonitrile (AN), trimethyl phosphate (TMP), triethyl phosphate (TEP), tris(2,2,2-trifluoroethyl) phosphate (FTEP). Figures reproduced with permission. Figure (b) reproduced from ref. 411 with permission. Copyright 2023 Royal Society of Chemistry. Figure (c) reproduced and adapted from ref. 257 Copyright 2021 Royal Society of Chemistry.

demonstrated that a combination of potassium bis(fluorosulphonyl)amide (KFSA) and potassium (3-methoxypropyl)((trifluoromethyl)sulphonyl)amide (KMPSA) can form a liquid state at remarkably low temperatures, as low as −13 °C.[429] This discovery represents the emergence of a room-temperature ionic liquid exclusively composed solely of K^+ cations, marking a significant milestone in the field. Anticipated future efforts are expected to be dedicated to mitigating the limitations associated with ionic liquids, including their elevated viscosities and relatively higher costs in comparison to conventional organic solvents. Additionally, it is worth noting that elevated temperatures can potentially unlock the latent performance of certain ionic liquids that exhibit suboptimal ionic conductivities at room temperature.

Aqueous electrolytes (Fig. 30b), utilising water as the solvent along with cost-effective salts like nitrates and sulphates, offer significant cost reduction and inherent safety advantages compared to non-aqueous electrolytes.[431–433] However, their applicability in organic electrolytes is limited due to their extreme insolubility in organic solvents. One of the key advantages of aqueous electrolytes over non-aqueous counterparts is their high ionic conductivity, contributing to excellent power density. Leveraging these advantages, aqueous KIBs have the potential to serve as high-power energy storage systems for grid-scale applications. Nonetheless, a notable disparity exists between aqueous KIBs and organic liquid electrolyte-based KIBs concerning energy density. The relatively lower energy density of aqueous KIBs primarily stems from the narrow electrochemical stability windows of aqueous electrolytes, resulting in limited working voltage. Conventionally, the electrochemical stability windows of typical aqueous electrolytes, thermodynamically restricted to 1.23 V, are narrower compared to those of organic electrolytes. Beyond this electrochemical stability window, water electrolysis gives rise to the evolution of oxygen or hydrogen, or both, adversely impacting the performance of aqueous KIBs. Moreover, the phase transition of water due to variations in temperature imposes limitations on the application of aqueous KIBs under elevated or sub-zero temperatures, consequently restricting the operational temperature windows of aqueous electrolytes. To overcome these challenges, it becomes imperative to explore novel water-in-salt-electrolytes (abbreviated as WiSE or WiS) that exhibit high electrode compatibility and ensure a wide electrochemical stability range.[434–438] By delving into WiSE technology, promising solutions can be envisioned to enhance the energy density and expand the temperature operability of aqueous KIBs, thereby propelling their practical adoption for diverse energy storage applications.

The advancement of all solid-state KIBs represents a burgeoning field,[440–442] inspired by the progress seen in LIB research, offering inherent safety benefits. A recent breakthrough involves an all-solid-state battery architecture comprising Prussian blue $K_xFe[Fe(CN)_6]$ as the cathode, K–C composite as the anode, and β/β''-Al_2O_3 solid electrolyte.[439] This design has demonstrated remarkable attributes, showcasing high energy density, excellent capacity retention, and satisfactory electrochemical performance across a wide temperature range of −20 °C to 120 °C (Fig. 31).[439] Despite the existence of polymer electrolytes exhibiting high K^+ conductivity, the

© 2024 The Author(s). Published by the Royal Society of Chemistry

Open Access Article. Published on 04 dicembre 2023. Downloaded on 11/06/2026 17:40:22.
This article is licensed under a Creative Commons Attribution-NonCommercial 3.0 Unported Licence.

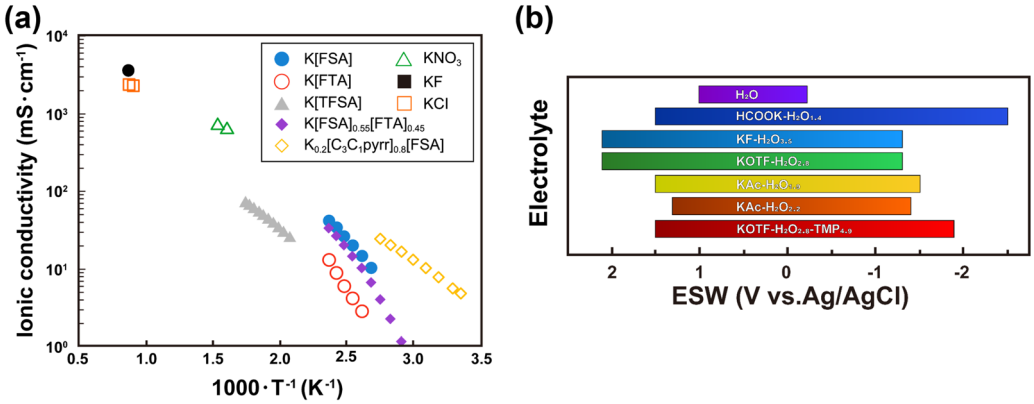

Fig. 30 (a) Arrhenius plot showcasing the ionic conductivity for chosen potassium single cation molten salts and room-temperature ionic liquids. Abbreviation: *N*-methyl-*N*-propylpyrrolidinium (C_3C_1pyrr). (b) Electrochemical stability window (ESW) of representative electrolytes for aqueous KIBs. Abbreviation: potassium acetate (KAc), potassium trifluoromethanesulphonate (KOTF). Figure (a) reproduced from ref. 428 with permission. Copyright 2020 American Chemical Society. Figure (b) reproduced from ref. 430 with permission. Copyright 2023 Wiley-VCH.

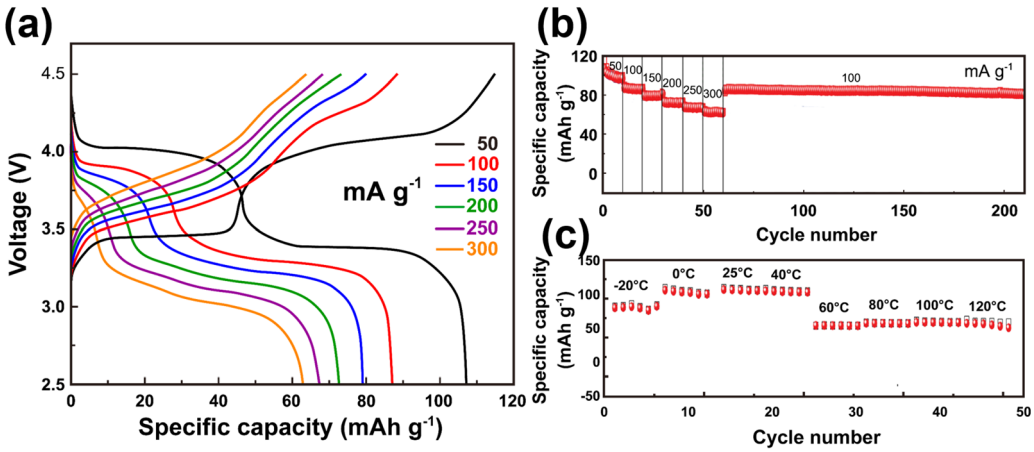

Fig. 31 Electrochemical performance of an all-solid-state potassium battery setup comprising Prussian blue $K_xFe[Fe(CN)_6]$ as cathode, K–C composite as the anode and β/β″-Al_2O_3 as solid electrolyte. (a) Voltage-capacity profiles at various current densities. (b) Cycle performance at various current densities. (c) Cycle performance at various temperature ranges. Figures reproduced with permission.[439] Copyright 2023 Wiley-VCH.

literature on solid-state potassium-ion conductors remains relatively scarce.[443–476] As a result, the current focus of research revolves around enhancing the ionic conductivity of solid-state potassium-ion conductors. However, it is essential to note that other pivotal electrochemical properties often remain insufficiently characterised, including electrochemical stability, ion selectivity, mechanical properties, and assembly techniques. As the field of all solid-state KIBs continues to progress, further investigations into these unexplored areas hold promise for bolstering the performance and reliability of these advanced energy storage systems. A comprehensive understanding of these key properties will pave the way for the development of safer, more efficient, and practical all-solid-state KIB technologies.

Indeed, the development of solid-state electrolytes has been a pivotal direction in the advancement of LIBs, and it is anticipated that a similar trend will unfold in the domain of KIBs.[444] (Fig. 32a–c) show the ionic conductivity data of various solid-state K^+ conductors, as documented within the existing literature. Notably, some of these materials (such as KSi_2P_3, β/β″-Al_2O_3, $K_{3-2x}Ba_xSbSe_4$ (x = 0, 0.2, 0.3 and 0.4), $K_{2+x}Zr_{1-x}Y_xCl_6$ (x = 0–1), *etc.*) exhibit appreciable ionic conductivity,[452,456–458,460–472,477–480] even under ambient room temperature conditions. Given the relatively large ionic radius of K^+, facilitating K^+ mobility within solid materials presents a significant challenge. To expedite research progress in this area, a synergistic approach that combines theoretical computations for materials screening with experimental studies is envisaged.[191] Such an integrated strategy can help identify suitable solid-state electrolytes with diverse dimensional frameworks (1D, 2D, or 3D) that exhibit high K^+ ionic conductivity.[481–487] However, similar to the challenges faced in LIBs and sodium-ion batteries, most solid electrolytes for KIBs may suffer from low ionic conductivity and substantial interphasial resistance with the electrodes. To overcome these hurdles, ionogel-electrolyte membranes, which encompass solid matrices combined with ionic liquids,

Open Access Article. Published on 04 dicembre 2023. Downloaded on 11/06/2026 17:40:22.
This article is licensed under a Creative Commons Attribution-NonCommercial 3.0 Unported Licence.

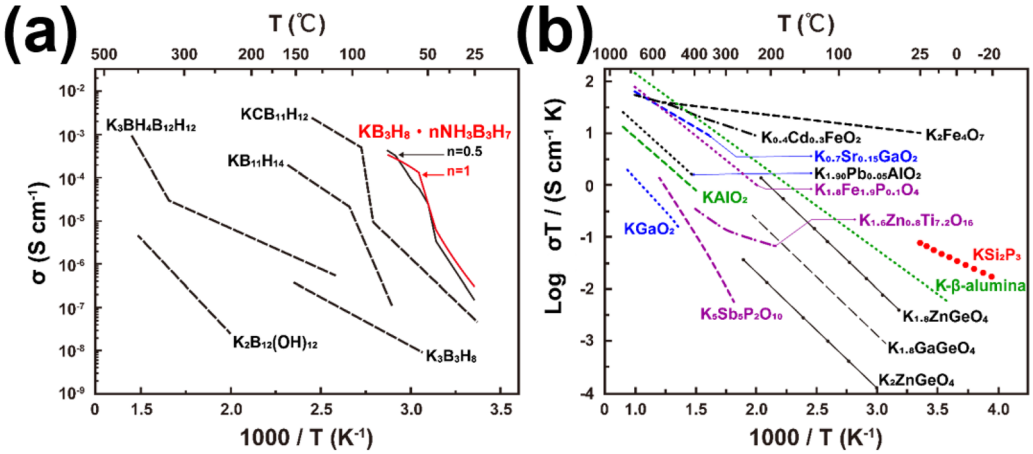

Fig. 32 Exemplars of inorganic compounds that can be utilised as solid-state potassium-ion conductors. (a) Borohydrides.[452] (b) Oxides (including cristoballite-type polyanion frameworks), antiperovskite phosphides and sulphides. Graph plotted from data derived from ref. 456–458, 460–472, 477 and 478. Figure (a) reproduced from ref. 425 with permission. Copyright 2022 American Chemical Society.

offer a promising avenue for exploration. These ionogel-electrolyte membranes possess desirable characteristics, including non-flammability, non-volatility, and superior electrochemical and physicochemical properties.[488] By leveraging such innovative materials, advancements in the development of solid-state electrolytes for KIBs are poised to accelerate, leading to enhanced performance and safety in potassium-ion battery technologies. Nevertheless, potassium metal's extreme reactivity ($1s^2 2s^2 2p^6 3s^2 3p^6 4s^1$) can raise safety issues when utilised as anode material. Designing all-solid-state KIBs using anode materials

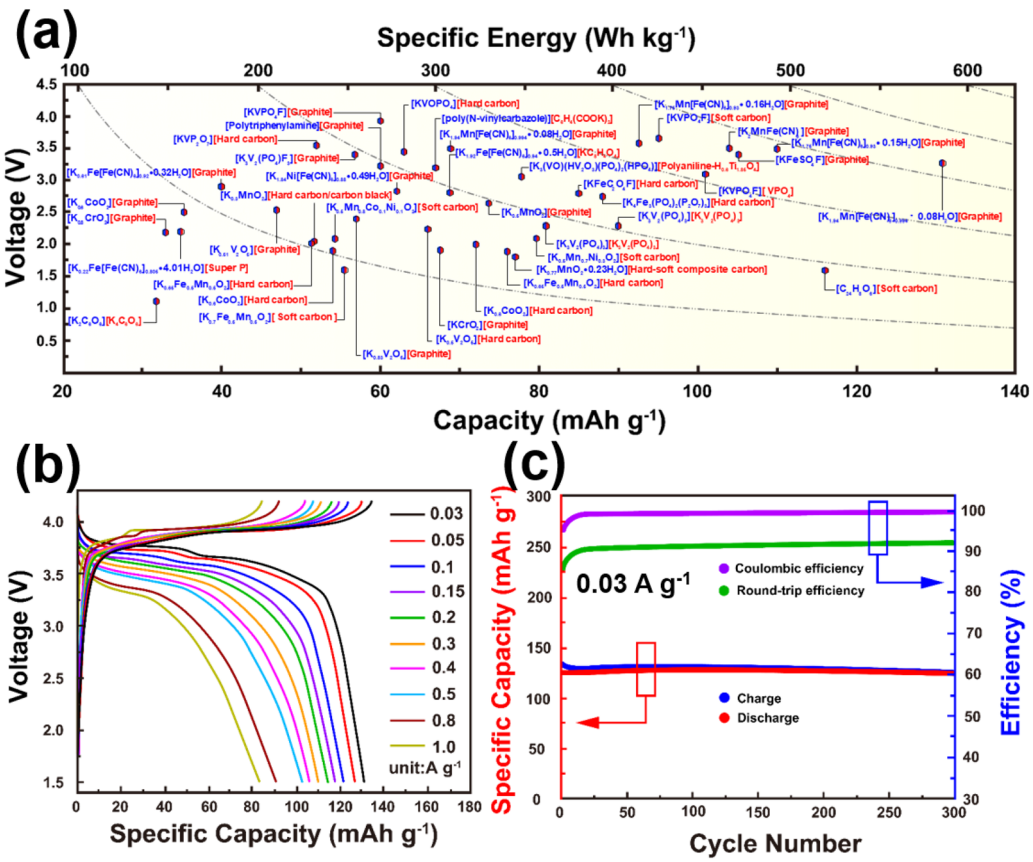

Fig. 33 (a) Ragone plot showing the energy densities, at a material level, attained by representative KIB full cells reported in existing literature. Cathode and anode materials are shown in blue and red, respectively. (b) Rate performance of a KIB full cell comprising $K_2MnFe(CN)_6$ as cathode and graphite as anode. (c) Corresponding cycle performance. Figures (b) and (c) reproduced and adapted from ref. 126 with permission. Copyright 2021 Springer Nature.

 © 2024 The Author(s). Published by the Royal Society of Chemistry

Open Access Article. Published on 04 dicembre 2023. Downloaded on 11/06/2026 17:40:22.
This article is licensed under a Creative Commons Attribution-NonCommercial 3.0 Unported Licence.

such as Sn composites, graphite or pre-potassiated graphite[53] has the potential to showcase their promise, mirroring the achievements seen in all-solid-state LIBs.

3.3 Full cell design

Various cathode materials have been employed in the design of high-voltage KIBs. Several high-performance KIB full cells have been developed, primarily falling within the following main categories: (i) non-aqueous batteries, exemplified by configurations such as $K_2Mn[Fe(CN)_6]$ cathode//1 M KFSA in $Pyr_{13}FSA$ ionic liquid electrolyte//graphite anode;[281,489] (ii) dual-ion batteries, featuring arrangements like graphite cathode//5 M KFSA in ethylene carbonate/dimethylene carbonate electrolyte//graphite anode;[490] (iii) aqueous batteries, comprising $K_2FeFe(CN)_6$ cathode//21 M KCF_3SO_3 water-in-salt electrolyte//$KTi_2(PO_4)_3$ anode;[491,492] (iv) all-organic flexible batteries, consisting of, for instance, potassium terephthalate ($K_4C_8H_4O_4$) as anode// 1 M KPF_6 in dimethoxyethanne as electrolyte//[N,N′-bis(2-anthraquinone)]-perylene-3,4,9,10-tetracarboxydiimide as an insoluble organic cathode;[493] and (v) all-solid-state batteries, which encompass combinations like $K_2FeFe(CN)_6$ cathode// $K_2Fe_4O_7$ solid–electrolyte//K metal anode.[454] Notably, non-aqueous KIB battery prototypes have exhibited energy densities comparable to those of LIBs, as illustrated in Fig. 33a. In particular, Fig. 33b and c demonstrate the electrochemical performance of a high-energy-density KIB full cell, employing graphite as the anode and Prussian blue ($K_2MnFe(CN)_6$) as the cathode, revealing minimal capacity decay and remarkable rate capability.[126] Fig. 34 further demonstrates the electrochemical performance of a KIB full cell, employing graphite as the anode and $KFeSO_4F$ polyanion-based compound as the cathode, revealing good rate capabilities along with noteworthy capacity retention following prolonged (dis)charge cycles.[14] These electrochemical performances substantiate the potential of KIBs as promising, high-performance, and cost-effective alternatives to traditional LIBs.

The operation of a potassium dual-ion battery involves the simultaneous insertion of K^+ ions into the anode and anions (such as ClO_4^-, PF_6^-, FSI^-, $TFSI^-$, $FTFSI^-$, $CF_3SO_3^-$, $BETI^-$, BF_4^-, etc.) into the cathode during the charging process. Subsequently, during the discharging process, both the anions and K^+ cations are extracted from the cathode and anode, returning to the electrolyte to combine once again. Remarkably, the high working voltage (>4.5 V) of potassium dual-ion batteries can reach as high as 5.0 V, depending on the specific anion employed.[422,490,494–499] Beyond their attainable high-voltage characteristics, potassium dual-ion batteries possess the advantages of being low-cost and delivering high capacities with excellent cyclability, rendering them sustainable high-energy-density battery systems. The most extensively researched dual-ion battery configurations utilise carbon materials (such as graphite) as both the cathode and anode. Fig. 35 illustrates the electrochemical performance of a potassium dual-ion battery featuring K metal as the anode, ionic liquid (1 M KFSI in $Pyr_{13}FSI$) as the electrolyte, and graphite as the cathode. To mitigate severe corrosion, typically observed in KFSI-based electrolytes at high voltages (>4.0 V),

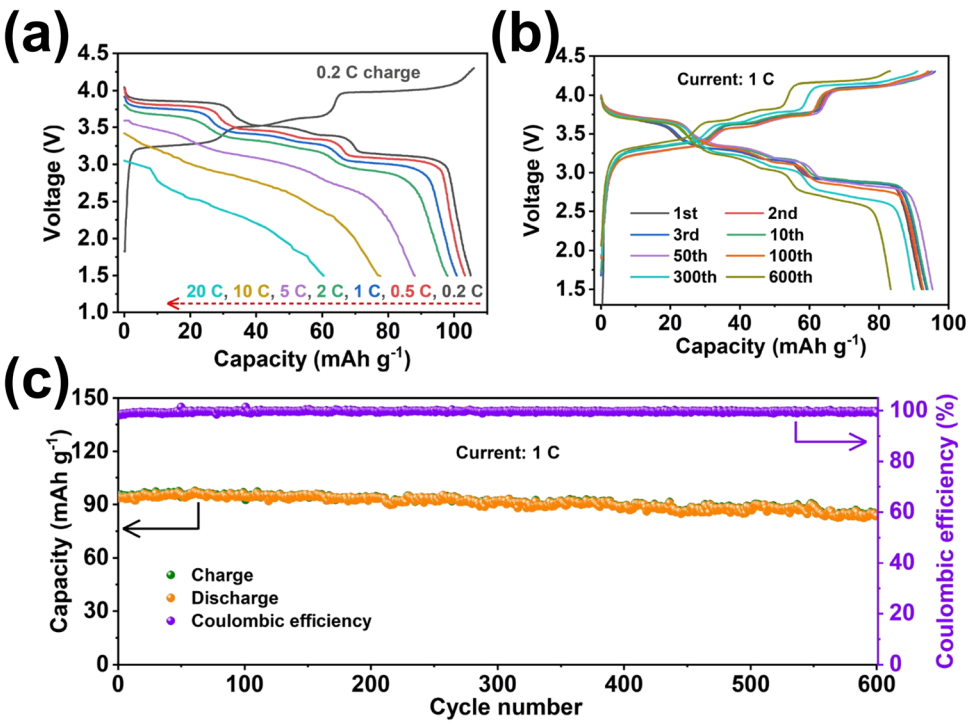

Fig. 34 Electrochemical performance of a KIB full cell, comprising $KFeSO_4F$ as cathode and graphite as anode material. (a) Voltage-capacity plots showing the rate performance. (b) Rate performance at a current density commensurate to 1C (1C = 127.6 mA g^{-1}). (c) Cycle performance. Figures reproduced from ref. 14 with permission. Copyright 2022 Elsevier.

Open Access Article. Published on 04 dicembre 2023. Downloaded on 11/06/2026 17:40:22.
This article is licensed under a Creative Commons Attribution-NonCommercial 3.0 Unported Licence.

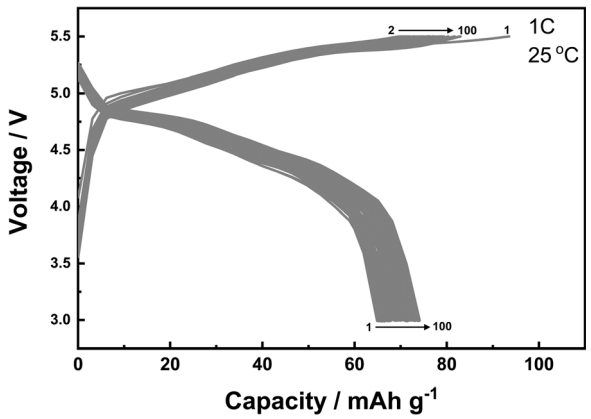

Fig. 35 Voltage-capacity profiles of a dual-ion battery setup, comprising graphite as the cathode and potassium metal as anode. A 1 M KFSI in $Pyr_{13}FSI$ ionic liquid was used as the electrolyte. Tungsten foils were used as the current collectors to avert corrosion typically observed in KFSI-based electrolytes. FSI^- can intercalate into graphite to form $C_6[FSI]_{0.5}$,[490] thus attaining a maximum intercalation capacity of 186 mA h g^{-1}. (1C = 186 mA g^{-1}).

on the aluminium current collector, tungsten foil was employed as the current collector in this particular system.

Demonstrations of KIBs prototypes with high voltage, resulting in elevated energy density and high power output, show promising results. KIBs offer a notable advantage over LIBs and sodium-ion batteries, owing to the wealth of commercial knowledge and extensive research derived from the widespread commercialization and implementation of LIBs, along with the ongoing investigation into sodium-ion batteries. Particularly, the expertise in high-voltage cathode materials discovery and characterisation from previous research will significantly expedite the material development and prototyping processes for high-performance KIBs. Learning from past mistakes, both commercial and academic, presents an opportunity to advance KIB technology further. The pursuit of practical high-performance KIB materials is currently employing a cornucopia of ideas, philosophies, and strategies, ranging from drawing parallels with LIB and sodium-ion battery materials to computation-guided screening and direct syntheses of novel functional materials. The vast compositional space of electrode and electrolyte materials applicable to realising KIB full cells underscores the importance of leveraging knowledge derived from LIBs and sodium-ion batteries to make informed decisions on material selection and chemical systems to be pursued by researchers. An under-explored area in KIB research remains the cost analyses[500] and environmental impact assessment. Although limited in scope for nascent KIBs, life-cycle assessment (LCA) proves to be a valuable tool for exploring potential combinations of high-energy-density electrodes, compatible electrolyte materials, and production processes with minimal environmental impact, ultimately leading to lower costs. Fig. 36 provides a succinct overview of the methodologies employable in research concerning potassium-ion batteries.

Furthermore, it is imperative to address practical considerations in the evaluation of KIB prototypes.[501] Currently, relying solely on material-level and half-cell tests for performance assessment proves to be inconsistent and inadequate. Assembling full-battery devices introduces greater complexity, making it essential to recognise that evaluating electrodes at the half-battery level is tantamount to overestimating their practical application. Crucial details relating to battery assembly are often overlooked during experiments, such as the mass ratio of inactive components (current collectors, binders), electrolyte loading, electrode thickness, and active material loading. Consequently, a shift in focus towards performance evaluation based on KIB full battery measurements through configuration

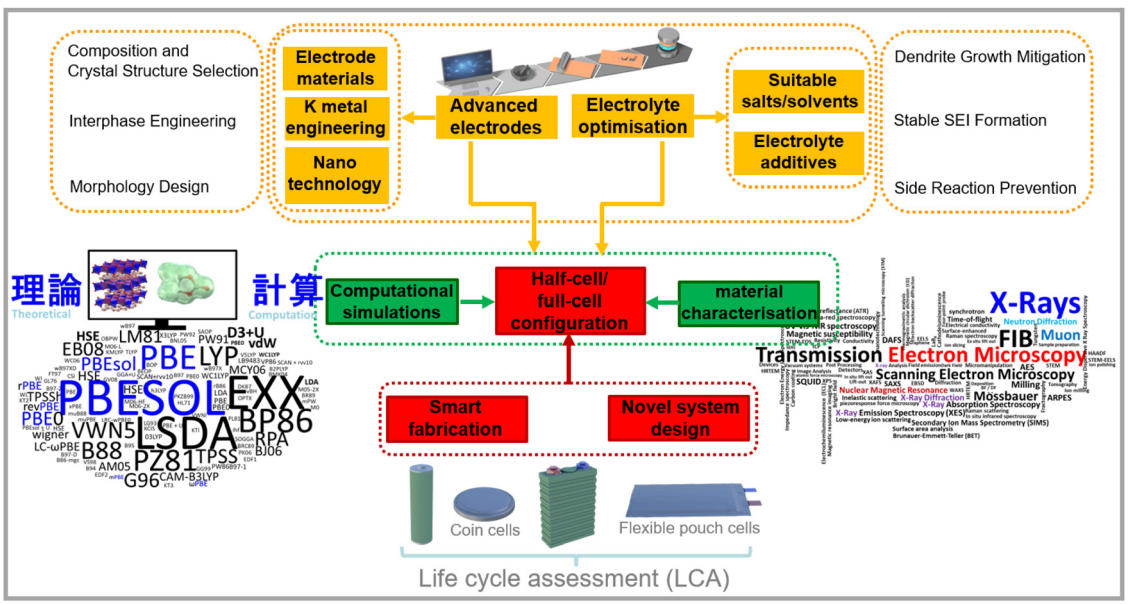

Fig. 36 Overview of the methodologies employed in research concerning potassium-ion batteries. Figure adapted from ref. 6 with permission. Copyright 2019 American Association for the Advancement of Science.

© 2024 The Author(s). Published by the Royal Society of Chemistry

Open Access Article. Published on 04 dicembre 2023. Downloaded on 11/06/2026 17:40:22.
This article is licensed under a Creative Commons Attribution-NonCommercial 3.0 Unported Licence.

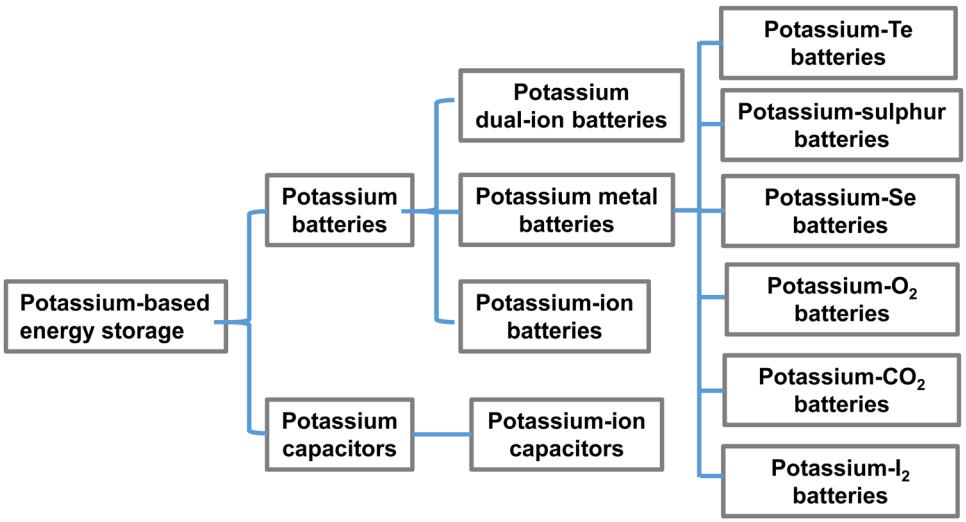

Fig. 37 Diversity of energy storage systems based on potassium-ion technology. Such diversification has the potential to facilitate the expansion into a variety of distinct target markets.

optimisation becomes necessary. This approach would provide a more comprehensive understanding of their real-world capabilities and limitations. Notably, early demonstrations of high-energy density KIB full cells and other potassium battery variants (Fig. 37) demonstrate promising potential for this sustainable battery class, which may serve as a captivating addition to the future energy storage landscape. In summary, the exciting prospects of KIBs and related potassium-based batteries lie in their potential contributions to a sustainable and diversified energy storage mix in the future. However, ensuring accurate performance evaluation at the full-battery level is crucial to realising their true capabilities and optimising their practical application.

Anode and cathode material combinations, as detailed in laboratory-scale full-cell potassium-ion battery (KIB) configurations (several of which are illustrated in Fig. 33a), have undergone comprehensive assessment through a pragmatic lens, encompassing pouch cell design.[501] Notably, non-aqueous KIB configurations leveraging graphite as the anode material have been shown to exhibit a propensity for yielding high energy densities. The peak of energy density achievement particularly in non-aqueous KIBs at the pouch cell level has been reported to culminate at approximately 150.0 W h kg^{-1} (attained by employing $KVPO_4F$ as the cathode material and graphite as the anode material).[501] This significant metric is on

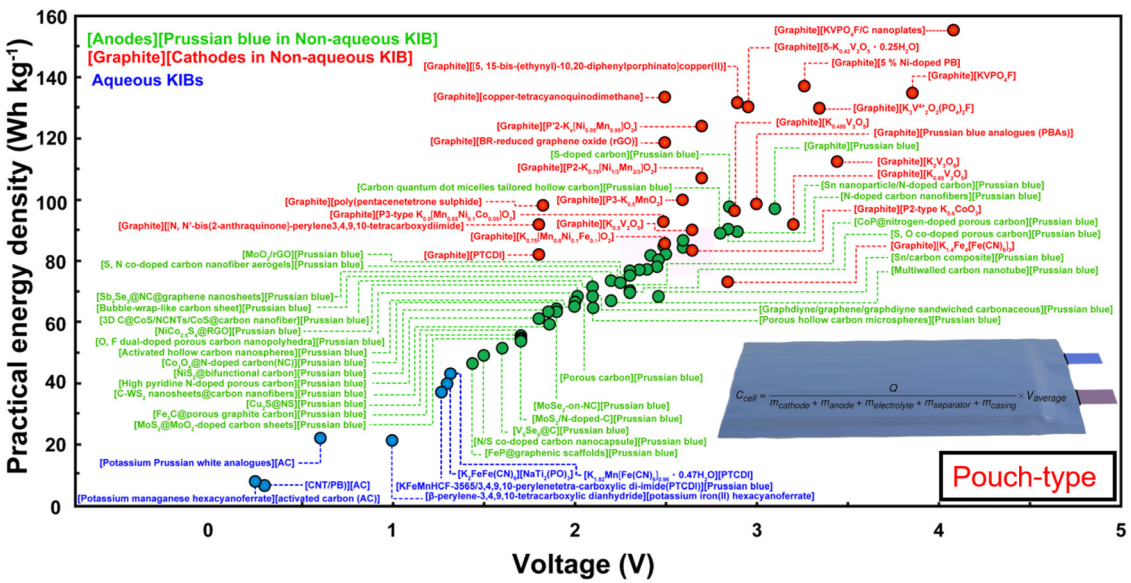

Fig. 38 Practical energy density projected based on reported KIB full cell material combinations. Graph plotted from data derived from ref. 501. In some instances, Prussian blue has been abbreviated as 'PB' for brevity's sake. Figure adapted with permission.[501] Copyright 2022 Springer Nature.

Open Access Article. Published on 04 dicembre 2023. Downloaded on 11/06/2026 17:40:22.
This article is licensed under a Creative Commons Attribution-NonCommercial 3.0 Unported Licence.

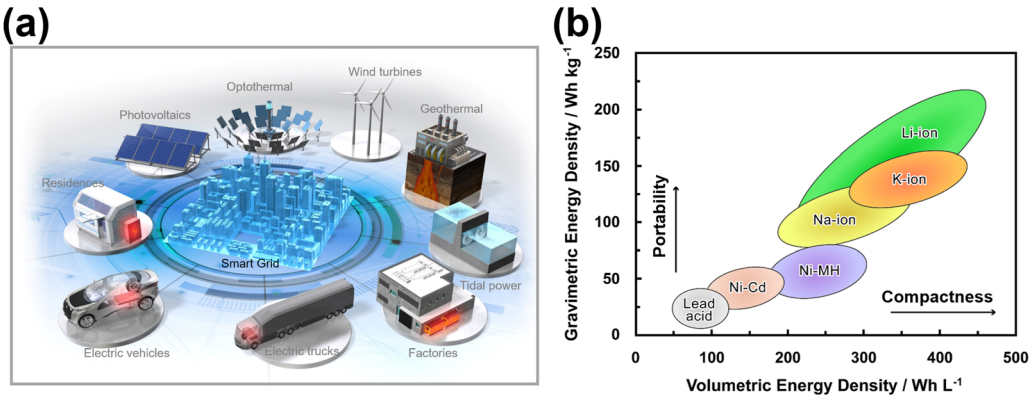

Fig. 39 (a) Applications envisioned for potassium-ion battery technology. Figure adapted from ref. 7 with permission. (b) Volumetric and gravimetric energy densities of rechargeable batteries. Figure adapted from ref. 124 with permission.

par with prevailing lithium-ion battery (LIB) cells, where lithium iron phosphate ($LiFePO_4$) serves as the cathode material and graphite as the anode material. The projected energy density enhances the potential for potassium-ion batteries to assert dominance within the mid- to low-tier market sectors, driven by their inherent cost-effectiveness. However, it should be acknowledged that the energy densities elucidated within the scope of laboratory-based cell configurations (such as those in Fig. 33a) lack a comprehensive consideration of the cumulative mass contributions of individual constituents comprising a KIB full-cell architecture—namely electrolytes, anodes (negative electrodes), cathodes (positive electrodes), separators, current collectors, and packaging casings. Therefore, the disclosed energy density values (Fig. 33a), whilst illustrative of maximal potential at the material level, are likely to exhibit much lower energy density values upon real-world full-cell evaluation, reflecting the multifaceted weight considerations intrinsic to practical implementations.

Fig. 38 displays the energy density of aqueous and non-aqueous potassium-ion batteries (KIBs) at the pouch cell level, calculated using various electrode combinations, as reported in ref. 501. Specifically, the figure illustrates that aqueous KIBs exhibit significantly lower energy density (<50 W h kg^{-1}) compared to non-aqueous KIBs due to their lower operating voltages. Achieving an energy density of >150 W h kg^{-1} is a realistic prospect for non-aqueous KIB systems. Whilst this projected energy density still falls short of that achieved by current lithium-ion batteries (LIBs), further enhancements in energy density are expected through battery assembly engineering and optimisation of electrode materials. Notably, KIBs that use graphite as an anode and polyanion-based cathode materials, such as $KVPO_4F$, demonstrate the highest energy density in terms of both high voltage and high capacity. Other cathode candidates include Prussian analogues, organic moieties, and manganese-based layered oxides, which show comparable energy density. Prussian analogues exhibit higher operating voltages but with lower specific capacities. Whilst research and development in practical KIBs are still in their early stages, there is ample room for exploration within the extensive electrode materials database to design high-energy-density KIBs surpassing >150 W h kg^{-1}.

4 Conclusion

This *Perspective* highlights significant advancements in high-performance cathode materials for potassium-ion batteries (KIBs), enabling readers to recognise the potential benefits of KIB technology when complementing lithium-ion battery (LIB) technology in high-voltage and high-power applications (Fig. 39a). Owing to the larger size of K^+ compared to Li^+, KIBs can be envisaged to effectively complement LIBs (Fig. 39b) in large-scale energy storage applications, addressing the limited paucity of terrestrial lithium reserves. One strategy to enhance KIB energy density involves designing suitable cathode materials and stable electrolytes for enduring long-term high-voltage operation. The practical evaluation of potassium-ion battery (KIB) full-cell designs envisions the possibility of achieving high voltage (in the 4 V range) and elevated energy density (>150 W h kg^{-1}),[501] positioning KIBs as competitive high-performance energy storage systems. Whilst KIB prototypes (designed at the laboratory scale) show promising electrochemical performance, proactive efforts from researchers are necessary to ensure the development of a commercially viable KIB and elevate the technology readiness level. This approach is crucial to meet the diverse energy demands of our society.

Furthermore, there is untapped potential in exploring the fundamental scientific principles and technological applications of multifunctional potassium-based cathode materials, particularly their honeycomb layered counterparts.[257,262] The field of KIBs holds uncharted territory, driving avant-garde innovation in K-ion technology. This journey encompasses a wide spectrum of discoveries, from novel phenomena in fundamental physics and chemistry, such as geometric and topological effects, to unprecedented degenerate cationic states triggering phase transitions through geometric distortions.[235] Additionally, groundbreaking technologies like Kitaev materials[502,503] in quantum computing[504] and feasible applications

© 2024 The Author(s). Published by the Royal Society of Chemistry

Open Access Article. Published on 04 dicembre 2023. Downloaded on 11/06/2026 17:40:22. This article is licensed under a Creative Commons Attribution-NonCommercial 3.0 Unported Licence.

in the realms of semiconductors and superconductors are emerging.[505] The saying 'strike while the iron is hot', which resonated even in the Iron Age, finds its parallel in the realm of KIBs, urging researchers in this field to seize the opportunities that the era of potassium holds.

Conflicts of interest

There are no conflicts to declare.

Acknowledgements

The authors would like to acknowledge the financial support of AIST Edge Runners Funding, Japan Society for the Promotion of Science (JSPS KAKENHI Grant Number 23K04922), TEPCO Memorial Foundation and Japan Prize Foundation.

References

1 Z. Yang, J. Zhang, M. C. Kintner-Meyer, X. Lu, D. Choi, J. P. Lemmon and J. Liu, *Chem. Rev.*, 2011, **111**, 3577–3613.
2 S. Ash, *Mineral commodity summaries 2019*, US Geological Survey Reston, VA, 2019.
3 C. Vaalma, D. Buchholz, M. Weil and S. Passerini, *Nat. Rev. Mater.*, 2018, **3**, 1–11.
4 R. Rajagopalan, Y. Tang, X. Ji, C. Jia and H. Wang, *Adv. Funct. Mater.*, 2020, **30**, 1909486.
5 K. Yoshii, T. Masese, M. Kato, K. Kubota, H. Senoh and M. Shikano, *ChemElectroChem*, 2019, **6**, 3901–3910.
6 W. Zhang, Y. Liu and Z. Guo, *Sci. Adv.*, 2019, **5**, eaav7412.
7 X. Min, J. Xiao, M. Fang, W. A. Wang, Y. Zhao, Y. Liu, A. M. Abdelkader, K. Xi, R. V. Kumar and Z. Huang, *Energy Environ. Sci.*, 2021, **14**, 2186–2243.
8 A. Eftekhari, Z. Jian and X. Ji, *ACS Appl. Mater. Interfaces*, 2017, **9**, 4404–4419.
9 X. Zhang, Z. Wei, K. N. Dinh, N. Chen, G. Chen, F. Du and Q. Yan, *Small*, 2020, **16**, 2002700.
10 Z.-X. Huang, Z.-Y. Gu, Y.-L. Heng, E. H. Ang, H.-B. Geng and X.-L. Wu, *Chem. Eng. J.*, 2023, **452**, 139438.
11 M. G. T. Nathan, H. Yu, G.-T. Kim, J.-H. Kim, J. S. Cho, J. Kim and J.-K. Kim, *Adv. Sci.*, 2022, **9**, 2105882.
12 L. Lander, G. Rousse, A. M. Abakumov, M. Sougrati, G. Van Tendeloo and J.-M. Tarascon, *J. Mater. Chem. A*, 2015, **3**, 19754–19764.
13 C. Ling and F. Mizuno, *J. Mater. Chem. A*, 2013, **1**, 8000–8006.
14 J. Liao, Q. Hu, Y. Du, J. Li, L. Duan, J. Bao and X. Zhou, *Sci. Bull.*, 2022, **67**, 2208–2215.
15 J. Dong, J. Liao, X. He, Q. Hu, Y. Yu and C. Chen, *Chem. Commun.*, 2020, **56**, 10050–10053.
16 P. R. Kumar, T. Hosaka, T. Shimamura, D. Igarashi and S. Komaba, *ACS Appl. Energy Mater.*, 2022, **5**, 13470–13479.
17 N. Recham, G. Rousse, M. T. Sougrati, J.-N. Chotard, C. Frayret, S. Mariyappan, B. C. Melot, J.-C. Jumas and J.-M. Tarascon, *Chem. Mater.*, 2012, **24**, 4363–4370.
18 K. Chihara, A. Katogi, K. Kubota and S. Komaba, *Chem. Commun.*, 2017, **53**, 5208–5211.
19 S. S. Fedotov, N. R. Khasanova, A. S. Samarin, O. A. Drozhzhin, D. Batuk, O. M. Karakulina, J. Hadermann, A. M. Abakumov and E. V. Antipov, *Chem. Mater.*, 2016, **28**, 411–415.
20 I. Gomez, O. Leonet, J. Alberto Blazquez, H.-J. Grande and D. Mecerreyes, *ACS Macro Lett.*, 2018, **7**, 419–424.
21 Z. Jian, Y. Liang, I. A. Rodrguez-Pérez, Y. Yao and X. Ji, *Electrochem. Commun.*, 2016, **71**, 5–8.
22 H. Wang, J. Lin and Z. X. Shen, *J. Sci.: Adv. Mater. Devices*, 2016, **1**, 225–255.
23 Y. Chen, W. Luo, M. Carter, L. Zhou, J. Dai, K. Fu, S. Lacey, T. Li, J. Wan and X. Han, *et al.*, *Nano Energy*, 2015, **18**, 205–211.
24 X. Wu, Z. Jian, Z. Li and X. Ji, *Electrochem. Commun.*, 2017, **77**, 54–57.
25 A. Eftekhari, Z. Jian and X. Ji, *ACS Appl. Mater. Interfaces*, 2017, **9**, 4404–4419.
26 A. Eftekhari, *J. Power Sources*, 2004, **126**, 221–228.
27 Q. Song, Z. Li, S. Gan, W.-S. Dong, W. Wang, J. Zhang and Q. Yu, *J. Mater. Chem. A*, 2023, **11**, 1532–1550.
28 S. Zhao, Z. Guo, K. Yan, X. Guo, S. Wan, F. He, B. Sun and G. Wang, *Small Struct.*, 2021, **2**, 2000054.
29 P. Padigi, J. Thiebes, M. Swan, G. Goncher, D. Evans and R. Solanki, *Electrochim. Acta*, 2015, **166**, 32–39.
30 J. Cattermull, K. Sada, K. Hurlbutt, S. J. Cassidy, M. Pasta and A. L. Goodwin, *Chem. Mater.*, 2022, **34**, 5000–5008.
31 R. Ma, Z. Wang, Q. Fu, W. Zhou, Y. Mo, J. Tu, Z. Wang, P. Gao, C. Fan and J. Liu, *J. Energy Chem.*, 2023, **83**, 16–23.
32 Z. Li, B. Ozdogru, B. Bal, M. Bowden, A. Choi, Y. Zhang, H. Wang, V. Murugesan, V. G. Pol and Ö. Ö. Çapraz, *Adv. Energy Mater.*, 2023, **13**, 2301329.
33 Y. Bai, K. Yuchi, X. Liu, S. Tian, S. Yang, X. Qian, B. Ma, M. Fang, Y. Liu and Z. Huang, *et al.*, *Eur. J. Inorg. Chem.*, 2023, e202300246.
34 L. Xue, Y. Li, H. Gao, W. Zhou, X. Lu, W. Kaveevivitchai, A. Manthiram and J. B. Goodenough, *J. Am. Chem. Soc.*, 2017, **139**, 2164–2167.
35 M. Okoshi, Y. Yamada, S. Komaba, A. Yamada and H. Nakai, *J. Electrochem. Soc.*, 2016, **164**, A54.
36 L. Ni, G. Xu, C. Li and G. Cui, *Exploration*, 2022, 20210239.
37 E. Nightingale Jr, *J. Phys. Chem.*, 1959, **63**, 1381–1387.
38 Y. Matsuda, H. Nakashima, M. Morita and Y. Takasu, *J. Electrochem. Soc.*, 1981, **128**, 2552.
39 M. Okoshi, Y. Yamada, S. Komaba, A. Yamada and H. Nakai, *J. Electrochem. Soc.*, 2016, **164**, A54.
40 S. Amara, J. Toulc'Hoat, L. Timperman, A. Biller, H. Galiano, C. Marcel, M. Ledigabel and M. Anouti, *ChemPhysChem*, 2019, **20**, 581–594.
41 Y. R. Dougassa, J. Jacquemin, L. El Ouatani, C. Tessier and M. Anouti, *J. Phys. Chem. B*, 2014, **118**, 3973–3980.
42 T. Hosaka, K. Kubota, A. S. Hameed and S. Komaba, *Chem. Rev.*, 2020, **120**, 6358–6466.
43 Y. Marcus, *Pure Appl. Chem.*, 1985, **57**, 1129–1132.

© 2024 The Author(s). Published by the Royal Society of Chemistry

Open Access Article. Published on 04 dicembre 2023. Downloaded on 11/06/2026 17:40:22.
This article is licensed under a Creative Commons Attribution-NonCommercial 3.0 Unported Licence.

44 S. Komaba, T. Hasegawa, M. Dahbi and K. Kubota, *Electrochem. Commun.*, 2015, **60**, 172–175.
45 Z. Jian, W. Luo and X. Ji, *J. Am. Chem. Soc.*, 2015, **137**, 11566–11569.
46 W. Luo, J. Wan, B. Ozdemir, W. Bao, Y. Chen, J. Dai, H. Lin, Y. Xu, F. Gu and V. Barone, *et al.*, *Nano Lett.*, 2015, **15**, 7671–7677.
47 X. Wang and H. Wang, *Adv. Powder Mater.*, 2022, **1**, 100057.
48 Z. Jian, W. Luo and X. Ji, *J. Am. Chem. Soc.*, 2015, **137**, 11566–11569.
49 W. Luo, J. Wan, B. Ozdemir, W. Bao, Y. Chen, J. Dai, H. Lin, Y. Xu, F. Gu and V. Barone, *et al.*, *Nano Lett.*, 2015, **15**, 7671–7677.
50 J. Liu, T. Yin, B. Tian, B. Zhang, C. Qian, Z. Wang, L. Zhang, P. Liang, Z. Chen and J. Yan, *et al.*, *Adv. Energy Mater.*, 2019, **9**, 1900579.
51 L. Fan, R. Ma, Q. Zhang, X. Jia and B. Lu, *Angew. Chem.*, 2019, **131**, 10610–10615.
52 H.-J. Liang, B.-H. Hou, W.-H. Li, Q.-L. Ning, X. Yang, Z.-Y. Gu, X.-J. Nie, G. Wang and X.-L. Wu, *Energy Environ. Sci.*, 2019, **12**, 3575–3584.
53 A. Iyo, H. Ogino, S. Ishida and H. Esaki, *Dramatically Accelerated Formation of Graphite Intercalation Compounds Catalyzed by Sodium*, 2023.
54 Y. Xu, T. Ding, D. Sun, X. Ji and X. Zhou, *Adv. Funct. Mater.*, 2023, **33**, 2211290.
55 L. Duan, Y. Xu, Z. Zhang, J. Xu, J. Liao, J. Xu, Y. Sun, Y. He and X. Zhou, *J. Mater. Chem. A*, 2021, **9**, 22820–22826.
56 Z. Zhang, Q. Hu, J. Liao, Y. Xu, L. Duan, R. Tian, Y. Du, J. Shen and X. Zhou, *Nano Lett.*, 2023, **23**, 694–700.
57 L. Duan, J. Xu, Y. Xu, R. Tian, Y. Sun, C. Zhu, X. Mo and X. Zhou, *J. Energy Chem.*, 2023, **76**, 332–338.
58 Y.-S. Xu, J.-C. Gao, X.-S. Tao, Y.-G. Sun, Y. Liu, A.-M. Cao and L.-J. Wan, *ACS Appl. Mater. Interfaces*, 2020, **12**, 15313–15319.
59 A. K. Pandey, B. D. Campéon, I. Konuma and N. Yabuuchi, *Energy Adv.*, 2023, **2**, 98–102.
60 Z. Zhang, J. Sun, L. Duan, Y. Du, J. Li, J. Shen and X. Zhou, *J. Mater. Chem. A*, 2022, **10**, 554–560.
61 W. Ko, J. Kim, J. Kang, H. Park, Y. Lee, J. Ahn, B. Ku, M. Choi, H. Ahn and G. Oh, *et al.*, *Mater. Today Energy*, 2023, 101356.
62 Y.-S. Xu, Y.-N. Zhou, Q.-H. Zhang, M.-Y. Qi, S.-J. Guo, J.-M. Luo, Y.-G. Sun, L. Gu, A.-M. Cao and L.-J. Wan, *Chem. Eng. J.*, 2021, **412**, 128735.
63 F. Li, X. Gu, S. Wu, S. Dong, J. Wang, P. Dai, L. Li, D. Liu and M. Wu, *Electrochim. Acta*, 2023, **439**, 141571.
64 H. Kim, D.-H. Seo, J. C. Kim, S.-H. Bo, L. Liu, T. Shi and G. Ceder, *Adv. Mater.*, 2017, **29**, 1702480.
65 H. Kim, J. C. Kim, S.-H. Bo, T. Shi, D.-H. Kwon and G. Ceder, *Adv. Energy Mater.*, 2017, **7**, 1700098.
66 Y. Hironaka, K. Kubota and S. Komaba, *Chem. Commun.*, 2017, **53**, 3693–3696.
67 J.-Y. Hwang, J. Kim, T.-Y. Yu, S.-T. Myung and Y.-K. Sun, *Energy Environ. Sci.*, 2018, **11**, 2821–2827.
68 T. Deng, X. Fan, J. Chen, L. Chen, C. Luo, X. Zhou, J. Yang, S. Zheng and C. Wang, *Adv. Funct. Mater.*, 2018, **28**, 1800219.
69 J. U. Choi, J. Kim, J.-Y. Hwang, J. H. Jo, Y.-K. Sun and S.-T. Myung, *Nano Energy*, 2019, **61**, 284–294.
70 J. U. Choi, J. Kim, J. H. Jo, H. J. Kim, Y. H. Jung, D.-C. Ahn, Y.-K. Sun and S.-T. Myung, *Energy Storage Mater.*, 2020, **25**, 714–723.
71 T. Masese, K. Yoshii, M. Kato, K. Kubota, Z. Huang, H. Senoh and M. A. Shikano, *Chem. Commun.*, 2019, **55**, 985–988.
72 T. Masese, K. Yoshii, Y. Yamaguchi, T. Okumura, Z. Huang, M. Kato, K. Kubota, J. Furutani, Y. Orikasa, H. Senoh and O. Rechargeable, *Nat. Commun.*, 2018, **9**, 1–12.
73 J. H. Jo, J. U. Choi, Y. J. Park, Y. H. Jung, D. Ahn, T.-Y. Jeon, H. Kim, J. Kim and S.-T. Myung, *Adv. Energy Mater.*, 2020, **10**, 1903605.
74 J.-Y. Hwang, J. Kim, T.-Y. Yu, H.-G. Jung, J. Kim, K.-H. Kim and Y.-K. Sun, *J. Mater. Chem. A*, 2019, **7**, 21362–21370.
75 B. Peng, Y. Li, J. Gao, F. Zhang, J. Li and G. Zhang, *J. Power Sources*, 2019, **437**, 226913.
76 L. Liu, J. Liang, W. Wang, C. Han, Q. Xia, X. Ke, J. Liu, Q. Gu, Z. Shi and S. Chou, *et al.*, *ACS Appl. Mater. Interfaces*, 2021, **13**, 28369–28377.
77 C.-L. Liu, S.-H. Luo, H.-B. Huang, X. Liu, Y.-C. Zhai and Z.-W. Wang, *Chem. Eng. J.*, 2019, **378**, 122167.
78 N. Naveen, S. C. Han, S. P. Singh, D. Ahn, K.-S. Sohn and M. Pyo, *J. Power Sources*, 2019, **430**, 137–144.
79 J. U. Choi, Y. J. Park, J. H. Jo, Y. H. Jung, D.-C. Ahn, T.-Y. Jeon, K.-S. Lee, H. Kim, S. Lee and J. Kim, *et al.*, *Energy Storage Mater.*, 2020, **27**, 342–351.
80 M. K. Cho, J. H. Jo, J. U. Choi and S.-T. Myung, *ACS Appl. Mater. Interfaces*, 2019, **11**, 27770–27779.
81 J. Hao, K. Xiong, J. Zhou, A. M. Rao, X. Wang, H. Liu and B. Lu, *Energy Environ. Mater.*, 2022, **5**, 261–269.
82 X. Zhang, D. Yu, Z. Wei, N. Chen, G. Chen, Z. X. Shen and F. Du, *ACS Appl. Mater. Interfaces*, 2021, **13**, 18897–18904.
83 J. Liang, C. Lin, X. Meng, M. Liang, J. Lai, X. Zheng, Q. Huang, L. Liu and Z. Shi, *J. Mater. Chem. A*, 2021, **9**, 17261–17269.
84 C.-L. Liu, S.-H. Luo, H.-B. Huang, Y.-C. Zhai and Z.-W. Wang, *ChemElectroChem*, 2019, **6**, 2308–2315.
85 T. Liu, S. Hou, Y. Li, S. Xue, J. Hu, H. Fu, C. Yang and L. Zhao, *J. Energy Chem.*, 2022, **64**, 335–343.
86 M. G. T. Nathan, N. Naveen, W. B. Park, K.-S. Sohn and M. Pyo, *J. Power Sources*, 2019, **438**, 226992.
87 C.-L. Liu, S.-H. Luo, H.-B. Huang, Y.-C. Zhai and Z.-W. Wang, *Electrochim. Acta*, 2018, **286**, 114–122.
88 R. Huang, Q. Xue, J. Lin, X. Zhang, J. Zhou, F. Wu, L. Li and R. Chen, *Nano Res.*, 2022, 1–7.
89 M. G. T. Nathan, W. B. Park, N. Naveen, S. Park, K.-S. Sohn and M. Pyo, *J. Electrochem. Soc.*, 2020, **167**, 100507.
90 R. Dang, Q.-B. Yan, E. Zhao, N. Li, K. Wu, Z. Chen, Z. Wu, X. Liu, Z. Hu and X. Xiao, *Sci. China: Mater.*, 2022, **65**, 1741–1750.
91 J. Feng, S.-H. Luo, L. Yang, K. Cai, Y. Dou, Q. Wang, Y. Zhang and X. Liu, *Energy Storage*, 2022, **4**, e277.
92 Y.-S. Xu, Q.-H. Zhang, D. Wang, J.-C. Gao, X.-S. Tao, Y. Liu, Y.-G. Sun, L. Gu, B.-B. Chang and C.-T. Liu, *et al.*, *Energy Storage Mater.*, 2020, **31**, 20–26.

© 2024 The Author(s). Published by the Royal Society of Chemistry

Open Access Article. Published on 04 dicembre 2023. Downloaded on 11/06/2026 17:40:22.
This article is licensed under a Creative Commons Attribution-NonCommercial 3.0 Unported Licence.

93 Z. Xiao, J. Meng, F. Xia, J. Wu, F. Liu, X. Zhang, L. Xu, X. Lin and L. Mai, *Energy Environ. Sci.*, 2020, **13**, 3129–3137.
94 X. Zhang, Y. Yang, X. Qu, Z. Wei, G. Sun, K. Zheng, H. Yu and F. Du, *Adv. Funct. Mater.*, 2019, **29**, 1905679.
95 W. Zhong, X. Liu, Q. Cheng, T. Tan, Q. Huang, Q. Deng, J. Hu and C. Yang, *Appl. Phys. Rev.*, 2021, **8**, 031412.
96 Q. Deng, F. Zheng, W. Zhong, Q. Pan, Y. Liu, Y. Li, G. Chen, Y. Li, C. Yang and M. Liu, *Chem. Eng. J.*, 2020, **392**, 123735.
97 Y. Huang, X. Zhang, H. Lin, Z. Wei, Y. Zeng, X. Ge, W. Zhang, X. Wang, X. Jin and Z. X. Shen, *et al.*, *Chem. Eng. J.*, 2023, **453**, 139571.
98 P. Bai, K. Jiang, X. Zhang, J. Xu, S. Guo and H. Zhou, *ACS Appl. Mater. Interfaces*, 2020, **12**, 10490–10495.
99 R.-J. Luo, X.-L. Li, J.-Y. Ding, J. Bao, C. Ma, C.-Y. Du, X.-Y. Cai, X.-J. Wu and Y.-N. Zhou, *Energy Storage Mater.*, 2022, **47**, 408–414.
100 R. Dang, N. Li, Y. Yang, K. Wu, Q. Li, Y. L. Lee, X. Liu, Z. Hu and X. Xiao, *J. Power Sources*, 2020, **464**, 228190.
101 Z. Caixiang, J. Hao, J. Zhou, X. Yu and B. Lu, *Adv. Energy Mater.*, 2023, **13**, 2203126.
102 J. Lv, B. Wang, J. Hao, H. Ding, L. Fan, R. Tao, H. Yang, J. Zhou and B. Lu, *eScience*, 2023, **3**, 100081.
103 Q. Zhang, C. Didier, W. K. Pang, Y. Liu, Z. Wang, S. Li, V. K. Peterson, J. Mao and Z. Guo, *Adv. Energy Mater.*, 2019, **9**, 1900568.
104 J. Liao, Y. Han, Z. Zhang, J. Xu, J. Li and X. Zhou, *Energy Environ. Mater.*, 2021, **4**, 178–200.
105 W. Li, Z. Bi, W. Zhang, J. Wang, R. Rajagopalan, Q. Wang, D. Zhang, Z. Li, H. Wang and B. Wang, *J. Mater. Chem. A*, 2021, **9**, 8221–8247.
106 L. Wu, M. Gu, Y. Feng, S. Chen, L. Fan, X. Yu, K. Guo, J. Zhou and B. Lu, *Adv. Funct. Mater.*, 2022, **32**, 2109893.
107 H. Kim, H. Ji, J. Wang and G. Ceder, *Trends Chem.*, 2019, **1**, 682–692.
108 X. Zhang, D. Yang, X. Rui, Y. Yu and S. Huang, *Curr. Opin. Electrochem.*, 2019, **18**, 24–30.
109 S. Wang, F. Chen, L.-M. Zhang, Y.-X. Li, N.-Q. Ren, K. Cao, J.-C. Xiao and C.-H. Chen, *Nanoscale*, 2022, **14**, 5347–5355.
110 S. Wang, B. Cui, Q. Zhuang, Y. Shi and H. Zheng, *Nanoscale Res. Lett.*, 2019, **14**, 1–11.
111 Y. Lee, J.-K. Yoo, H. Park, W. Ko, J. Kang, J. H. Jo, G. Yoon, H.-G. Im, H. Yashiro and S.-T. Myung, *et al.*, *J. Mater. Chem. A*, 2021, **9**, 5475–5484.
112 Z. Tai, M. Shi, S. Chong, Y. Chen, Q. Tan, C. Shu and Y. Liu, *Sustainable Energy Fuels*, 2019, **3**, 736–743.
113 S. Wang, Y. Chen, B. Cui, B. Li, S. Wang, Y. Cui, Z. Ju and Q. Zhuang, *Appl. Surf. Sci.*, 2020, **514**, 145954.
114 Y. E. A. Sakurai, *Post lithium ion secondary battery development*, NTS Inc., Tokyo, 2023, pp. 12–28.
115 X. Bie, K. Kubota, T. Hosaka, K. Chihara and S. Komaba, *J. Mater. Chem. A*, 2017, **5**, 4325–4330.
116 S. Chong, Y. Chen, Y. Zheng, Q. Tan, C. Shu, Y. Liu and Z. Guo, *J. Mater. Chem. A*, 2017, **5**, 22465–22471.
117 J. Liao, Q. Hu, Y. Yu, H. Wang, Z. Tang, Z. Wen and C. Chen, *J. Mater. Chem. A*, 2017, **5**, 19017–19024.
118 X. Ma, Y. Guo, C. Yu, X. Chen, L. Gui, N. Cheng, J. Sun, P. Chen, J. Chen and Z. Zi, *et al.*, *J. Alloys Compd.*, 2022, **904**, 164049.
119 S. Chong, Y. Wu, S. Guo, Y. Liu and G. Cao, *Energy Storage Mater.*, 2019, **22**, 120–127.
120 Y. Pei, C. Mu, H. Li, F. Li and J. Chen, *ChemSusChem*, 2018, **11**, 1285–1289.
121 Y. Lu, L. Wang, J. Cheng and J. B. Goodenough, *Chem. Commun.*, 2012, **48**, 6544–6546.
122 X. Bie, K. Kubota, T. Hosaka, K. Chihara and S. Komaba, *J. Power Sources*, 2018, **378**, 322–330.
123 L. Wang, J. Song, R. Qiao, L. A. Wray, M. A. Hossain, Y.-D. Chuang, W. Yang, Y. Lu, D. Evans and J.-J. Lee, *et al.*, *J. Am. Chem. Soc.*, 2015, **137**, 2548–2554.
124 K. Kubota, M. Dahbi, T. Hosaka, S. Kumakura and S. Komaba, *Chem. Rec.*, 2018, **18**, 459–479.
125 X. Wu, S. Qiu, Y. Liu, Y. Xu, Z. Jian, J. Yang, X. Ji and J. Liu, *Adv. Mater.*, 2022, **34**, 2106876.
126 L. Deng, J. Qu, X. Niu, J. Liu, J. Zhang, Y. Hong, M. Feng, J. Wang, M. Hu and L. Zeng, *et al.*, *Nat. Commun.*, 2021, **12**, 2167.
127 M. Tang, Y. Wu, Y. Chen, C. Jiang, S. Zhu, S. Zhuo and C. Wang, *J. Mater. Chem. A*, 2019, **7**, 486–492.
128 S.-Y. Yang, Y.-J. Chen, G. Zhou and Z.-W. Fu, *J. Electrochem. Soc.*, 2018, **165**, A1422.
129 M. Kato, T. Masese, M. Yao, N. Takeichi and T. Kiyobayashi, *New J. Chem.*, 2019, **43**, 1626–1631.
130 H. Gao, L. Xue, S. Xin and J. B. Goodenough, *Angew. Chem.*, 2018, **130**, 5547–5551.
131 W. Guo, Y.-X. Yin, S. Xin, Y.-G. Guo and L.-J. Wan, *Energy Environ. Sci.*, 2012, **5**, 5221–5225.
132 T. Zhou, W. Jin, W. Xue, B. Dai, C. Feng, X. Huang, P. Théato and Y. Li, *J. Power Sources*, 2021, **483**, 229136.
133 F. A. Obrezkov, A. F. Shestakov, V. F. Traven, K. J. Stevenson and P. A. Troshin, *J. Mater. Chem. A*, 2019, **7**, 11430–11437.
134 L. Fan, Q. Liu, Z. Xu and B. Lu, *ACS Energy Lett.*, 2017, **2**, 1614–1620.
135 F. A. Obrezkov, V. Ramezankhani, I. Zhidkov, V. F. Traven, E. Z. Kurmaev, K. J. Stevenson and P. A. Troshin, *J. Phys. Chem. Lett.*, 2019, **10**, 5440–5445.
136 C. Li, J. Xue, A. Huang, J. Ma, F. Qing, A. Zhou, Z. Wang, Y. Wang and J. Li, *Electrochim. Acta*, 2019, **297**, 850–855.
137 K. Minami, T. Masese and K. Yoshii, *New J. Chem.*, 2021, **45**, 4921–4924.
138 Y. Chen, W. Luo, M. Carter, L. Zhou, J. Dai, K. Fu, S. Lacey, T. Li, J. Wan and X. Han, *et al.*, *Nano Energy*, 2015, **18**, 205–211.
139 R. R. Kapaev and P. A. Troshin, *J. Mater. Chem. A*, 2020, **8**, 17296–17325.
140 J. J. Shea and C. Luo, *ACS Appl. Mater. Interfaces*, 2020, **12**, 5361–5380.
141 S. Xu, Y. Chen and C. Wang, *J. Mater. Chem. A*, 2020, **8**, 15547–15574.
142 W. Zhang, W. Huang and Q. Zhang, *Chem. – Eur. J.*, 2021, **27**, 6131–6144.

© 2024 The Author(s). Published by the Royal Society of Chemistry

Open Access Article. Published on 04 dicembre 2023. Downloaded on 11/06/2026 17:40:22.
This article is licensed under a Creative Commons Attribution-NonCommercial 3.0 Unported Licence.

143 M. Radhakrishnan, S. Prabhu, M. Arockiaraj and M. Arulperumjothi, *Int. J. Quantum Chem.*, 2022, **122**, e26818.
144 Ž. Tomovi, M. D. Watson and K. Müllen, *Angew. Chem., Int. Ed.*, 2004, **43**, 755–758.
145 A. Soncini, E. Steiner, P. W. Fowler, R. W. Havenith and L. W. Jenneskens, *Chem. – Eur. J.*, 2003, **9**, 2974–2981.
146 I. A. Popov and A. I. Boldyrev, *Eur. J. Org. Chem.*, 2012, 3485–3491.
147 K. Namsheer and C. S. Rout, *RSC Adv.*, 2021, **11**, 5659–5697.
148 A. Duan, Z. Wang, X. Huang and Y. Li, *Angew. Chem., Int. Ed.*, 2023, e202302754.
149 J. Liao, Q. Hu, J. Mu, X. He, S. Wang and C. Chen, *Chem. Commun.*, 2019, **55**, 659–662.
150 A. S. Hameed, A. Katogi, K. Kubota and S. Komaba, *Adv. Energy Mater.*, 2019, **9**, 1902528.
151 Y. Wang, X. Zhao, Y. Wang, W. Qiu, E. Song, S. Wang and J. Liu, *ACS Appl. Mater. Interfaces*, 2022, **15**, 1129–1137.
152 A. Slesarenko, I. K. Yakuschenko, V. Ramezankhani, V. Sivasankaran, O. Romanyuk, A. V. Mumyatov, I. Zhidkov, S. Tsarev, E. Z. Kurmaev and A. F. Shestakov, *et al.*, *J. Power Sources*, 2019, **435**, 226724.
153 R. Shi, S. Jiao, Q. Yue, G. Gu, K. Zhang and Y. Zhao, *Exploration*, 2022, 20220066.
154 J. Hu, Y. Hong, M. Guo, Y. Hu, W. Tang, S. Xu, S. Jia, B. Wei, S. Liu and C. Fan, *et al.*, *Energy Storage Mater.*, 2023, **56**, 267–299.
155 X. Zhu, R. N. Ali, M. Song, Y. Tang and Z. Fan, *Polymers*, 2022, **14**, 5538.
156 V. Ramezankhani, I. K. Yakuschenko, S. Vasilyev, T. A. Savinykh, A. V. Mumyatov, I. S. Zhidkov, E. V. Shchurik, E. Z. Kurmaev, A. F. Shestakov and P. A. Troshin, *J. Mater. Chem. A*, 2022, **10**, 3044–3050.
157 B. Tian, J. Zheng, C. Zhao, C. Liu, C. Su, W. Tang, X. Li and G.-H. Ning, *J. Mater. Chem. A*, 2019, **7**, 9997–10003.
158 C. Masquelier and L. Croguennec, *Chem. Rev.*, 2013, **113**, 6552–6591.
159 H. Kim, D.-H. Seo, M. Bianchini, R. J. Clément, H. Kim, J. C. Kim, Y. Tian, T. Shi, W.-S. Yoon and G. Ceder, *Adv. Energy Mater.*, 2018, **8**, 1801591.
160 A. Manthiram and J. Goodenough, *J. Power Sources*, 1989, **26**, 403–408.
161 X. Lin, J. Huang, H. Tan, J. Huang and B. Zhang, *Energy Storage Mater.*, 2019, **16**, 97–101.
162 J. Han, G.-N. Li, F. Liu, M. Wang, Y. Zhang, L. Hu, C. Dai and M. Xu, *Chem. Commun.*, 2017, **53**, 1805–1808.
163 Z. Zhang, R. Wang, Z. Chen, X. Liu, Z. Liu, J. Zeng, X. Zhao, K. Peng, Q. Yao and X. Zhang, *et al.*, *Chem. Eng. J.*, 2022, **436**, 135235.
164 K.-Y. Zhang, Z.-Y. Gu, E. H. Ang, J.-Z. Guo, X.-T. Wang, Y. Wang and X.-L. Wu, *Mater. Today*, 2022, **54**, 189–201.
165 T. Hosaka, T. Shimamura, K. Kubota and S. Komaba, *Chem. Rec.*, 2019, **19**, 735–745.
166 H. He, K. Cao, S. Guo, W. Yao, F. Chen and C.-H. Chen, *et al.*, *J. Power Sources*, 2023, **564**, 232862.
167 J. Wang, B. Ouyang, H. Kim, Y. Tian, G. Ceder and H. Kim, *J. Mater. Chem. A*, 2021, **9**, 18564–18575.
168 S. Li, M. Li, R. Shen, Z. Liu, X. Lv, J. Su, H. Kuai and Y. Wen, *J. Alloys Compd.*, 2023, 172446.
169 T. Jenkins, J. A. Alarco and I. D. Mackinnon, *ACS Omega*, 2021, **6**, 1917–1929.
170 H.-X. Kuai, J.-F. Lu, X.-Y. Lv, Y.-F. Long and Y.-X. Wen, *Ionics*, 2022, **28**, 3817–3831.
171 X. Yang, D. Yan, T. Chou and J. C. Kim, *J. Mater. Chem. A*, 2023, **11**, 14304–14310.
172 H. Park, W. Ko, Y. Lee, J. Kang, J. Ahn, J.-K. Yoo and J. Kim, *J. Mater. Chem. A*, 2021, **9**, 11802–11811.
173 L. Larbi, R. Wernert, P. Fioux, L. Croguennec, L. Monconduit and C. Matei Ghimbeu, *ACS Appl. Mater. Interfaces*, 2023, **15**, 18992–19001.
174 J. Liao, C. Chen, Q. Hu, Y. Du, Y. He, Y. Xu, Z. Zhang and X. Zhou, *Angew. Chem.*, 2021, **133**, 25779–25786.
175 J. Li, Y. Zheng, K. San Hui, K. Wang, C. Zha, D. A. Dinh, J. Tu, Z. Shao and K. N. Hui, *Energy Storage Mater.*, 2023, 102852.
176 W. B. Park, S. C. Han, C. Park, S. U. Hong, U. Han, S. P. Singh, Y. H. Jung, D. Ahn, K.-S. Sohn and M. Pyo, *Adv. Energy Mater.*, 2018, **8**, 1703099.
177 X.-D. He, J.-Y. Liao, T. Chen, L.-M. Zhang, X. Ding, J.-R. Wang, S. Wang, Z.-Y. Wen and C.-H. Chen, *J. Alloys Compd.*, 2021, **884**, 161126.
178 I. V. Tereshchenko, D. A. Aksyonov, A. Zhugayevych, E. V. Antipov and A. M. Abakumov, *Solid State Ionics*, 2020, **357**, 115468.
179 M. Ohara, A. S. Hameed, K. Kubota, A. Katogi, K. Chihara, T. Hosaka and S. Komaba, *Chem. Sci.*, 2021, **12**, 12383–12390.
180 S. S. Fedotov, N. D. Luchinin, D. A. Aksyonov, A. V. Morozov, S. V. Ryazantsev, M. Gaboardi, J. R. Plaisier, K. J. Stevenson, A. M. Abakumov and E. V. Antipov, *Nat. Commun.*, 2020, **11**, 1484.
181 O. Yakubovich, N. Khasanova and E. Antipov, *Minerals*, 2020, **10**, 524.
182 A. M. Abakumov, S. S. Fedotov, E. V. Antipov and J.-M. Tarascon, *Nat. Commun.*, 2020, **11**, 4976.
183 H. He, K. Cao, S. Zeng, J. Si, Y. Zhu and C.-H. Chen, *J. Power Sources*, 2023, **587**, 233715.
184 L. Lander, G. Rousse, D. Batuk, C. V. Colin, D. A. Dalla Corte and J.-M. Tarascon, *Inorg. Chem.*, 2017, **56**, 2013–2021.
185 I. Sultana, M. M. Rahman, S. Mateti, N. Sharma, S. Huang and Y. Chen, *Batteries Supercaps*, 2020, **3**, 450–455.
186 J. Bodart, N. Eshraghi, T. Carabin, B. Vertruyen, R. Cloots, F. Boschini and A. Mahmoud, *J. Power Sources*, 2020, **480**, 229057.
187 H.-X. Kuai, J.-F. Lu, X.-Y. Lv, Y.-F. Long and Y.-X. Wen, *Ionics*, 2022, **28**, 3817–3831.
188 S. Zheng, S. Cheng, S. Xiao, L. Hu, Z. Chen, B. Huang, Q. Liu, J. Yang and Q. Chen, *J. Alloys Compd.*, 2020, **815**, 152379.
189 J. Huang, X. Cai, H. Yin, Y. Li, W. Lin, S. Huang and Y. Zhang, *J. Phys. Chem. Lett.*, 2021, **12**, 2721–2726.
190 A. Bocchini, U. Gerstmann, T. Bartley, H.-G. Steinrück, G. Henkel and W. Schmidt, *Phys. Rev. Mater.*, 2022, **6**, 105401.

© 2024 The Author(s). Published by the Royal Society of Chemistry

Open Access Article. Published on 04 dicembre 2023. Downloaded on 11/06/2026 17:40:22.
This article is licensed under a Creative Commons Attribution-NonCommercial 3.0 Unported Licence.

191 R. Eremin, N. Kabanova, Y. A. Morkhova, A. Golov and V. Blatov, *Solid State Ionics*, 2018, **326**, 188–199.
192 K. Li, X. Fan, D. J. Singh and W. Zheng, *J. Energy Chem.*, 2021, **54**, 377–385.
193 L. Wu and M. Liu, *Ind. Eng. Chem. Res.*, 2007, **46**, 6494–6500.
194 W. Yuan, Q. Zhang, J. Kano and F. Saito, *et al.*, *Powder Technol.*, 2014, **260**, 22–26.
195 H. B. Yahia, E. Gaudin and J. Darriet, *Z. Naturforsch. B*, 2007, **62**, 873–880.
196 H. B. Yahia, R. Essehli, I. Belharouak and E. Gaudin, *Mater. Res. Bull.*, 2015, **71**, 7–10.
197 Y. Wang and R. Li, *J. Solid State Chem.*, 2010, **183**, 1221–1225.
198 Z.-G. Hu, T. Higashiyama, M. Yoshimura, Y. K. Yap, Y. Mori and T. Sasaki, *Jpn. J. Appl. Phys.*, 1998, **37**, L1093.
199 V. Krasilnikov and V. Bamburov, *Dokl. Chem.*, 2007, 247–250.
200 V. Krasilnikov, *Russ. J. Inorg. Chem.*, 2007, **52**, 258–262.
201 X. Ge, Y. Chen, S. Liu, X. Yang and K. Feng, *J. Solid State Electrochem.*, 2022, **26**, 1627–1636.
202 R. Fehrmann, B. Krebs, G. Papatheodorou, R. W. Berg and N. J. Bjerrum, *Inorg. Chem.*, 1986, **25**, 1571–1577.
203 S. F. Linnell, J. L. Payne, D. M. Pickup, A. V. Chadwick, A. R. Armstong and J. T. Irvine, *J. Mater. Chem. A*, 2020, **8**, 19502–19512.
204 A. ElMaadi, A. Boukhari and E. Holt, *J. Alloys Compd.*, 1995, **223**, 13–17.
205 R. Nath, D. Kasinathan, H. Rosner, M. Baenitz and C. Geibel, *Phys. Rev. B: Condens. Matter Mater. Phys.*, 2008, **77**, 134451.
206 H. Yaghoobnejad Asl and A. Choudhury, *Chem. Mater.*, 2016, **28**, 5029–5036.
207 H. Park, H. Kim, W. Ko, J. H. Jo, Y. Lee, J. Kang, I. Park, S.-T. Myung and J. Kim, *Energy Storage Mater.*, 2020, **28**, 47–54.
208 J. Kang, H. Park, W. Ko, Y. Lee, J. Ahn, J.-K. Yoo, S. H. Song, H. Kim and J. Kim, *J. Mater. Chem. A*, 2021, **9**, 9898–9908.
209 F. Wang, S. Liu, Q. Jiang, K. Feng, X. Yang, X. Li, H. Zhang, M. Xia and H. Zhang, *J. Power Sources*, 2020, **452**, 227835.
210 S. Dai, T. Feng, C. Chen, X. Li and M. Wu, *J. Electrochem. Soc.*, 2020, **167**, 110517.
211 J. Vaughey, W. T. Harrison and A. J. Jacobson, *J. Solid State Chem.*, 1994, **110**, 305–313.
212 O. V. Yakubovich, E. V. Yakovleva, A. N. Golovanov, A. S. Volkov, O. S. Volkova, E. A. Zvereva, O. V. Dimitrova and A. N. Vasiliev, *Inorg. Chem.*, 2013, **52**, 1538–1543.
213 A. Zhao, Y. Fang, X. Ai, H. Yang and Y. Cao, *J. Energy Chem.*, 2021, **60**, 635–648.
214 L. Zhu, M. Wang, S. Xiang, D. Sun, Y. Tang and H. Wang, *Adv. Energy Mater.*, 2023, 2302046.
215 C. Delmas, C. Fouassier and P. Hagenmuller, *Phys. B + C*, 1980, **99**, 81–85.
216 J.-J. Braconnier, C. Delmas, C. Fouassier and P. Hagenmuller, *Mater. Res. Bull.*, 1980, **15**, 1797–1804.
217 R. Hoppe and H. Sabrowsky, *Z. Anorg. Allg. Chem.*, 1965, **339**, 144–154.
218 C. Fouassier, C. Delmas and P. Hagenmuller, *Mater. Res. Bull.*, 1975, **10**, 443–449.
219 C. Vaalma, G. A. Giffin, D. Buchholz and S. Passerini, *J. Electrochem. Soc.*, 2016, **163**, A1295.
220 J. C. Pramudita, D. Sehrawat, D. Goonetilleke and N. Sharma, *Adv. Energy Mater.*, 2017, **7**, 1602911.
221 Y.-S. Xu, S.-J. Guo, X.-S. Tao, Y.-G. Sun, J. Ma, C. Liu and A.-M. Cao, *Adv. Mater.*, 2021, **33**, 2100409.
222 Z. Xiao, F. Xia, L. Xu, X. Wang, J. Meng, H. Wang, X. Zhang, L. Geng, J. Wu and L. Mai, *Adv. Funct. Mater.*, 2022, **32**, 2108244.
223 W. Li, Z. Bi, W. Zhang, J. Wang, R. Rajagopalan, Q. Wang, D. Zhang, Z. Li, H. Wang and B. Wang, *J. Mater. Chem. A*, 2021, **9**, 8221–8247.
224 H. Park, Y. Lee, W. Ko, M. Choi, B. Ku, H. Ahn, J. Kim, J. Kang, J.-K. Yoo and J. Kim, *Batteries Supercaps*, 2023, **6**, e202200486.
225 X. Ding, Y. Wang, X. Wang, L. Geng, C. Guo, W. Liu, H. Wang, C. Sun and C. Han, *Chem. Eng. J.*, 2023, **466**, 143331.
226 M. G. T. Nathan, H. Yu, G.-T. Kim, J.-H. Kim, J. S. Cho, J. Kim and J.-K. Kim, *Adv. Sci.*, 2022, **9**, 2105882.
227 J. Liao, Y. Han, Z. Zhang, J. Xu, J. Li and X. Zhou, *Energy Environ. Mater.*, 2021, **4**, 178–200.
228 Z. Liu, H. Su, Y. Yang, T. Wu, S. Sun and H. Yu, *Energy Storage Mater.*, 2021, **34**, 211–228.
229 Z. Wu, J. Zou, S. Chen, X. Niu, J. Liu and L. Wang, *J. Power Sources*, 2021, **484**, 229307.
230 B. Pandit, E. S. Goda, M. Ubaidullah, S. F. Shaikh, U. T. Nakate, A. P. Khedulkar, D. Kumar and R.-A. Doong, *et al.*, *Ceram. Int.*, 2022, **48**, 28856–28863.
231 N. Naveen, W. B. Park, S. P. Singh, S. C. Han, D. Ahn, K.-S. Sohn and M. Pyo, *Small*, 2018, **14**, 1803495.
232 H. Kim, D.-H. Seo, A. Urban, J. Lee, D.-H. Kwon, S.-H. Bo, T. Shi, J. K. Papp, B. D. McCloskey and G. Ceder, *Chem. Mater.*, 2018, **30**, 6532–6539.
233 O. Smirnova, V. Nalbandyan, M. Avdeev, L. Medvedeva, B. Medvedev, V. Kharton and F. Marques, *J. Solid State Chem.*, 2005, **178**, 172–179.
234 L. Duan, H. Tang, X. Xu, J. Liao, X. Li, G. Zhou and X. Zhou, *Energy Storage Mater.*, 2023, **62**, 102950.
235 G. M. Kanyolo and T. Masese, *Advances in Honeycomb Layered Oxides: Part II-Theoretical advances in the characterisation of honeycomb layered oxides with optimised lattices of cations*, 2022.
236 C.-L. Liu, S.-H. Luo, H.-B. Huang, Y.-C. Zhai and Z.-W. Wang, *Chem. Eng. J.*, 2019, **356**, 53–59.
237 K. Sada and P. Barpanda, *Chem. Commun.*, 2020, **56**, 2272–2275.
238 T. Masese, K. Yoshii, K. Tada, M. Kato, S. Uchida, K. Kubota, T. Ina, T. Okumura, Z.-D. Huang and J. Furutani, *et al.*, *Energy Technol.*, 2020, **8**, 2000039.
239 C. Liu, S. Luo, H. Huang, Z. Wang, A. Hao, Y. Zhai and Z. Wang, *Electrochem. Commun.*, 2017, **82**, 150–154.
240 S. Zhao, K. Yan, P. Munroe, B. Sun and G. Wang, *Adv. Energy Mater.*, 2019, **9**, 1803757.

Open Access Article. Published on 04 dicembre 2023. Downloaded on 11/06/2026 17:40:22.
This article is licensed under a Creative Commons Attribution-NonCommercial 3.0 Unported Licence.

241 M. Clites, J. L. Hart, M. L. Taheri and E. Pomerantseva, *ACS Energy Lett.*, 2018, **3**, 562–567.
242 B. Tian, W. Tang, C. Su and Y. Li, *ACS Appl. Mater. Interfaces*, 2018, **10**, 642–650.
243 K. Yuan, R. Ning, M. Bai, N. Hu, K. Zhang, J. Gu, Q. Li, Y. Huang, C. Shen and K. Xie, *Energy Technol.*, 2020, **8**, 1900796.
244 A. Bhatia, J.-P. Pereira-Ramos, N. Emery and R. Baddour-Hadjean, *Chem. Mater.*, 2021, **33**, 5276–5289.
245 X. Niu, J. Qu, Y. Hong, L. Deng, R. Wang, M. Feng, J. Wang, L. Zeng, Q. Zhang and L. Guo, *et al.*, *J. Mater. Chem. A*, 2021, **9**, 13125–13134.
246 Y. Wu, G. Chen, X. Wu, L. Li, J. Yue, Y. Guan, J. Hou, F. Shi and J. Liang, *J. Semiconductors*, 2023, **44**, 041701.
247 J. H. Jo, J.-Y. Hwang, J. U. Choi, H. J. Kim, Y.-K. Sun and S.-T. Myung, *J. Power Sources*, 2019, **432**, 24–29.
248 W. Sohn, J. S. Chae, G. H. Lim and K. C. Roh, *J. Alloys Compd.*, 2022, **898**, 162904.
249 L. Wu, M. Gu, Y. Feng, S. Chen, L. Fan, X. Yu, K. Guo, J. Zhou and B. Lu, *Adv. Funct. Mater.*, 2022, **32**, 2109893.
250 S. C. Han, W. B. Park, K.-S. Sohn and M. Pyo, *Inorg. Chem. Front.*, 2020, **7**, 2023–2030.
251 D. Sumner, *Canadian Mathematical Bull.*, 1964, **7**, 65–75.
252 S. Troscheit, *Mathematical Proceedings of the Cambridge Philosophical Society*, 2014, pp. 295–311.
253 K. J. Falconer, *Mathematical Proceedings of the Cambridge Philosophical Society*, 2004, pp. 167–174.
254 R. Darst, *Proc. Am. Math. Soc.*, 1993, **119**, 105–108.
255 D. Groult, C. Mercey and B. Raveau, *J. Solid State Chem. France*, 1980, **32**, 289–296.
256 J. Liao, Q. Hu, X. Sheng, Z. Zhang, Y. Xu, X. Mo and X. Zhou, *ACS Mater. Lett.*, 2022, **4**, 1653–1659.
257 G. M. Kanyolo, T. Masese, N. Matsubara, C.-Y. Chen, J. Rizell, Z.-D. Huang, Y. Sassa, M. Månsson, H. Senoh and H. Matsumoto, *Chem. Soc. Rev.*, 2021, **50**, 3990–4030.
258 T. Masese, Y. Miyazaki, G. Mbiti Kanyolo, T. Takahashi, M. Ito, H. Senoh and T. Saito, *ACS Appl. Nano Mater.*, 2021, **4**, 279–287.
259 G. M. Kanyolo and T. Masese, *J. Phys. Commun.*, 2022, **6**, 041001.
260 G. M. Kanyolo and T. Masese, *Reproducing the asymptotic behaviour of galaxy rotation curves by a novel constraint in general relativity*, 2021.
261 T. Masese, G. M. Kanyolo, Y. Miyazaki, M. Ito, N. Taguchi, J. Rizell, S. Tachibana, K. Tada, Z.-D. Huang and A. Alshehabi, *et al.*, *Adv. Sci.*, 2022, 2204672.
262 G. M. Kanyolo, T. Masese, A. Alshehabi and Z.-D. Huang, *Advances in honeycomb layered oxides: Part I-Syntheses and Characterisations of Pnictogen-and Chalcogen-Based Honeycomb Layered Oxides*, 2022.
263 G. Kanyolo and T. Masese, *Sci. Rep.*, 2020, **10**, 1–13.
264 G. Kanyolo and T. Masese, *Sci. Rep.*, 2022, **12**, 1–14.
265 T. Masese, Y. Miyazaki, J. Rizell, G. Kanyolo, C. Chen, H. Ubukata, K. Kubota, K. Sau, T. Ikeshoji, Z. Huang and O. Mixed, *Nat. Commun.*, 2021, **12**, 1–16.
266 G. Kanyolo and T. Masese, Partition function for quantum gravity in 4 dimensions as a 1/*N* expansion, preprint: hal-03335930 technical report, 2021.
267 Y. Kee, N. Dimov, A. Staykov and S. Okada, *Mater. Lett.*, 2016, **183**, 187–190.
268 Y. Kee, B. Put, N. Dimov, A. Staykov and S. Okada, *Batteries Supercaps*, 2020, **3**, 390–391.
269 L. Xiao, Z. Din, Q. Huang, C. Chen, Y. Feng, C. Liang, P. Gao and W. Wei, *Acta Mater.*, 2020, **199**, 34–41.
270 D. Bérardan, S. Franger, A. Meena and N. Dragoe, *J. Mater. Chem. A*, 2016, **4**, 9536–9541.
271 C. M. Rost, E. Sachet, T. Borman, A. Moballegh, E. C. Dickey, D. Hou, J. L. Jones, S. Curtarolo and J.-P. Maria, *Nat. Commun.*, 2015, **6**, 1–8.
272 Y. Cai, X. Zeng, D. Pang, Y. Gu, J. Qi, T. Masese, F. Chang, Y. Li, S. Wang and Z. Li, *et al.*, *Materialia*, 2023, **27**, 101674.
273 A. Sagot, L. Stievano and V. Pralong, *ACS Appl. Energy Mater.*, 2023, **6**, 7785–7789.
274 S. Park, S. Park, Y. Park, M. H. Alfaruqi, J.-Y. Hwang and J. Kim, *Energy Environ. Sci.*, 2021, **14**, 5864–5874.
275 R. Maleki, M. Asadnia and A. Razmjou, *Adv. Intell. Syst.*, 2022, **4**, 2200073.
276 M.-F. Ng, Y. Sun and Z. W. Seh, *Energy Adv.*, 2023, **2**, 449–464.
277 Y. Chen and C. Wang, *Acc. Chem. Res.*, 2020, **53**, 2636–2647.
278 A. Zhou, W. Cheng, W. Wang, Q. Zhao, J. Xie, W. Zhang, H. Gao, L. Xue and J. Li, *Adv. Energy Mater.*, 2021, **11**, 2000943.
279 W. Shu, C. Han and X. Wang, *Adv. Funct. Mater.*, 2023, 2309636.
280 T. Hosaka, K. Kubota, H. Kojima and S. Komaba, *Chem. Commun.*, 2018, **54**, 8387–8390.
281 H. Onuma, K. Kubota, S. Muratsubaki, T. Hosaka, R. Tatara, T. Yamamoto, K. Matsumoto, T. Nohira, R. Hagiwara and H. Oji, *et al.*, *ACS Energy Lett.*, 2020, **5**, 2849–2857.
282 Y. Liu, Z.-Y. Gu, Y.-L. Heng, J.-Z. Guo, M. Du, H.-J. Liang, J.-L. Yang, K.-Y. Zhang, K. Li and X.-L. Wu, *Green Energy Environ.*, 2023, DOI: **10.1016/j.gee.2023.10.004**.
283 L. Wu, J. Sun, Y. Zhang, S. Jin, Y. Kong and J. Xu, *Inorg. Chem.*, 2010, **49**, 2715–2720.
284 L. Wu, B. Wang, Y. Zhang, L. Li, H. Wang, H. Yi, Y. Kong and J. Xu, *Dalton Trans.*, 2014, **43**, 13845–13851.
285 Y. Yao, K. Satoh, T. Takahashi and T. Yoneyama, *Soil Sci. Plant Nutrition*, 2006, **52**, 133.
286 Y. Luo, Z. Xia, H. Liu and Y. He, *Opt. Mater.*, 2014, **36**, 723–726.
287 E. Arroyabe and V. Kahlenberg, *Eur. J. Mineral.*, 2011, **23**, 101–110.
288 Z. Leng, D. Zhang, H. Bai, P. She, J. Zhao and Z. Tang, *Opt. Mater.*, 2021, **118**, 111293.
289 Y. Cai, W. Liu, F. Chang, S. Jin, X. Yang, C. Zhang, L. Bai, T. Masese, Z. Li and Z.-D. Huang, *ACS Appl. Mater. Interfaces*, 2023, **15**, 48277–48286.
290 V. S. K. Sungjemmenla, C. B. Soni, V. Kumar and Z. W. Seh, *Energy Technol.*, 2022, **10**, 2200421.
291 E. M. Erickson, W. Li, A. Dolocan and A. Manthiram, *ACS Appl. Mater. Interfaces*, 2020, **12**, 16451–16461.
292 K. Edstroem, T. Gustafsson and J. O. Thomas, *Electrochim. Acta*, 2004, **50**, 397–403.

© 2024 The Author(s). Published by the Royal Society of Chemistry

Open Access Article. Published on 04 dicembre 2023. Downloaded on 11/06/2026 17:40:22.
This article is licensed under a Creative Commons Attribution-NonCommercial 3.0 Unported Licence.

293 H. Maleki Kheimeh Sari and X. Li, *Adv. Energy Mater.*, 2019, **9**, 1901597.
294 S. Malmgren, K. Ciosek, M. Hahlin, T. Gustafsson, M. Gorgoi, H. Rensmo and K. Edström, *Electrochim. Acta*, 2013, **97**, 23–32.
295 K. Nie, Y. Hong, J. Qiu, Q. Li, X. Yu, H. Li and L. Chen, *Front. Chem.*, 2018, **6**, 616.
296 M. Gauthier, T. J. Carney, A. Grimaud, L. Giordano, N. Pour, H.-H. Chang, D. P. Fenning, S. F. Lux, O. Paschos and C. Bauer, *et al.*, *J. Phys. Chem. Lett.*, 2015, **6**, 4653–4672.
297 H. Liu, Y. He, K. Cao, S. Wang, Y. Jiang, X. Liu, K.-J. Huang, Q.-S. Jing and L. Jiao, *Small*, 2021, **17**, 2008133.
298 K. Cao, S. Wang, Y. Jia, D. Xu, H. Liu, K.-J. Huang, Q.-S. Jing and L. Jiao, *Chem. Eng. J.*, 2021, **406**, 126902.
299 Y. Chen, H. Qin, J. Zhou, T. Yang, B. Sun, Y. Ni, H. Wang, S. A. Redfern, M. Miao and H.-Q. Lin, *et al.*, *J. Phys. Chem. Lett.*, 2022, **13**, 7439–7447.
300 X. L. Huang, F. Zhao, Y. Qi, Y.-A. Qiu, J. S. Chen, H. K. Liu, S. X. Dou and Z. M. Wang, *Energy Storage Mater.*, 2021, **42**, 193–208.
301 Q. Yang, Z. Tai, Q. Xia, W. Lai, W. Wang, B. Zhang, Z. Yan, J. Peng, H. Yang and H. Liu, *et al.*, *J. Mater. Chem. A*, 2021, **9**, 8378–8385.
302 E. J. Canto-Aguilar, M. A. Oliver-Tolentino, G. Ramos-Sánchez and I. González, *Electrochim. Acta*, 2021, **371**, 137828.
303 A. P. Vijaya Kumar Saroja, Z. Wang, H. R. Tinker, F. R. Wang, P. R. Shearing and Y. Xu, *SusMat*, 2023, **3**, 222–234.
304 C. He, J. Zou, C.-F. Sun and Q. Liu, *Mater. Lett.*, 2023, 134627.
305 X. Niu, Y. Zhang, L. Tan, Z. Yang, J. Yang, T. Liu, L. Zeng, Y. Zhu and L. Guo, *Energy Storage Mater.*, 2019, **22**, 160–167.
306 Y. Wu, H.-B. Huang, Y. Feng, Z.-S. Wu and Y. Yu, *Adv. Mater.*, 2019, **31**, 1901414.
307 Y. Liu, Y.-X. Lu, Y.-S. Xu, Q.-S. Meng, J.-C. Gao, Y.-G. Sun, Y.-S. Hu, B.-B. Chang, C.-T. Liu and A.-M. Cao, *Adv. Mater.*, 2020, **32**, 2000505.
308 I. Sultana, M. M. Rahman, Y. Chen and A. M. Glushenkov, *Adv. Funct. Mater.*, 2018, **28**, 1703857.
309 X. Yuan, B. Zhu, J. Feng, C. Wang, X. Cai and R. Qin, *Chem. Eng. J.*, 2021, **405**, 126897.
310 K.-X. Lei, J. Wang, C. Chen, S.-Y. Li, S.-W. Wang, S.-J. Zheng and F.-J. Li, *Rare Met.*, 2020, **39**, 989–1004.
311 S. Imtiaz, I. S. Amiinu, Y. Xu, T. Kennedy, C. Blackman and K. M. Ryan, *Mater. Today*, 2021, **48**, 241–269.
312 H. Gao, X. Guo, S. Wang, F. Zhang, H. Liu and G. Wang, *EcoMat*, 2020, **2**, e12027.
313 W. Li, Z. Li, C. Zhang, W. Liu, C. Han, B. Yan, S. An and X. Qiu, *Solid State Ionics*, 2020, **351**, 115319.
314 J. Wang, H. Wang, X. Zang, D. Zhai and F. Kang, *Batteries Supercaps*, 2021, **4**, 554–570.
315 G. Luo, X. Feng, M. Qian, W. Zhang, W. Qin, C. Wu and L. Pan, *Mater. Chem. Front.*, 2023, **7**, 3011–3036.
316 K.-H. Nam, V. Ganesan, K. H. Chae and C.-M. Park, *Carbon*, 2021, **181**, 290–299.
317 Z. Li, J. Wen, Y. Cai, F. Lv, X. Zeng, Q. Liu, T. Masese, C. Zhang, X. Yang and Y. Ma, *et al.*, *Adv. Funct. Mater.*, 2023, 2300582.
318 Y. Xu, J. Zhang and D. Li, *Chem. – Asian J.*, 2020, **15**, 1648–1659.
319 S. Liu, L. Kang, J. Henzie, J. Zhang, J. Ha, M. A. Amin, M. S. A. Hossain, S. C. Jun and Y. Yamauchi, *ACS Nano*, 2021, **15**, 18931–18973.
320 J. Zheng, Y. Wu, Y. Sun, J. Rong, H. Li and L. Niu, *Nano-Micro Lett.*, 2021, **13**, 1–37.
321 Z. Hong, H. Maleki, T. Ludwig, Y. Zhen, M. Wilhelm, D. Lee, K.-H. Kim and S. Mathur, *J. Energy Chem.*, 2021, **62**, 660–691.
322 Y. Huang, R. Haider, S. Xu, K. Liu, Z.-F. Ma and X. Yuan, *Energy Storage Mater.*, 2022, **51**, 327–360.
323 N. Khan, G. Han and S. A. Mazari, *J. Electroanal. Chem.*, 2022, **907**, 116051.
324 Q. Xue, D. Li, Y. Huang, X. Zhang, Y. Ye, E. Fan, L. Li, F. Wu and R. Chen, *J. Mater. Chem. A*, 2018, **6**, 12559–12564.
325 J. Rehman, X. Fan, A. Laref, V. A. Dinh and W. Zheng, *J. Alloys Compd.*, 2021, **865**, 158782.
326 G. Suo, Y. Cheng, J. Zhang and S. M. Ahmed, *ChemNano-Mat*, 2021, **7**, 1291–1308.
327 S. Yu, S.-O. Kim, H.-S. Kim and W. Choi, *Int. J. Energy Res.*, 2019, **43**, 7646–7654.
328 L. Zhang, W. Wang, S. Lu and Y. Xiang, *Adv. Energy Mater.*, 2021, **11**, 2003640.
329 J. Wang, H. Wang, X. Zang, D. Zhai and F. Kang, *Batteries Supercaps*, 2021, **4**, 554–570.
330 T. Yamamoto, A. Yadav and T. Nohira, *J. Electrochem. Soc.*, 2022, **169**, 050507.
331 J. Wang, Z. Liu, J. Zhou, K. Han and B. Lu, *ACS Mater. Lett.*, 2021, **3**, 1572–1598.
332 L. Xue, H. Gao, W. Zhou, S. Xin, K. Park, Y. Li and J. B. Goodenough, *Adv. Mater.*, 2016, **28**, 9608–9612.
333 S. Dong, Y. Song, Y. Fang, K. Zhu, K. Ye, Y. Gao, J. Yan, G. Wang and D. Cao, *Carbon*, 2021, **178**, 1–9.
334 Y.-Z. Fang, R. Hu, K. Zhu, K. Ye, J. Yan, G. Wang and D. Cao, *Adv. Funct. Mater.*, 2020, **30**, 2005663.
335 X. Li, J. Li, L. Ma, C. Yu, Z. Ji, L. Pan and W. Mai, *Energy Environ. Mater.*, 2022, **5**, 458–469.
336 H. Lei, J. Li, X. Zhang, L. Ma, Z. Ji, Z. Wang, L. Pan, S. Tan and W. Mai, *InfoMat*, 2022, **4**, e12272.
337 Y.-Y. Zhu, Y.-H. Wang, Y.-T. Wang, T.-J. Xu and P. Chang, *Carbon Energy*, 2022, **4**, 1182–1213.
338 M. Shen, H. Ding, L. Fan, A. M. Rao, J. Zhou and B. Lu, *Adv. Funct. Mater.*, 2023, 2213362.
339 F. Yuan, Y. Li, D. Zhang, Z. Li, H. Wang, B. Wang, Y. Wu and Y. A. Wu, *Inorg. Chem. Front.*, 2023, **10**, 2547–2573.
340 A. K. Thakur, M. S. Ahmed, J. Park, R. Prabakaran, S. Sidney, R. Sathyamurthy, S. C. Kim, S. Periasamy, J. Kim and J.-Y. Hwang, *Int. J. Energy Res.*, 2022, **46**, 4033–4070.
341 Y.-h Wu, X.-n Wu, Y.-y Guan, Y. Xu, F.-n Shi and J.-y Liang, *New Carbon Mater.*, 2022, **37**, 852–874.
342 T. Zhu, B. Mai, P. Hu, C. Cai, B. Xing, Z. Wei, C. Chen, H. Fan, M. Li and X. Wang, *ACS Appl. Energy Mater.*, 2023, **6**, 2370–2377.
343 W.-J. Deng, X.-D. He, L.-M. Zhang, J.-R. Wang and C.-H. Chen, *Energy Technol.*, 2021, **9**, 2100644.

© 2024 The Author(s). Published by the Royal Society of Chemistry

Open Access Article. Published on 04 dicembre 2023. Downloaded on 11/06/2026 17:40:22.
This article is licensed under a Creative Commons Attribution-NonCommercial 3.0 Unported Licence.

344 J. Zou, C. He, J. Bao, C.-F. Sun and Y. Li, *Ionics*, 2023, 1–7.
345 Y. Liu, Y.-X. Lu, Y.-S. Xu, Q.-S. Meng, J.-C. Gao, Y.-G. Sun, Y.-S. Hu, B.-B. Chang, C.-T. Liu and A.-M. Cao, *Adv. Mater.*, 2020, **32**, 2000505.
346 X. Wu, Y. Chen, Z. Xing, C. W. K. Lam, S.-S. Pang, W. Zhang and Z. Ju, *Adv. Energy Mater.*, 2019, **9**, 1900343.
347 Z. Jian, S. Hwang, Z. Li, A. S. Hernandez, X. Wang, Z. Xing, D. Su and X. Ji, *Adv. Funct. Mater.*, 2017, **27**, 1700324.
348 Z. Tai, Q. Zhang, Y. Liu, H. Liu and S. Dou, *Carbon*, 2017, **123**, 54–61.
349 L. Wang, J. Yang, J. Li, T. Chen, S. Chen, Z. Wu, J. Qiu, B. Wang, P. Gao and X. Niu, *et al.*, *J. Power Sources*, 2019, **409**, 24–30.
350 Z. Xing, Y. Qi, Z. Jian and X. Ji, *ACS Appl. Mater. Interfaces*, 2017, **9**, 4343–4351.
351 X. Yuan, B. Zhu, J. Feng, C. Wang, X. Cai and R. Qin, *Chem. Eng. J.*, 2021, **405**, 126897.
352 J. Zhou and S. Guo, *SmartMat*, 2021, **2**, 176–201.
353 X. Wang, K. Han, D. Qin, Q. Li, C. Wang, C. Niu and L. Mai, *Nanoscale*, 2017, **9**, 18216–18222.
354 X. Li, J. Li, L. Ma, C. Yu, Z. Ji, L. Pan and W. Mai, *Energy Environ. Mater.*, 2022, **5**, 458–469.
355 M. Sha, L. Liu, H. Zhao and Y. Lei, *Carbon Energy*, 2020, **2**, 350–369.
356 X. He, J. Liao, Z. Tang, L. Xiao, X. Ding, Q. Hu, Z. Wen and C. Chen, *J. Power Sources*, 2018, **396**, 533–541.
357 Q. Wang, C. Gao, W. Zhang, S. Luo, M. Zhou, Y. Liu, R. Liu, Y. Zhang, Z. Wang and A. Hao, *Electrochim. Acta*, 2019, **324**, 134902.
358 Y. Feng, S. Chen, D. Shen, J. Zhou and B. Lu, *Energy Environ. Mater.*, 2021, **4**, 451–457.
359 Z. Wu, J. Zou, S. Shabanian, K. Golovin and J. Liu, *Chem. Eng. J.*, 2022, **427**, 130972.
360 F. Yuan, J. Hu, Y. Lei, R. Zhao, C. Gao, H. Wang, B. Li, F. Kang and D. Zhai, *ACS Nano*, 2022, **16**, 12511–12519.
361 J. Han, M. Xu, Y. Niu, G.-N. Li, M. Wang, Y. Zhang, M. Jia and C. ming Li, *Chem. Commun.*, 2016, **52**, 11274–11276.
362 Y. Dong, Z.-S. Wu, S. Zheng, X. Wang, J. Qin, S. Wang, X. Shi and X. Bao, *ACS Nano*, 2017, **11**, 4792–4800.
363 W. D. McCulloch, X. Ren, M. Yu, Z. Huang and Y. Wu, *ACS Appl. Mater. Interfaces*, 2015, **7**, 26158–26166.
364 M. Shimizu, R. Yatsuzuka, T. Koya, T. Yamakami and S. Arai, *ACS Appl. Energy Mater.*, 2018, **1**, 6865–6870.
365 K. Cao, H. Liu, W. Li, C. Xu, Q. Han, Z. Zhang and L. Jiao, *J. Electroanal. Chem.*, 2019, **841**, 51–55.
366 C. Liu, H. Wang, S. Zhang, M. Han, Y. Cao, S. Liu, Z. Yang, A. Chen and J. Sun, *Nanoscale*, 2020, **12**, 11427–11434.
367 B. Kishore, G. Venkatesh and N. Munichandraiah, *J. Electrochem. Soc.*, 2016, **163**, A2551.
368 S. Zhao, L. Dong, B. Sun, K. Yan, J. Zhang, S. Wan, F. He, P. Munroe, P. H. Notten and G. Wang, *Small*, 2020, **16**, 1906131.
369 P. R. Kumar, K. Kubota, D. Igarashi and S. Komaba, *J. Phys. Chem.*, 2021, **125**, 24823–24830.
370 N. Voronina, J. H. Jo, A. Konarov, J. Kim and S.-T. Myung, *Small*, 2020, **16**, 2001090.
371 J. Han, Y. Niu, S.-J. Bao, Y.-N. Yu, S.-Y. Lu and M. Xu, *Chem. Commun.*, 2016, **52**, 11661–11664.
372 K. Lei, F. Li, C. Mu, J. Wang, Q. Zhao, C. Chen and J. Chen, *Energy Environ. Sci.*, 2017, **10**, 552–557.
373 I. Sultana, M. M. Rahman, Y. Chen and A. M. Glushenkov, *Adv. Funct. Mater.*, 2018, **28**, 1703857.
374 J. Huang, X. Lin, H. Tan and B. Zhang, *Adv. Energy Mater.*, 2018, **8**, 1703496.
375 I. Sultana, T. Ramireddy, M. M. Rahman, Y. Chen and A. M. Glushenkov, *Chem. Commun.*, 2016, **52**, 9279–9282.
376 S. Chong, M. Ma, L. Yuan, S. Qiao, S. Dong, H. Liu and S. Dou, *Energy Environ. Mater.*, 2023, e12458.
377 T. Sun, J. Xie, W. Guo, D.-S. Li and Q. Zhang, *Adv. Energy Mater.*, 2020, **10**, 1904199.
378 L. Zhu, G. Ding, L. Xie, X. Cao, J. Liu, X. Lei and J. Ma, *Chem. Mater.*, 2019, **31**, 8582–8612.
379 E. R. Wolfson, L. Schkeryantz, E. M. Moscarello, J. P. Fernandez, J. Paszek, Y. Wu, C. M. Hadad and P. L. McGrier, *ACS Appl. Mater. Interfaces*, 2021, **13**, 41628–41636.
380 J. Sun, Y. Xu, A. Li, R. Tian, Y. Fei, B. Chen and X. Zhou, *ACS Appl. Nano Mater.*, 2022, **5**, 15592–15599.
381 H. Wang, D. Zhai and F. Kang, *Energy Environ. Sci.*, 2020, **13**, 4583–4608.
382 F. Yuan, Z. Li, D. Zhang, Q. Wang, H. Wang, H. Sun, Q. Yu, W. Wang and B. Wang, *Adv. Sci.*, 2022, **9**, 2200683.
383 X. Zhang, J. Meng, X. Wang, Z. Xiao, P. Wu and L. Mai, *Energy Storage Mater.*, 2021, **38**, 30–49.
384 H. Wang, J. Hu, J. Dong, K. C. Lau, L. Qin, Y. Lei, B. Li, D. Zhai, Y. Wu and F. Kang, *Adv. Energy Mater.*, 2019, **9**, 1902697.
385 N. Daumas and A. Hérold, *Sci. Paris C*, 1969, **268**, 373.
386 A. Lerf, *Dalton Trans.*, 2014, **43**, 10276–10291.
387 W. Rüdorff and U. Hofmann, *Z. Anorg. Allg. Chem.*, 1938, **238**, 1–50.
388 A. Kushima, X. Qian, P. Zhao, S. Zhang and J. Li, *Nano Lett.*, 2015, **15**, 1302–1308.
389 M. Barsoum and G. Tucker, *Scr. Mater.*, 2017, **139**, 166–172.
390 J. G. McHugh, P. Mouratidis and K. Jolley, *Phys. Rev. B*, 2021, **103**, 195436.
391 H. O. Badr and M. W. Barsoum, *Carbon*, 2023, **201**, 599–615.
392 M. W. Barsoum, *Front. Mater.*, 2020, **7**, 146.
393 Y. Lei, D. Han, J. Dong, L. Qin, X. Li, D. Zhai, B. Li, Y. Wu and F. Kang, *Energy Storage Mater.*, 2020, **24**, 319–328.
394 J. Park, Y. Jeong, M. H. Alfaruqi, Y. Liu, X. Xu, S. Xiong, M.-G. Jung, H.-G. Jung, J. Kim and J.-Y. Hwang, *et al.*, *ACS Energy Lett.*, 2021, **7**, 401–409.
395 M. Zhou, P. Bai, X. Ji, J. Yang, C. Wang and Y. Xu, *Adv. Mater.*, 2021, **33**, 2003741.
396 Y. Liu, C. Gao, L. Dai, Q. Deng, L. Wang, J. Luo, S. Liu and N. Hu, *Small*, 2020, **16**, 2004096.
397 Y. Lei, L. Qin, R. Liu, K. C. Lau, Y. Wu, D. Zhai, B. Li and F. Kang, *ACS Appl. Energy Mater.*, 2018, **1**, 1828–1833.
398 J. Li, Y. Hu, H. Xie, J. Peng, L. Fan, J. Zhou and B. Lu, *Angew. Chem.*, 2022, **134**, e202208291.

© 2024 The Author(s). Published by the Royal Society of Chemistry

Open Access Article. Published on 04 dicembre 2023. Downloaded on 11/06/2026 17:40:22.
This article is licensed under a Creative Commons Attribution-NonCommercial 3.0 Unported Licence.

399 L. Fan, Y. Hu, A. M. Rao, J. Zhou, Z. Hou, C. Wang and B. Lu, *Small Methods*, 2021, **5**, 2101131.
400 Y. Hu, L. Fan, A. M. Rao, W. Yu, C. Zhuoma, Y. Feng, Z. Qin, J. Zhou and B. Lu, *Natl. Sci. Rev.*, 2022, **9**, nwac134.
401 T. Hosaka, T. Matsuyama, K. Kubota, S. Yasuno and S. Komaba, *ACS Appl. Mater. Interfaces*, 2020, **12**, 34873–34881.
402 T. Hosaka, T. Fukabori, T. Matsuyama, R. Tatara, K. Kubota and S. Komaba, *ACS Energy Lett.*, 2021, **6**, 3643–3649.
403 M. Zhou, Y. Fan, Y. Gao, Z. Ma, Z. Liu, W. Wang, H. A. Younus, Z. Chen, X. Wang and S. Zhang, *ACS Appl. Mater. Interfaces*, 2022, **14**, 44429–44438.
404 Z. T. Gossage, T. Hosaka, T. Matsuyama, R. Tatara and S. Komaba, *J. Mater. Chem. A*, 2023, **11**, 914–925.
405 J. Popovic, *J. Electrochem. Soc.*, 2022, **169**, 030510.
406 Z. Zhao, H. Zhang, F. Li, L. Zhao, Q. Li and H. Li, *Nano Lett.*, 2022, **22**, 10102–10110.
407 H. Wang, D. Zhai and F. Kang, *Energy Environ. Sci.*, 2020, **13**, 4583–4608.
408 G. Liu, Z. Cao, L. Zhou, J. Zhang, Q. Sun, J.-Y. Hwang, L. Cavallo, L. Wang, Y.-K. Sun and J. Ming, *Adv. Funct. Mater.*, 2020, **30**, 2001934.
409 G. Zeng, S. Xiong, Y. Qian, L. Ci and J. Feng, *J. Electrochem. Soc.*, 2019, **166**, A1217–A1222.
410 S. Ji, J. Li, J. Li, C. Song, S. Wang, K. Wang, K. S. Hui, C. Zha, Y. Zheng and D. A. Dinh, *et al.*, *Adv. Funct. Mater.*, 2022, **32**, 2200771.
411 L. Fan, H. Xie, Y. Hu, Z. Caixiang, A. M. Rao, J. Zhou and B. Lu, *Energy Environ. Sci.*, 2023, **16**, 305–315.
412 X. Feng, Z. Zhang, R. Li, W. Xiong, B. Yu, M. Wang, J. Chen, Z. Ma, B. Guo and Y. Huang, *et al.*, *Sustainable Energy Fuels*, 2022, **6**, 2198–2206.
413 Y. Gu, S. Fang, L. Yang and S.-I. Hirano, *ACS Appl. Energy Mater.*, 2021, **4**, 4919–4927.
414 Y. Zheng, D. Wang, S. Kaushik, S. Zhang, T. Wada, J. Hwang, K. Matsumoto and R. Hagiwara, *EnergyChem*, 2022, **4**, 100075.
415 T. Yamamoto, R. Matsubara and T. Nohira, *J. Chem. Eng. Data*, 2021, **66**, 1081–1088.
416 T. Yamamoto, A. Yadav and T. Nohira, *J. Electrochem. Soc.*, 2022, **169**, 050507.
417 T. Yamamoto and T. Nohira, *Chem. Rec.*, 2023, e202300169.
418 T. Yamamoto, *Electrochemistry*, 2022, **90**, 101005.
419 W. Zhang, H. Tian, J. Wang, H. Sun, J. Wang and W. Huang, *ACS Appl. Mater. Interfaces*, 2022, **14**, 38887–38894.
420 H. Sun, P. Liang, G. Zhu, W. H. Hung, Y.-Y. Li, H.-C. Tai, C.-L. Huang, J. Li, Y. Meng and M. Angell, *et al.*, *Proc. Natl. Acad. Sci. U. S. A.*, 2020, **117**, 27847–27853.
421 M. Fiore, S. Wheeler, K. Hurlbutt, I. Capone, J. Fawdon, R. Ruffo and M. Pasta, *Chem. Mater.*, 2020, **32**, 7653–7661.
422 K. Beltrop, S. Beuker, A. Heckmann, M. Winter and T. Placke, *Energy Environ. Sci.*, 2017, **10**, 2090–2094.
423 T. Yamamoto, K. Matsumoto, R. Hagiwara and T. Nohira, *J. Phys. Chem. C*, 2017, **121**, 18450–18458.
424 M. Arnaiz, A. Bothe, S. Dsoke, A. Balducci and J. Ajuria, *J. Electrochem. Soc.*, 2019, **166**, A3504.
425 W. Zhou, M. Zhang, X. Kong, W. Huang and Q. Zhang, *Adv. Sci.*, 2021, **8**, 2004490.
426 Y. Chen, S. Liu, Z. Bi, Z. Li, F. Zhou, R. Shi and T. Mu, *Green Energy Environ.*, 2023, DOI: 10.1016/j.gee.2023.05.002.
427 I. A. Shkrob, L. A. Robertson, Z. Yu, R. S. Assary, L. Cheng, L. Zhang, E. Sarnello, X. Liu, T. Li and A. P. Kaur, *et al.*, *J. Mol. Liq.*, 2021, **334**, 116533.
428 H. Yamamoto, C.-Y. Chen, K. Kubota, K. Matsumoto and R. Hagiwara, *J. Phys. Chem. B*, 2020, **124**, 6341–6347.
429 L. Schkeryantz, P. Nguyen, W. D. McCulloch, C. E. Moore, K. C. Lau and Y. Wu, *J. Phys. Chem. C*, 2022, **126**, 11407–11413.
430 J. Chen, S. Lei, S. Zhang, C. Zhu, Q. Liu, C. Wang, Z. Zhang, S. Wang, Y. Shi and L. Yin, *et al.*, *Adv. Funct. Mater.*, 2023, 2215027.
431 X. Zhang, T. Xiong, B. He, S. Feng, X. Wang, L. Wei and L. Mai, *Energy Environ. Sci.*, 2022, **15**, 3750–3774.
432 L. Jiang, Y. Lu, C. Zhao, L. Liu, J. Zhang, Q. Zhang, X. Shen, J. Zhao, X. Yu and H. Li, *et al.*, *Nat. Energy*, 2019, **4**, 495–503.
433 J. Han, A. Mariani, S. Passerini and A. Varzi, *Energy Environ. Sci.*, 2023, **16**, 1480–1501.
434 P. Kulkarni, D. Ghosh and R. G. Balakrishna, *Sustainable Energy Fuels*, 2021, **5**, 1619–1654.
435 D. P. Leonard, Z. Wei, G. Chen, F. Du and X. Ji, *ACS Energy Lett.*, 2018, **3**, 373–374.
436 H. Chen, Z. Zhang, Z. Wei, G. Chen, X. Yang, C. Wang and F. Du, *Sustainable Energy Fuels*, 2020, **4**, 128–131.
437 L. Droguet, A. Grimaud, O. Fontaine and J.-M. Tarascon, *Adv. Energy Mater.*, 2020, **10**, 2002440.
438 D. Xiao, L. Zhang, Z. Li, H. Dou and X. Zhang, *Energy Storage Mater.*, 2022, **44**, 10–28.
439 J.-F. Wu, W. Zhou, Z. Wang, W.-W. Wang, X. Lan, H. Yan, T. Shi, R. Hu, X. Cui and C. Xu, *et al.*, *Adv. Mater.*, 2023, 2209833.
440 H. Fei, Y. Liu, Y. An, X. Xu, J. Zhang, B. Xi, S. Xiong and J. Feng, *J. Power Sources*, 2019, **433**, 226697.
441 G. Du, M. Tao, D. Liu, M. K. Aslam, Y. Qi, J. Jiang, Y. Li, S.-J. Bao and M. Xu, *J. Colloid Interface Sci.*, 2021, **582**, 932–939.
442 T. Masese and G. M. Kanyolo, *Storing Energy*, Elsevier, 2022, pp. 265–307.
443 J. Zheng, H. Fang, L. Fan, Y. Ren, P. Jena and Y. Wu, *J. Phys. Chem. Lett.*, 2021, **12**, 7120–7126.
444 H. Aziam, B. Larhrib, C. Hakim, N. Sabi, H. B. Youcef and I. Saadoune, *Renewable Sustainable Energy Rev.*, 2022, **167**, 112694.
445 H. Fei, Y. Liu, Y. An, X. Xu, G. Zeng, Y. Tian, L. Ci, B. Xi, S. Xiong and J. Feng, *J. Power Sources*, 2018, **399**, 294–298.
446 E. Manarin, F. Corsini, S. Trano, L. Fagiolari, J. Amici, C. Francia, S. Bodoardo, S. Turri, F. Bella and G. Griffini, *ACS Appl. Polym. Mater.*, 2022, **4**, 3855–3865.
447 M. Elmanzalawy, E. Sanchez-Ahijón, O. Kisacik, J. Carretero-González and E. Castillo-Martnez, *ACS Appl. Energy Mater.*, 2022, **5**, 9009–9019.
448 A. D. Khudyshkina, P. A. Morozova, A. J. Butzelaar, M. Hoffmann, M. Wilhelm, P. Theato, S. S. Fedotov and F. Jeschull, *ACS Appl. Polym. Mater.*, 2022, **4**, 2734–2746.

© 2024 The Author(s). Published by the Royal Society of Chemistry

Open Access Article. Published on 04 dicembre 2023. Downloaded on 11/06/2026 17:40:22.
This article is licensed under a Creative Commons Attribution-NonCommercial 3.0 Unported Licence.

449 A. D. Khudyshkina, A. J. Butzelaar, Y. Guo, M. Hoffmann, T. Bergfeldt, M. Schaller, S. Indris, M. Wilhelm, P. Théato and F. Jeschull, *Electrochim. Acta*, 2023, **454**, 142421.
450 Y. Zhang, A. Bahi, F. Ko and J. Liu, *Small*, 2022, **18**, 2107186.
451 J. Zheng, B. Perry and Y. Wu, *ACS Mater. Au*, 2021, **1**, 92–106.
452 Y. Zhang, P. Qiu, J. Zheng, X. Chen, X.-M. Chen, S. Li, C. Ji, Y. Wu and X. Chen, *ACS Appl. Mater. Interfaces*, 2022, **14**, 17378–17387.
453 J. Shao, J. Zheng, L. Qin, S. Zhang, Y. Ren and Y. Wu, *Angew. Chem.*, 2022, **134**, e202200606.
454 H. Yuan, H. Li, T. Zhang, G. Li, T. He, F. Du and S. Feng, *J. Mater. Chem. A*, 2018, **6**, 8413–8418.
455 Y.-J. Gu, Y.-A. Lo, A.-C. Li, Y.-C. Chen, J.-H. Li, Y.-S. Wang, H.-K. Tian, W. Kaveevivitchai and C.-W. Kung, *ACS Appl. Energy Mater.*, 2022, **5**, 8573–8580.
456 E. Burmakin, B. Antonov and G. S. Shekhtman, *Inorg. Mater.*, 2010, **46**, 540–544.
457 G. Nechaev and E. Burmakin, *Russ. J. Electrochem.*, 2011, **47**, 1411–1414.
458 E. Burmakin and G. Nechaev, *Russ. J. Electrochem.*, 2013, **49**, 1001–1003.
459 V. R. Jeedi, K. K. Ganta, Y. Mallaiah, R. Swarnalatha, S. N. Reddy and A. S. Chary, *J. Polym. Res.*, 2022, **29**, 64.
460 G. Nechaev and E. Burmakin, *Russ. J. Electrochem.*, 2011, **47**, 457–460.
461 E. Burmakin, G. Nechaev and G. S. Shekhtman, *Russ. J. Electrochem.*, 2008, **44**, 1386–1392.
462 E. Burmakin, G. Nechaev, G. S. Shekhtman and S. Plaksin, *Russ. J. Electrochem.*, 2009, **45**, 934–937.
463 E. Burmakin and G. S. Shekhtman, *Inorg. Mater.*, 2008, **44**, 882–885.
464 N. V. Proskurnina, V. I. Voronin, G. S. Shekhtman, L. N. Maskaeva, N. A. Kabanova, A. A. Kabanov and V. A. Blatov, *J. Phys. Chem. C*, 2017, **121**, 21128–21135.
465 T. Takahashi and K. Kuwabara, *Electrochim. Acta*, 1978, **23**, 375–379.
466 S. Yamamoto, S. Tamura and N. Imanaka, *J. Alloys Compd.*, 2006, **418**, 226–229.
467 Y. W. Kim, A. Oda and N. Imanaka, *Electrochem. Commun.*, 2003, **5**, 94–97.
468 J.-M. Doux, N. Stephant, A. L. G. La Salle, O. Joubert, D. Guyomard and E. Quarez, *CrystEngComm*, 2019, **21**, 594–601.
469 J.-M. Doux, L. Leguay, A. L. G. La Salle, O. Joubert and E. Quarez, *Solid State Ionics*, 2018, **324**, 260–266.
470 E. Wang and M. Greenblatt, *Chem. Mater.*, 1991, **3**, 542–546.
471 C. Delmas, A. Maazaz and P. Hagenmuller, *Solid State Ionics*, 1983, **9**, 83–88.
472 A. Maazaz and C. Delmas, *Solid State Ionics*, 1982, **6**, 261–266.
473 J. Zheng, L. Schkeryantz, G. Gourdin, L. Qin and Y. Wu, *ACS Appl. Energy Mater.*, 2021, **4**, 4156–4164.
474 B. Babu, C. Neumann, S. Muench, M. Enke, L. Medenbach, C. Leibing, A. Lex-Balducci, A. Turchanin, U. S. Schubert and A. Balducci, *Energy Storage Mater.*, 2023, **56**, 342–350.
475 V. Madhani, M. S. Rathore and D. Kumar, *High Performance Polymers*, 2023, **35**, 28–35.
476 A. Kotronia, K. Edström, D. Brandell and H. D. Asfaw, *Adv. Energy Sustainability Res.*, 2022, **3**, 2100122.
477 J. Grins and M. Nygren, *Solid State Ionics*, 1983, **9**, 869–876.
478 A. Haffner, A.-K. Hatz, O. E. Zeman, C. Hoch, B. V. Lotsch and D. Johrendt, *Angew. Chem., Int. Ed.*, 2021, **60**, 13641–13646.
479 J. Shao, H. Ao, L. Qin, J. Elgin, C. E. Moore, Y. Khalifa, S. Zhang and Y. Wu, *Adv. Mater.*, 2023, 2306809.
480 Y. Okada, A. Nasu, T. Kimura, H. Tsukasaki, S. Mori, H. Ben Yahia, K. Motohashi, A. Sakuda and A. Hayashi, *Chem. Mater.*, 2023, **35**, 7422–7429.
481 B. He, A. Ye, S. Chi, P. Mi, Y. Ran, L. Zhang, X. Zou, B. Pu, Q. Zhao and Z. Zou, *et al.*, *Sci. Data*, 2020, **7**, 153.
482 V. Gulino, A. Wolczyk, A. A. Golov, R. A. Eremin, M. Palumbo, C. Nervi, V. A. Blatov, D. M. Proserpio and M. Baricco, *Inorg. Chem. Front.*, 2020, **7**, 3115–3125.
483 R. A. Eremin, P. N. Zolotarev, A. A. Golov, N. A. Nekrasova and T. Leisegang, *J. Phys. Chem. C*, 2019, **123**, 29533–29542.
484 L. Fiedler, K. Shah, M. Bussmann and A. Cangi, *Phys. Rev. Mater.*, 2022, **6**, 040301.
485 A. P. Shevchenko, R. A. Eremin and V. A. Blatov, *CrystEngComm*, 2020, **22**, 7298–7307.
486 R. Xiao, H. Li and L. Chen, *J. Mater. Chem. A*, 2020, **8**, 5157–5162.
487 Y. Wang, S. Wu, W. Shao, X. Sun, Q. Wang, R. Xiao and H. Li, *J. Materiomics*, 2022, **8**, 1038–1047.
488 S. Wang, Y. Jiang and X. Hu, *Adv. Mater.*, 2022, **34**, 2200945.
489 M. Fiore, S. Wheeler, K. Hurlbutt, I. Capone, J. Fawdon, R. Ruffo and M. Pasta, *Chem. Mater.*, 2020, **32**, 7653–7661.
490 K. V. Kravchyk, P. Bhauriyal, L. Piveteau, C. P. Guntlin, B. Pathak and M. V. Kovalenko, *Nat. Commun.*, 2018, **9**, 1–9.
491 Y. Li, W. Deng, Z. Zhou, C. Li, M. Zhang, X. Yuan, J. Hu, H. Chen and R. Li, *J. Mater. Chem. A*, 2021, **9**, 2822–2829.
492 J. Ge, X. Yi, L. Fan and B. Lu, *J. Energy Chem.*, 2021, **57**, 28–33.
493 Y. Hu, W. Tang, Q. Yu, X. Wang, W. Liu, J. Hu and C. Fan, *Adv. Funct. Mater.*, 2020, **30**, 2000675.
494 B. Ji, F. Zhang, X. Song and Y. Tang, *Adv. Mater.*, 2017, **29**, 1700519.
495 J. Zhu, Y. Li, B. Yang, L. Liu, J. Li, X. Yan and D. He, *Small*, 2018, **14**, 1801836.
496 L. Fan, Q. Liu, S. Chen, K. Lin, Z. Xu and B. Lu, *Small*, 2017, **13**, 1701011.
497 A. Yu, Q. Pan, M. Zhang, D. Xie and Y. Tang, *Adv. Funct. Mater.*, 2020, **30**, 2001440.
498 B. Ji, F. Zhang, N. Wu and Y. Tang, *Adv. Energy Mater.*, 2017, **7**, 1700920.

© 2024 The Author(s). Published by the Royal Society of Chemistry

Open Access Article. Published on 04 dicembre 2023. Downloaded on 11/06/2026 17:40:22.
This article is licensed under a Creative Commons Attribution-NonCommercial 3.0 Unported Licence.

499 M. Zhang, J. Zhong, W. Kong, L. Wang, T. Wang, H. Fei, H. Luo, J. Zhu, J. Hu and B. Lu, *Energy Environ. Mater.*, 2021, **4**, 413–420.
500 Z. Yan and M. Obrovac, *J. Power Sources*, 2020, **464**, 228228.
501 L. Sun, G. Li, S. Zhang, S. Liu, J. Yuwono, J. Mao and Z. Guo, *Sci. China: Chem.*, 2022, 1–9.
502 S. Trebst and C. Hickey, *Phys. Rep.*, 2022, **950**, 1–37.
503 S. M. Winter, A. A. Tsirlin, M. Daghofer, J. van den Brink, Y. Singh, P. Gegenwart and R. Valent, *J. Phys.: Condens. Matter*, 2017, **29**, 493002.
504 A. Kitaev, *Ann. Phys.*, 2006, **321**, 2–111.
505 Y.-Z. You, I. Kimchi and A. Vishwanath, *Phys. Rev. B: Condens. Matter Mater. Phys.*, 2012, **86**, 085145.